Universidade Estadual de Campinas
Faculdade de Engenharia Elétrica e de Computação

RAFAEL BRITO SAMPAIO

DEVELOPMENT OF RADIOFREQUENCY SYSTEM FOR BANKNOTES AND DOCUMENTS IDENTIFICATION

DESENVOLVIMENTO DE SISTEMA DE RADIOFREQUÊNCIA PARA IDENTIFICAÇÃO DE CÉDULAS MONETÁRIAS E DOCUMENTOS

Campinas
2017

RAFAEL BRITO SAMPAIO

DEVELOPMENT OF RADIOFREQUENCY SYSTEM FOR BANKNOTES AND DOCUMENTS IDENTIFICATION

DESENVOLVIMENTO DE SISTEMA DE RADIOFREQUÊNCIA PARA IDENTIFICAÇÃO DE CÉDULAS MONETÁRIAS E DOCUMENTOS

Dissertação apresentada à Faculdade de Engenharia Elétrica e de Computação da Universidade Estadual de Campinas como parte dos requisitos exigidos para a obtenção do título de Mestre em Engenharia Elétrica, na Área de Telecomunicações e Telemática.

Dissertation presented to the Faculty of Electrical and Computer Engineering of the University of Campinas in partial fulfillment of the requirements for the degree of Master in the area of Telecommunications and Telematics.

Advisor: Prof. Dr. Hugo Enrique Hernandez Figueroa.

Este exemplar corresponde à versão final da dissertação defendida pelo aluno Rafael Brito Sampaio e orientado pelo Prof. Dr. Hugo Enrique Hernandez Figueroa.

Campinas
2017

Agência(s) de fomento e nº(s) de processo(s): CAPES

Ficha catalográfica
Universidade Estadual de Campinas
Biblioteca da Área de Engenharia e Arquitetura
Luciana Pietrosanto Milla - CRB 8/8129

Sa47d

Sampaio, Rafael Brito, 1991-
Development of radiofrequency system for banknotes and documents identification / Rafael Brito Sampaio. – Campinas, SP : [s.n.], 2017.

Orientador: Hugo Enrique Hernández-Figueroa.
Dissertação (mestrado) – Universidade Estadual de Campinas, Faculdade de Engenharia Elétrica e de Computação.

1. Etiqueta chipless RFID. 2. Ressonadores. 3. Falsificação - Prevenção. I. Hernández-Figueroa, Hugo Enrique,1959-. II. Universidade Estadual de Campinas. Faculdade de Engenharia Elétrica e de Computação. III. Título.

Informações para Biblioteca Digital

Título em outro idioma: Desenvolvimento de sistema de radiofrequência para identificação de cédulas monetárias e documentos
Palavras-chave em inglês:
RFID chipless tag
Resonators
Falsification - Prevention
Área de concentração: Telecomunicações e Telemática
Titulação: Mestre em Engenharia Elétrica
Banca examinadora:
Hugo Enrique Hernández-Figueroa [Orientador]
Leonardo Lorenzo Bravo Roger
João Roberto Moreira Neto
Data de defesa: 01-09-2017
Programa de Pós-Graduação: Engenharia Elétrica

COMISSÃO JULGADORA – DISSERTAÇÃO DE MESTRADO

Candidato: Rafael Brito Sampaio RA: 103830

Data da Defesa: 01 de setembro de 2017

Título da Dissertação: "Development of Radiofrequency System for Banknotes and Documents Identification".

"Desenvolvimento de Sistema de Radiofrequência para Identificação de Cédulas Monetárias e Documentos".

Prof. Dr. Hugo Enrique Hernández Figueroa (Presidente, FEEC/UNICAMP)
Prof. Dr. Leonardo Lorenzo Bravo Roger (UNICAMP - Campus Limeira)
Dr. João Roberto Moreira Neto (Bradar Indústria S.A.)

A ata de defesa, com as respectivas assinaturas dos membros da Comissão Julgadora, encontra-se no processo de vida acadêmica do aluno.

To my mother Elizabete.

Acknowledgments

First, I thank the supreme Lord of the universe, who always gives me strength and guidance in my journeys.

To my parents Jairon and Elizabete for the encouragement to study and to my brothers Rone and Ricardo for the always given support.

To Prof. Hugo Figueroa for the opportunity of insertion in the academic environment and for the scientific orientation, disposition and motivation spent over the last years.

To the colleagues from the applied electromagnetism working group of the LEMAC 3, especially to Dr. Luciano Prado for the teachings and collaborations throughout the development of this work.

To Capes for the financial support and FEEC/UNICAMP for the physical structure offered to its students and researchers.

To my friends Márcio, José Carlos, Germano, Paulo and Juan Pablo for the tips, suggestions and discussions of great value for life.

Finally, I thank everyone who have contributed to this moment, directly or indirectly, and have been motivating me or cheering for my success.

Abstract

This work describes the development of a low-cost and efficient radiofrequency system for banknotes and documents identification intending to avoid counterfeiting. The proposed system is based on the microstrip and chipless RFID technologies; however, the identification is carried out through the contact of the object with the reader. In order to make this possible, the spiral resonators in the reader are placed next to a transmission line, each resonator represents a data bit, they resonate freely until a banknote or a document is placed and aligned properly. Each banknote or document must have a metallic mark printed on its inner layer, because it makes falsification difficult and the electromagnetic waves can cross the paper, in such a way that each metallic mark establishes a binary code. The metallic marks suppress the resonances of the resonators located in the reader. In other words, the marks can change the bits state, 0 or 1, corresponding to the presence and absence of resonance, respectively. The system also has the potential to increase the volume of data encoding with the possibility of the ternary system, when the resonances have three states. Simulation and measurement results are also presented in this work.

Keywords: radiofrequency, banknotes, counterfeiting, chipless RFID, spiral resonators, metallic marks, microstrip.

Resumo

Este trabalho descreve o desenvolvimento de um sistema de radiofrequência, eficaz e de baixo custo, para identificação de cédulas monetárias e documentos com a intenção de evitar falsificações. O sistema proposto é baseado nas tecnologias de linha de microfita e RFID sem chip, porém, a identificação é feita através do contato do objeto com a leitora. Para que essa identificação ocorra, na leitora, ressoadores em formato espiral são dispostos próximos a uma linha de transmissão, cada ressoador representando um bit de dado, e ressoam livremente até que uma cédula ou documento seja colocada em contato e devidamente alinhada. Cada cédula ou documento deve possuir uma marca metálica impressa em camada interna, pois dificulta falsificações e as ondas eletromagnéticas conseguem atravessar o papel, de forma que cada marca defina o código binário de cada objeto, uma vez que essas marcas metálicas suprimem as ressonâncias dos ressoadores situados na leitora. Em outras palavras, as marcas metálicas transformam o estado do bit de dado, bit 0 ou 1, correspondendo aos estados de presença e ausência de ressonância, respectivamente. O sistema também tem potencial para aumento do volume de codificação de dados com a possibilidade do sistema ternário, quando as ressonâncias possuem três estados. Resultados de simulações e resultados de medições também são apresentados neste trabalho.

Palavras-chave: radiofrequência, cédulas monetárias, falsificação, RFID sem chip, ressoadores, marcas metálicas, microfita.

List of Illustrations

List of Tables

Contents

Chapter 1

Introduction and Objectives

Counterfeiters around the world have long targeted banknotes or paper currency, especially the ones with higher value, and even metallic coins. Such action can represent a threat to the economy of a country depending on the volume of counterfeits. Even with several security measures developed along the past years in order to harden counterfeiting, such as magnetized iron oxide inks, organic pigments, varnishes and additives, holographic bands and watermarks, banknotes are always falsified. Oftentimes these situations constitute historical events as exemplified in the next paragraphs.

The first illustrated case refers to the astronomer, philosopher, alchemist, theologian and English scientist Isaac Newton who, in 1696, was nominated to the post of director of the English Royal Mint, responsible for the production of England's money. Three years later, Newton was promoted master of the Royal Mint, a position he held until his death, in 1727. During his stay, Newton did not spare efforts to take out of circulation all the old coins of the country and replace them with more reliable ones. He also investigated counterfeiters and as a result, he ended up familiar with the underworld of the city. He attended brothels and bars in the effort to hunt down and interrogate counterfeiters while receiving death threats in that period. Several counterfeiters he helped to arrest were sent to the gallows, drawn and quartered [1], [2].

Another example occurred during the World War II, when the Nazis gathered inside a fortress, in Salzburg, Austria, experts collected throughout occupied Europe to make pounds sterling and dollars. One of the forgers was the Czech Franz Xaver Ribka. After the war, Ribka run away to Brazil. In the late 70's, he sold pictures of his own, and falsifications from famous painters in the fairs and art galleries of Rio de Janeiro. Years after the end of the war, Hitler's fake banknotes still appeared around the world. In the early 50's, the Bank of England put an end to the nightmare: it removed all 5-pound bills of circulation and issued new banknotes with a magnetic thread embedded in paper. The Americans were more radical and defrayed Hitler's counterfeit to keep the credibility of their currency [3].

A large spill of fake, almost perfect, U$ 100 banknotes began in the 1990's in the Middle East. They faithfully reproduced the special paper, with red and blue microfibers and embossed printing. A United States House of Representatives Committee said the notes were made by Iran as part of an economic war plan against the United States [3].

The cited cases are only some examples of counterfeiting around the world. In Brazil, there are many cases every year of false money seizures by the federal police. Furthermore, there is still a lot of fake money being manufactured and put into circulation, which the authorities cannot identify.

It is in this context that the exposed work in this master's dissertation is introduced, since the work motivation is to research, simulate, construct and test the electromagnetic response of tags to be utilized for the identification of banknotes and/or documents intending to make it even more difficult or avoid counterfeiting. In other words, the main motivation of the project is the development of a RFID (Radio-Frequency IDentification) system, using passive tags, in order to avoid forgeries of banknotes and/or documents. Passive tags mean the non-existence of chip for data storage, for that reason the technology, which uses these tags, is denominated chipless RFID. The absence of chip drastically reduces the tags production cost in such a way that it constitutes an indispensable advantage when considering the tagging of large amounts of objects, banknotes and documents in this case. Furthermore, the proposed system in this work can be implemented commercially after certain adjustments and the full development of the reader in the proper frequency band.

That way, chipless RFID tags consist of a promising solution for low cost item tagging. The data encoding can be done by time domain reflectometry (TDR) or spectral signature. The proposed system uses the spectral signature, i.e., the resonators resonate at different frequencies so that its resonances can be cancelled out or not for the frequency domain data encoding.

Among examples of similar systems, however, similar concerning the purpose established here, found in the literature, the following stand out: the commercial chipless RFID system developed by RFSAW in which the tag is based on surface acoustic waves and uses the TDR coding scheme [4, Chapter 1, pp. 1-4]. The CorssID telecommunications company reported the development of a chipless RFID system that provides a solution for identifying multiple objects, including banknotes. That reported system uses manometric particles of chemicals with varying degrees of magnetism that resonate when bombarded by electromagnetic waves, however, there is no further information about the prototype and its

costs since it was introduced in 2004 [5, Chapter 1, p. 14]. Spiral resonators along microstrip line or coplanar waveguide has already been thought as a solution to avoid counterfeiting, nevertheless, the system presented in [6] has the whole apparatus, namely, transmission line, resonators and antennas, embedded in the banknotes. The developed system proposed in this work is different and will be analyzed in detail over the next chapters.

1.1. Text Organization

This text is divided in the following way: in Chapter 2 is presented the theory involved in the project development, which includes the initial studies about terahertz at the time a solution for the presented problem was sought. It also talks about microstrip line and stripline detailing its techniques for calculating dimensions for given impedances. It also talks about the resonance of a resonator emphasizing the spiral resonator along a microstrip line. Lastly, Chapter 2 presents the theory of chipless RFID showing illustrative examples of the base technology of the proposed system.

Chapter 3 presents the work methodology highlighting the numerical results of the proposed system. The results encompass, but not limit to, the individual spiral-resonator modeling, the modeling of the system with ten resonators along a microstrip line and results of the ternary system of data encoding. Chapter 4 shows the laboratory measurement results for concept proof. It is divided into two sections, which represent the two sets of measurements carried out to attest the system feasibility. Ultimately, Chapter 5 presents the work conclusions as well as suggestions for future endeavors.

Chapter 2

Theoretical Foundation

The following topics provide the theoretical foundation necessary for the development of the work here described. As the project consists of an identification system of objects based on resonators along a transmission line, it is necessary a descriptive theory about transmission lines, such as microstrip and stripline; also, about resonators and about chipless RFID, being the latter the technological base of this project. Besides, the project has passed through steps until the most appropriate solution for the application was found. Among the initial steps, initial studies about terahertz resonators deserved attention, being that the subject of the first section of this chapter.

2.1. Terahertz Resonators

The initial idea for the solution of this project was based on the utilization of the terahertz frequency band, mainly due to resonators micrometric dimensions.

Terahertz radiation (THz) is an electromagnetic radiation in the frequency range of 0.3 to 10 THz (1 mm to 30 μm in wavelength) [7, Preface]. Such a band is situated between microwave and infrared frequencies. Until recently, a very large portion of the spectrum has not been useful due to the non-existence of appropriate emitters to send controlled terahertz signals and efficient sensors to collect and record information [7, Chapter 1, p. 1].

Since this project consists of obtaining and developing a tag for placement inside banknotes and/or documents, preliminarily, it was thought that the project in the THz band would meet the specifications. That is because the size of the tags must be small so that the resonators are imperceptible when embedded in the bills. The resonators are tiny in the THz band. However, in addition to the lack of appropriated emitters and receptors, there is the manufacturing difficulty of devices with such dimensions; for example, it would be very hard to obtain a substrate with micrometric thickness not to mention that it would result in low mechanical rigidity. For the application of this project, it would be necessary a rather thin substrate in order to be imperceptible inside the banknotes, otherwise, there would be an unwanted protuberance on the banknote or document.

It would be utilized resonators on non-dopped silicon substrate with ground plane, whose electrical characteristics are known in the THz band, in such a way that the tag identification were done by means of the electromagnetic wave reflection on the resonators structure. It is important to notice that the tag identification can also be done by the transmission of the electromagnetic wave through the resonators structure; in this case, there would be no ground plane on the back of the silicon substrate.

For this initial stage of ideas, the shape of the resonators was defined taking into account simplicity, because it is intended a possible posterior commercial application. Among several shapes found in literature, initially, it was opted for the ring, circular or square, with or without gap. Fig. 2.1 shows some resonator geometries suitable for terahertz operation [8].

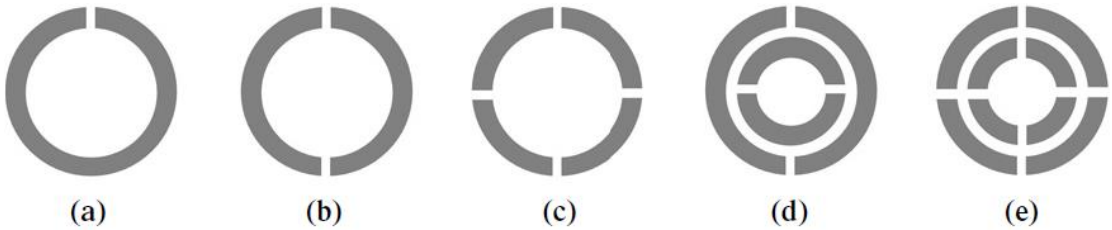

Fig. 2.1 - Sketches of different resonator shapes: (a) single ring with gap, (b) single ring with two gaps, (c) single ring with four gaps, (d) SRR (Split Ring Resonator) with two gaps and (e) SRR with four gaps.

A SRR (Split Ring Resonator) as that of Fig. 2.1(d) or (e) is not easy to manufacture for high frequency operation, due to the fact that when the structure is scaled to these frequencies the gap dimensions get very tiny. That way, the gap-reduced dimensions could eventually cause contact problems between metallic regions [8]. Thus, the chosen geometry for the first trials was the single ring without gap, similar to that of Fig. 2.1(a), however, without gap and in square shape. The electromagnetics simulation results are presented in Chapter 3, in section 3.2.

2.2. Microstrip Line

The technology utilized for the construction of the resonators and concept proof in this work is the microstrip line. Although the system can also be implemented with stripline technology for possible subsequent commercial application, the theoretical description of the microstrip is similar in some aspects to the stripline. In addition, microstrip is easier to build for making measurements and concept proof.

In a microstrip line, the dominant mode of electromagnetic wave transmission of lowest order is Quasi-TEM, due to the existence of low intensity fields in the longitudinal direction of the line resultant from the inhomogeneity of the line. In other words, the electric and magnetic fields are present in two distinct regions during the propagation of an electromagnetic wave, dielectric and air. Fig. 2.2 shows the arrangement of the electric and magnetic field lines in a microstrip line, the substrate has dielectric constant εr and is h thick, the conducting line has thickness t and width w, ground plane has thickness t. From Fig. 2.2, it is noticed that the electric field travels a path from the microstrip line through the air and the dielectric to the ground plane, so that the electromagnetic waves propagate through the air as well as through the substrate. This last statement is also true for magnetic field lines. However, most fields are concentrated in the dielectric.

The microstrip line can be thought as a transmission line inserted into a homogeneous dielectric medium whose dielectric constant is larger than that of air and smaller than that of the substrate. In the direction of the wave propagation, phase constant β is the same in both air and substrate and depends on the effective dielectric constant of the structure.

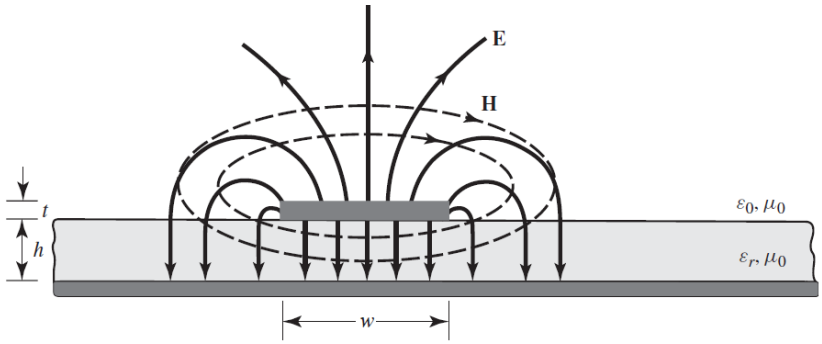

Fig. 2.2 - Electric and magnetic field lines when there exists signal propagation through a microstrip line seen in cross-section.

Due to the boundary conditions of the problem, the electric and magnetic fields tangential to the air-dielectric interface are the same. The electric field tangential to metals (line and ground) is zero. The E and H components in the direction of propagation are small compared to the transverse components so that the field configuration of this structure, which satisfies the boundary conditions, is that corresponding to the Quasi-TEM mode.

The calculation presented below familiarizes the reader on how to calculate the dimensions of a microstrip line with given substrate and characteristic impedance. First, the characteristic impedance Zc of the line can be estimated by equations (2.1) and (2.2) below:

$$Zc = \sqrt{\frac{L}{C}}\ (\Omega), \qquad (2.1)$$

$$Zc = 31.6\sqrt{\frac{L(nH)}{C(pF)}}\ (\Omega), \qquad (2.2)$$

where L and C represent the inductance and capacitance per unit length, respectively. The values of L (nH) and C (pF) can be estimated using the following equations [9]:

$$L \cong 2xln\left(\frac{5.98h}{0.8w+t}\right)\ (nH), \qquad (2.3)$$

$$C \cong \frac{0.264x(\varepsilon r+1.41)}{\ln\left(\frac{5.98h}{0.8w+t}\right)}\ (pF). \qquad (2.4)$$

That way, it is possible to obtain a good estimate of the microstrip line width value for a given characteristic impedance, once the dielectric constant εr, the height h of the substrate, the metal thickness t and the length x of the line are defined.

For a more precise calculation, it can be used the following equations suitable for calculation at low frequencies [10]:

$$\frac{weff(0)}{h} = \frac{weff(f=0)}{h} = \frac{w}{h} + \left(\frac{1.25}{\pi}\right)\frac{t}{h}\left[1+\ln\left(2\frac{h}{t}\right)\right]\ para\ \frac{w}{h} \geq \frac{1}{2\pi} \qquad (2.5)$$

$$\frac{weff(0)}{h} = \frac{weff(f=0)}{h} = \frac{w}{h} + \left(\frac{1.25}{\pi}\right)\frac{t}{h}\left[1+\ln\left(4\pi\frac{w}{t}\right)\right]\ para\ \frac{w}{h} < \frac{1}{2\pi} \qquad (2.6)$$

The value of w/h can be estimated initially using equations (2.2) to (2.4) such that (2.5) or (2.6) is the most appropriate equation to find the effective value of the line width over the height of the substrate weff(0)/h. Once the value of weff(0)/h is defined, the following equations allow to find the characteristic impedance Zc(0) and the effective dielectric constant εr,eff(0) values at low frequencies [10]:

$$For\ \frac{weff(0)}{h} \leq 1$$

$$Zc(0) = Zc(f = 0) = \frac{60}{\sqrt{\varepsilon r, \text{eff}(0)}} \ln\left[8\frac{h}{weff(0)} + \frac{weff(0)}{4}h\right], \quad (2.7)$$

$$\varepsilon r, \text{eff}(0) = \varepsilon r, \text{eff}(\text{f} = 0)$$

$$= \frac{\varepsilon r + 1}{2} + \frac{\varepsilon r - 1}{2}\left\{\left[1 + 12\frac{\text{h}}{\text{weff}(0)}\right]^{-\frac{1}{2}} + 0.04\left[1 - \frac{weff(0)}{h}\right]^2\right\}. \quad (2.8)$$

$$For\ \frac{weff(0)}{h} > 1$$

$$Zc(0) = Zc(f = 0)$$

$$= 120\frac{\pi}{\sqrt{\varepsilon r, \text{eff}(0)}} / \{\frac{\text{weff}(0)}{\text{h}} + 1.393$$

$$+ 0.667 \ln\left[\frac{weff(0)}{h} + 1.444\right]\}, \quad (2.9)$$

$$\varepsilon r, \text{eff}(0) = \varepsilon r, \text{eff}(\text{f} = 0) = \frac{\varepsilon r + 1}{2} + \frac{\varepsilon r - 1}{2}\left[1 + 12\frac{\text{h}}{\text{weff}(0)}\right]^{-1/2}. \quad (2.10)$$

Thus, the value of w can be varied in order to reach the desired value of Zc(0). According to equation (2.2), larger values of w imply in larger lines causing greater capacitance and lower inductance, and in this case, the characteristic impedance tends to decrease. The opposite is also valid, lower values of w imply lower capacitance and higher characteristic impedance.

Microstrip lines are considered dispersive transmission lines for relatively high frequencies, these values of frequencies are, in general, above 3 GHz. This indicates that $\varepsilon_{r,\text{eff}}$ and Zc vary with frequency. Then, according to [10], the following equations provide the precise calculation for a given frequency:

$$Zc(f) = Zc(0)\left[\frac{\varepsilon r, \text{eff}(0)}{\varepsilon r, \text{eff}(\text{f})}\right]^{1/2}, \quad (2.11)$$

$$\varepsilon r, \text{eff}(\text{f}) = \varepsilon r - \left[\frac{\varepsilon r - \varepsilon r, \text{eff}(0)}{1 + \left(\frac{\varepsilon r, \text{eff}(0)}{\varepsilon r}\right)\left(\frac{f}{ft}\right)^2}\right], \quad (2.12)$$

$$ft = \frac{Zc(0)}{2\mu oh}, \quad (2.13)$$

$$v(f) = vo/(\sqrt{\mu r.\, \varepsilon r, \text{eff}(\text{f})}. \quad (2.14)$$

In (2.14), v(f) represents the propagation velocity of the wave in the line at an established frequency and v_o is the speed of light in vacuum, μr represents the relative magnetic permeability of the medium.

The losses associated with the microstrip line are due to ohmic losses in the metal, losses in the substrate and losses by radiation. They are represented by an attenuation constant α added to the field equations and depend on the frequency. For the substrate, its losses can be associated to a loss tangent given by $tan\theta = \frac{\sigma}{\omega.\varepsilon}$, where σ represents the electrical conductivity, ω represents the angular frequency and ε stands for the dielectric constant of the material. The attenuation constant is calculated according to the material in which the wave propagates. Depending on the material, there are approximations more suitable for dielectric or conductive media.

The equations in this section show how to calculate the width of a microstrip line. Moreover, they provide an intuitive idea to the designer on how to proceed in the calculation of a microstrip line in the software simulations phase.

2.3. Stripline

A stripline consists of a structure in which the line is centered between two ground planes so that between the line and the ground planes exists a dielectric. Fig. 2.3 shows the geometry of this type of transmission line, as well as the layout of the field lines. The dimension h corresponds to the total height of the stripline, b represents the thickness of the dielectric, and w expresses the width of the line.

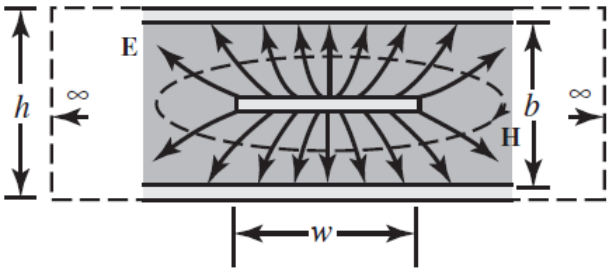

Fig. 2.3 - Electric and magnetic field lines when there exists signal propagation through a stripline line seen in cross-section.

Because the stripline has two conductors and a homogeneous dielectric, it supports a TEM wave and this is its usual mode of operation [11, Chapter 3, pp. 141-144].

Variations of the geometry shown in Fig. 2.3 include different substrate thicknesses above and below the line (asymmetric stripline) or even different dielectric constants; furthermore, air dielectrics can be used for low loss propagation [11, Chapter 3, pp. 141-144]. The structure also accepts higher order modes. In order to prevent modes other than TEM from propagating in the line, ground planes must be connected, usually via paths.

In comparison to the microstrip line, striplines offer better noise immunity, better insulation between adjacent lines, thinner lines, and is a non-dispersive transmission line. Nonetheless, as drawbacks, there is slower propagation speed, higher manufacturing cost and greater difficulty of integration with encapsulated devices.

As in the previous section, the following calculation familiarizes the reader on how to calculate the dimensions of a stripline with a given substrate for a given characteristic impedance. For the stipline, equation (2.1) of the previous section is also valid, repeated here for convenience:

$$Zc\ (\Omega) = \sqrt{\frac{L}{C}}. \qquad (2.15)$$

As the wave propagates only in the dielectric substrate, the effective dielectric constant of the structure corresponds to the dielectric constant of the substrate. Thus, the equation of the signal propagation velocity is given by:

$$vp = \frac{vo}{\sqrt{\varepsilon \mathrm{r}}} = \frac{1}{\sqrt{LC}}. \quad (2.16)$$

As $\varepsilon_{r,eff}$ of the microstrip line is smaller than the ε_r of the substrate, equation (2.16) proves that the propagation velocity in the stripline is lower. Combining (2.15) and (2.16), it is obtained that [10]:

$$Zc = \frac{\sqrt{\mu r \varepsilon \mathrm{r}}}{\mathrm{voC}}, \qquad (2.17)$$

so that the characteristic impedance of the line can be found by knowing the value of the line capacitance per unit length. The capacitances of a stripline are the capacitances between the line and the ground plane and the capacitances resulting from fringe effects within the

structure. The following equation gives an approximation of the value of Zc [11, Chapter 3, pp. 141-144]:

$$Zc = \frac{30\pi}{\sqrt{\varepsilon r}} \frac{b}{We + 0.441b}, \qquad (2.18)$$

where We is the effective width of the center conductor and is given by:

$$\frac{We}{b} = \frac{w}{b} - 0 \quad for\ \frac{w}{b} > 0{,}35, \qquad (2.19a)$$

$$\frac{We}{b} = \left(0.35 - \frac{w}{b}\right)^2 \quad for\ \frac{w}{b} < 0.35. \qquad (2.19b)$$

In order to find w/b, the following formulas are used [11, Chapter 3, pp. 141-144]:

$$\frac{w}{b} = x \ \ for\ \sqrt{\varepsilon r}\mathrm{Zo} < 120\Omega, \qquad (2.20a)$$

$$\frac{w}{b} = 0.85 - \sqrt{0.6 - x}\ \ for\ \sqrt{\varepsilon r}\mathrm{Zo} > 120\Omega, \qquad (2.20b)$$

where x is defined in the following way:

$$x = \frac{30\pi}{\sqrt{\varepsilon r}\mathrm{Zo}} - 0.441. \qquad (2.21)$$

In these equations, Zo is a given characteristic impedance value.

Once again, as in the previous section, the above equations show how the quantitative calculation of a stripline is done. Also, they provide an intuitive idea to the designer on how to proceed in the design of a stripline in the preliminary phase to software simulations. From equations (2.19a) and (2.19b), it can be seen that the narrower the central conductor of a stripline, the greater its characteristic impedance, and vice versa.

Concerning losses, these are due to ohmic losses in the metal and losses in the substrate.

Finally, the precise calculation for a stripline is long and tedious, of little practical interest for the purposes of this work.

2.4. Resonator Resonance

Microwave resonators are used in a variety of applications such as filters, amplifiers and RFID. The operation of the microwave resonators is very similar to that of lumped element circuits.

At frequencies close to resonance, a microwave resonator can be modeled by an equivalent circuit of series or parallel lumped elements [11, Chapter 6, pp. 272-277]. A resonator designed in microstrip line or stripline has capacitances, inductances and resistances. For example, capacitors are formed in gaps in the structure and between the structure and the ground plane, while the length and width of tracks, that make up the resonator, represent their inductances.

Thus, by modeling the microwave resonator as a series or parallel RLC circuit, it is obtained that the angular resonance frequency (wo) is given by the equation below:

$$wo = \frac{1}{\sqrt{L.C}}, \quad (2.22)$$

where L and C are the inductance and capacitance of the resonator, respectively.

What happens in a resonator when an electromagnetic wave hits it with certain power is that magnetic energy is stored in its inductor, electrical energy is stored in its capacitor, and there will also be losses due to the presence of the conductor resistance, losses by radiation, as well as losses in the dielectric. Resonance occurs when the stored average magnetic energy equals the stored average electric energy [11, Chapter 6, pp. 272-277], which is when equation (2.22) is defined. The impedance level in this situation consists only of a small resistance. Therefore, a situation of near short-circuit is generated between the transmission line and ground plane.

However, for the situation described in the previous paragraph be achieved, it is necessary that the resonator be coupled to an external circuit, such as a transmission line. In practice, it depends on the type of resonator under consideration. The level of coupling required between the resonator and its attached external circuit depends on the application [11, Chapter 6, pp. 297-306]. The coupling of most interest in this work is the gap coupling in microstrip line or stripline. In Fig. 2.4, a spiral shaped resonator is positioned near a 50 Ω microstrip line. It is noted the conductor, separated by the ground plane by a substrate with

dielectric constant given by ε_r, together with the resonator in a spiral format gap-coupled to the line.

The spiral resonator can be modeled as a series RLC circuit, as seen in Fig. 2.5 a), due to the low impedance path created in the resonance situation, characteristic of a series RLC circuit [4, Chapter 3, pp. 25-29]. When the spiral is coupled to the microstrip line, the entire circuit (microstrip line, coupling gap and spiral resonator) is modeled as a parallel equivalent RLC circuit due to its stop-band characteristic, such situation can be seen in Fig. 2.5 b) [4, Chapter 3, pp. 25-29]. In Fig. 2.5, CD, LD and RD are the distributed capacitance, the distributed inductance and the resistance of losses of the spiral resonator, respectively. R_s, C_s e L_T represent, respectively, the resistance of losses, the capacitance between the line and the ground plane and the total inductance of the microstrip line. Z_0 corresponds to the characteristic impedance of the line and the source. L_e, C_e e R_e constitute equivalent inductance, capacitance, and resistance losses.

Therefore, the angular resonance frequency of the spiral resonator coupled to the microstrip line is given by:

$$wo = \frac{1}{\sqrt{Le.Ce}} \qquad (2.23)\ [4, Chapter\ 3, pp. 25-29]$$

In summary, the spiral resonator shown in Fig. 2.4 creates a low-impedance path between the microstrip line and the ground plane at its resonance, so that it absorbs much of the energy that propagates through the line at that frequency.

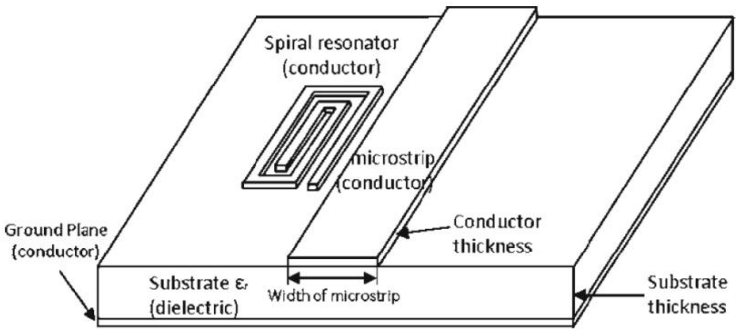

Fig. 2.4 - Spiral resonator gap-coupled to a microstrip line.

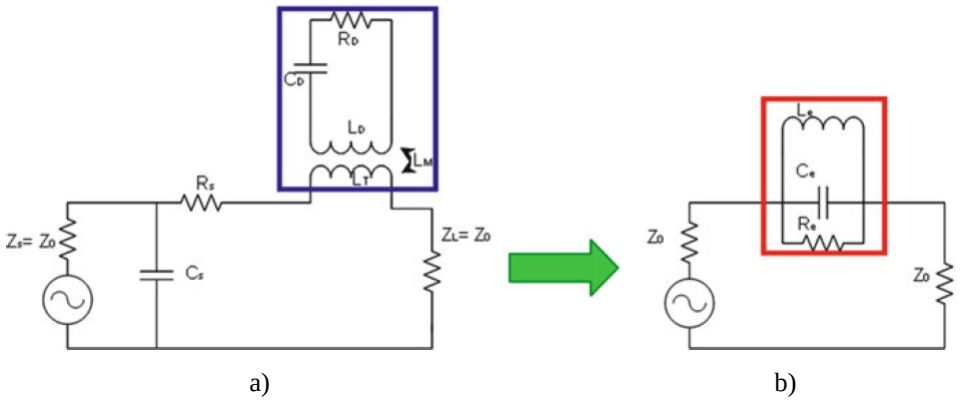

a) b)

Fig. 2.5 - Equivalent circuit model of a spiral resonator coupled to a microstrip line.

Another important parameter on the resonators approach is the quality factor, usually known as Q of the resonator or circuit. The quality factor is defined by equation (2.24) below [11, Chapter 6, pp. 272-277]:

$$Q = w\frac{average\ stored\ energy}{energy\ loss/second}. \qquad (2.24)$$

In other words, the Q of the circuit is related to its losses. According to equation (2.24), the smaller the losses, the larger the Q and vice versa. For the case of Fig. 2.4, the Q of the circuit is different from that calculated when considering only the resonator in a spiral format, because a resonator, in practice, is invariably coupled to other circuit(s) whose effect is to reduce the total quality factor [11, Chapter 6, pp. 272-277]. Considering this case, when it is modeled as a parallel RLC circuit as shown in Fig. 2.5 b), another resistor is added in parallel to the resistor of the resonator itself. The parallel combination results in a smaller equivalent resistance R_e between the resonator and the ground plane, which leads to more losses and lower quality factor.

2.5. Chipless RFID

One of the great advantages of RFID technology, compared to other identification technologies, is the option of automatic tracking and identification; this is possible because there is no need for line-of-sight, during identification, enabled by the use of radio waves [4, Chapter 1, pp. 1-4]. Its main applications include supply chain management and logistics, electronic article surveillance, document and baggage tracking, vehicle and livestock tagging

etc [4, Chapter 1, pp 1-4]. Although RFID has a great range of applications in many areas, there is no single system that meets all of the requirements because certain features are required in some applications while are not in others. Hence, the design and requirements of an RFID system is defined, in general, for its specific application.

Firstly, it is necessary to emphasize the differences between conventional RFID and chipless RFID. The best-known and currently used type is still conventional RFID based on the use of integrated circuit (IC) chip where data is stored; this chip is connected to an antenna [12]. The IC also performs the essential tasks of data processing. In the case of passive ICs, the chip is powered by the energy emitted by the reader's interrogation signal; on the other hand, in the case of active ICs, they have built-in battery so that identification can be achieved at greater distances with the loss of greater tag cost [4, Preface]. In a conventional system, the main tag cost is related to the chip, and this has been limiting the application of this technology in large scale in the substitution of bar codes, despite demonstrating advantages such as no need for line-of-sight, remote identification and the possibility of automatic identification.

The total cost of an RFID system depends primarily on the tag cost. However, the last statement is only true when there are a significant number of tags in the system, in this case, the reader does not contribute significantly to the operational cost because it constitutes a fixed value [5, Chapter 1, p. 8]. That way, the following is true:

System Cost = (fixed cost) + N(tag cost),
N = number of tags,
Fixed Cost = (reader + software)
If $N \rightarrow \infty$,
System Cost $\cong N$*(tag cost)*

Chipless RFID appears as a cost-effective tagging solution resulting in a competitive price comparing to a barcode identification system. It is in this context that the peculiarities of chipless RFID are highlighted: no need for line-of-sight, low cost and smaller reading distances compared to conventional RFID due to the absence of chip and battery. Nevertheless, in technological developments, there is always a tradeoff between performance and cost. With lower cost, the main challenges of chipless RFID lie in the development of unconventional coding techniques; shorter identification distances, since all the power involved in the reading comes from the power of the reader's interrogation signal; and less

coded bits compared to the conventional case [4, Preface]. In recent years, efforts have been made in the development of chipless technology, so that there are already some consolidated and functional systems. As examples, it is presented the ones in [13] and [14] where, for coding, electromagnetic waves are transformed into surface acoustic waves (SAW). It is used, in this system, the time domain reflection scheme for signal coding. There is also the system presented in [6] where the identification is achieved by the spectral signature left by the resonances.

The theoretical foundation presented in this section about chipless RFID refers to the option by which the execution of the main idea of the project was highly inspired. Chipless RFID tags are classified based on data encoding. Thus, there are two classifications, the first one is based on time domain signal reflection (TDR-based) and the second is based on the spectral signature [4, Preface]. The focus of this work lies in the second type, that is, the coding is carried out by means of variations in the spectral curves of the resonant structures.

A chipless RFID tag is composed of several resonators resonating at different frequencies, i.e., each tag has its own identification code. In addition, when the resonators are defined in a microstrip line, antennas are used to receive and transmit the signal with the electromagnetic mark of the resonators. Electromagnetic marks stand for the information encoded by the resonators. This way, for each identification code, a set of resonators must be defined. In general, it is used binary code, in such a way that each resonator composing the tag constitutes an information bit. The bit must be 0 or 1 for the presence or absence of resonance, or reciprocally 1 or 0 for the presence or absence of resonance, respectively. The amount of bits a tag can hold depends on the available frequency band, since the resonance of each resonator occupies a fraction of the band.

The spiral resonator is a simple, compact and narrowband resonator. Despite it is not the highest quality factor resonator found in the literature, the spire has resonance attenuations with acceptable values. An important factor for the cascade resonator modeling is that the resonators require a smaller resonance spacing in the spectrum. This is an advantage of the spiral resonator due to its narrowband characteristic. In addition, it is possible to position spires on both sides of the microstrip line or in a stripline. This action saves space for cases where a large amount of data encoding is required. In [15] there is a coplanar waveguide resonator with a quality factor slightly better than that of the spiral resonator, however, there is no possibility of positioning resonators on both sides of the line, as it can be seen in Fig.

2.6. This peculiarity would result in a very long line in a situation where a large amount of bits is needed.

In [6], a small short-circuit is used between the arms of the spiral resonator so that the resonance is removed, or, in other words, so that the state of the bit is modified from 0 to 1, as mentioned earlier. However, in practice, the resonance is not actually removed; it is only shifted to a higher frequency and becomes weakened, as can be seen in Fig 2.7.

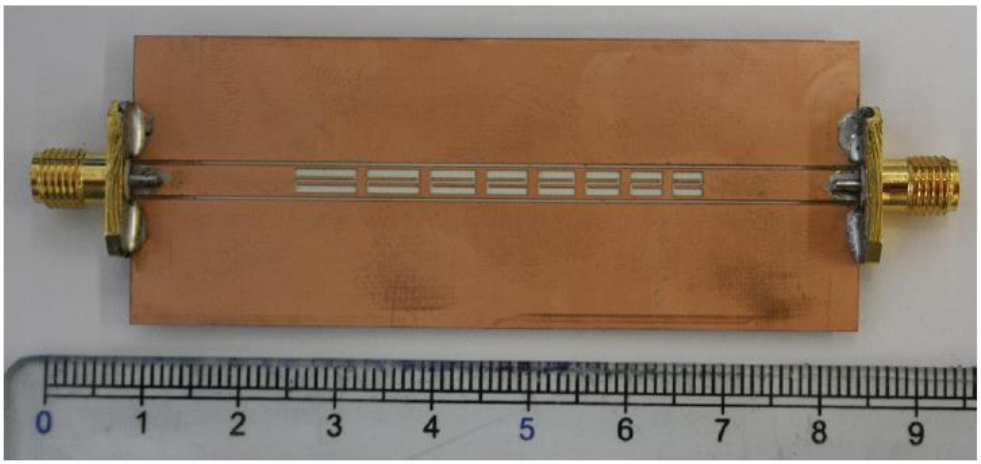

Fig. 2.6 - Coplanar waveguide resonators. Although it has a larger Q, the resonance takes up more space in the spectrum and the resonator occupies more space compared to the spiral.

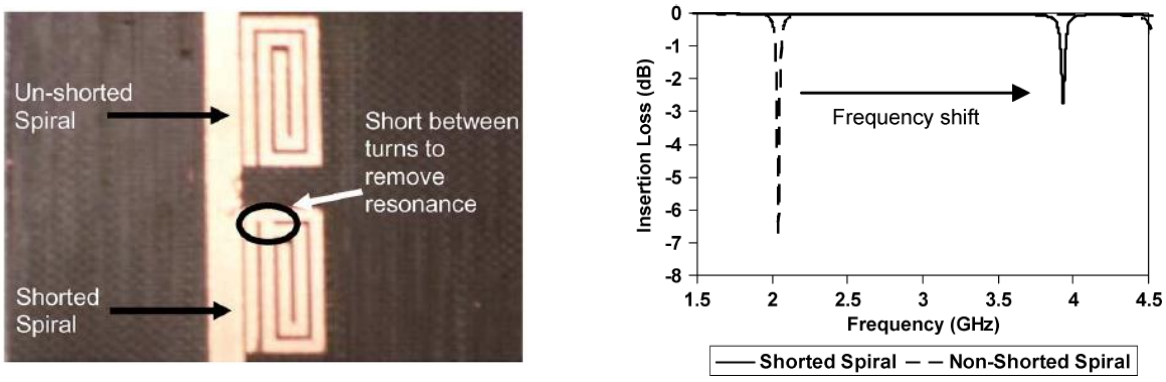

a) b)

Fig. 2.7 - Spiral resonator next to microstrip line; a) Normal and short-circuited spire; b) Resonant frequency displacement when spire is short-circuited.

That resonance offset limits the frequency band used, resulting in less amount of bits for encoding of information. Another option would be the complete removal of the spire in places where resonances are not desirable. In this case, the resonance would be removed including its harmonics. Nonetheless, in practical terms this becomes an unwanted action. Since in mass production it would be more practical for all the spiral-shaped resonators of the

tag to be manufactured with short-circuits. In such a way that the specific code of each tag was defined by eliminating these short circuits at the desired spirals.

To illustrate the chipless RFID operation, it is presented the following example of a tag using the previously described microstrip line technology: first, the label is illuminated by a wideband signal with constant amplitude and phase, as seen in Fig. 2.8, which covers the band of frequencies used in the design of the resonators, coming from a reader. The tag-receiving antenna Rx receives the signal and the circuit resonates at the frequencies for which it was designed. The resonances create attenuations in the amplitude of the signal and phase leaps, as can be observed in Fig. 2.8 [12]:

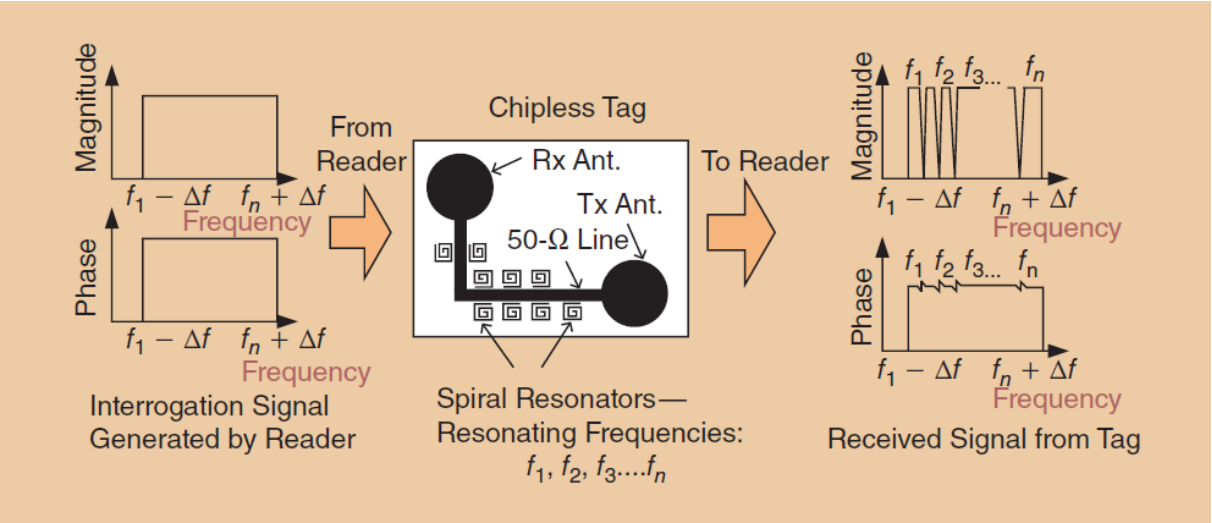

Fig. 2.8 - Principle of operation of a spectral signature chipless RFID tag.

The modified signal is retransmitted to the reader via the tag transmitting antenna Tx to be processed and decoded. Then, the tag's intrinsic code can be identified, with its pre-established short-circuited spires. The data encoding in the spectrum, both in amplitude and phase, allows the reader to use two criteria for data decoding: amplitude and phase. As seen, the system does not work by RCS backscattering, but relapses in the retransmission of the interrogation signal with the coded spectral identity [6].

In Fig. 2.8, the tag antennas Rx and Tx are printed circular monopoles. These antennas are omni-directional, compact, fully-printed and wideband, projected for the same band to which the resonators are designed. Furthermore, the radiation pattern remains at an acceptable degree of constancy along the band. Such characteristics are indispensable for the remote reading of the information contained in the tag. As said above, these antennas retain the function of receiving the interrogation signal from the reader and transmitting the signal back after performing its spectral modulation through the resonators [4, Chapter 1, pp. 1-4].

From Fig. 2.8, it can be seen that these antennas are linearly polarized, one of them vertically and the other horizontally polarized, this is adopted as an isolation mechanism between the interrogation signal sent by the reader to the tag and the signal retransmitted by the tag [4, Chapter 4, p. 54].

In such a system, the reader can obtain the information and decode the data in many ways. As examples, the reader could only read the amplitude information or read both the amplitude and phase information. For the simplest case, which only consists of reading the spectral amplitude of the signal, the reader RF circuit would consist of transmitting and receiving antennas, LNA, amplifiers, filters and a rectifier diode that would identify at each frequency a voltage value that would be sent to the reader's digital module. However, the reading details are outside the scope of this work, whose focus is the design of a tag and its identification mode as will be shown in the following chapters.

Chapter 3

Methodology and Presentation of the System

In this chapter, the norms and methods established in the development of the project will be described, as well as descriptions of the proposed system. The motivation of the project was to find a solution for banknotes and documents identification. However, when feasible solutions are envisaged, a number of ideas about how this solution could be implemented arises, in many cases, encountering some obstacles such as manufacturing difficulties, impracticability and high costs.

The methodology used to carry out the project was divided into the following topics. In summary, the following topics summarize the simulated results of some proposals for terahertz tags, and then show the methods and descriptions used in microwave frequencies.

3.1. Simulation Software: CST Studio Suite

First, it is important to highlight the general characteristics of the simulation software adopted in this project. CST Studio Suite consists in a software that provides efficient and accurate computational solutions for an electromagnetic design and/or analysis. The three-dimensional electromagnetic simulation software has a user-friendly interface and allows choosing the most appropriate method for the project, as well as optimizing devices over a wide range of frequencies [16]. This software was of fundamental importance in the adjustments and achievements of the results throughout the project. Adjustments for example in resonator dimensions and resonance positioning, port placement, mode excitation, parameter sweeps etc.

3.2. Terahertz Tag

Some simulation attempts have been made successfully. Fig. 3.1 presents a ten-bit tag with square ring resonators, whose dimensions are micrometric. Its main dimensions, named, square resonator lengths and widths, are showed. Each resonator resonates at its

designed frequency. The image shows the tag seen from above, the resonators are on a silicon substrate and there is a ground plane on its opposite side as it can be seen in the tag side view of Fig. 3.2. The resonator would be simpler to manufacture in this format.

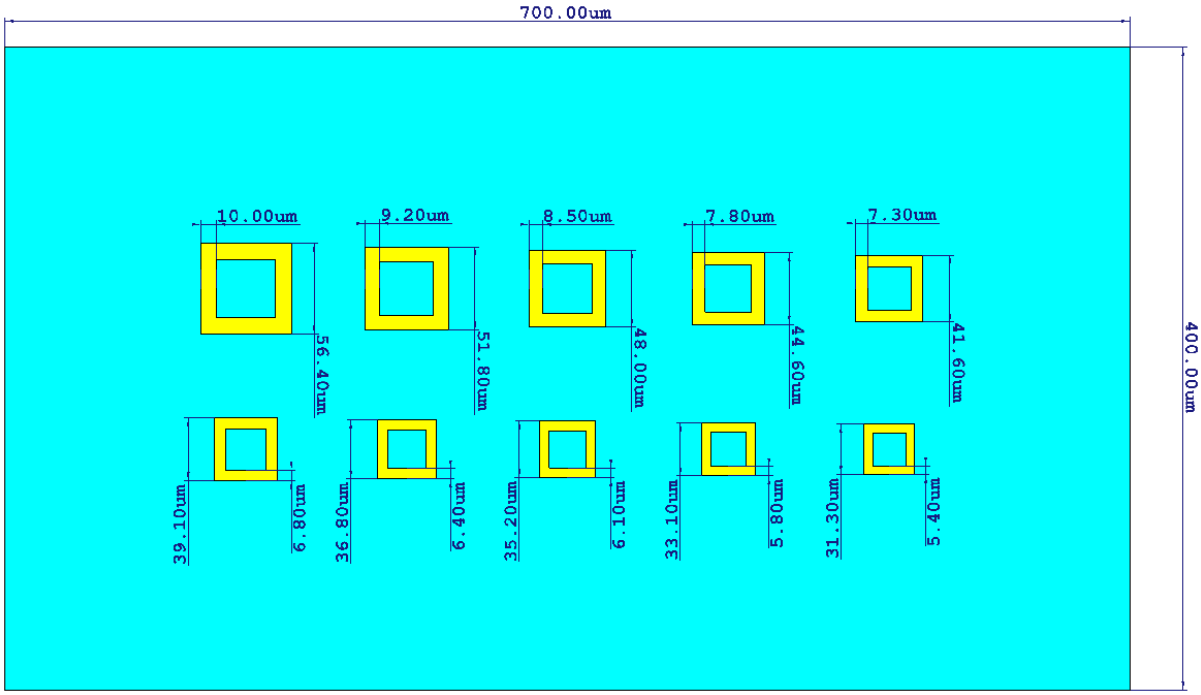

Fig. 3.1 - Set of resonators in silicon substrate, metal in yellow and silicon in blue.

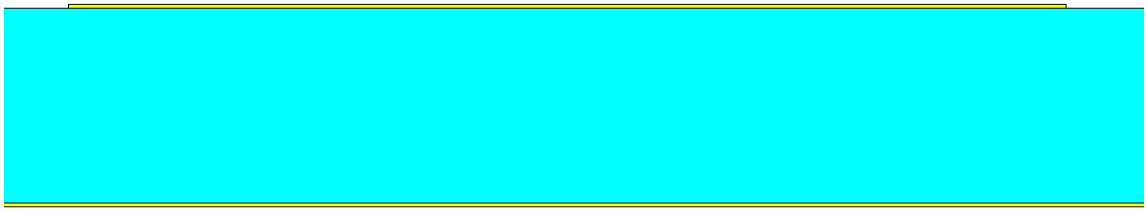

Fig. 3.2 - Tag side view highlighting resonator and ground plane.

In the modeling, a non-doped silicon substrate (blue color in Figures 3.1 and 3.2) was used, the dielectric constant and loss tangent value of this material is found in the literature for the range in which it was simulated, being 11.67 [17] and 15.4 x 10^{-6} [18], respectively. The silicon dielectric is 10-µm width. Moreover, the chosen metal was gold, since it is a low-loss conductor, which increases the resonators quality factor (Q). Gold can be considered as a perfect electric conductor in the terahertz band [19].

In the simulation, it was used a plane wave as excitation, so that the electric field vector reaches the resonators of Fig. 3.1 parallel to the page in the vertical position, as can be seen in Fig. 3.3.

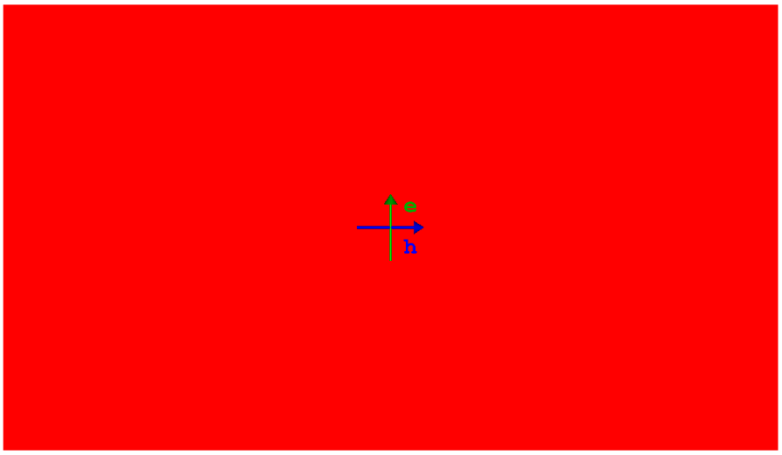

Fig. 3.3 - Configuration of the electric and magnetic field vectors of the plane wave that excites the tag.

Fig. 3.4 displays the dielectric loss curve, in watts, of the tag as a function of frequency, in the range of 0.5 to 1.2 THz.

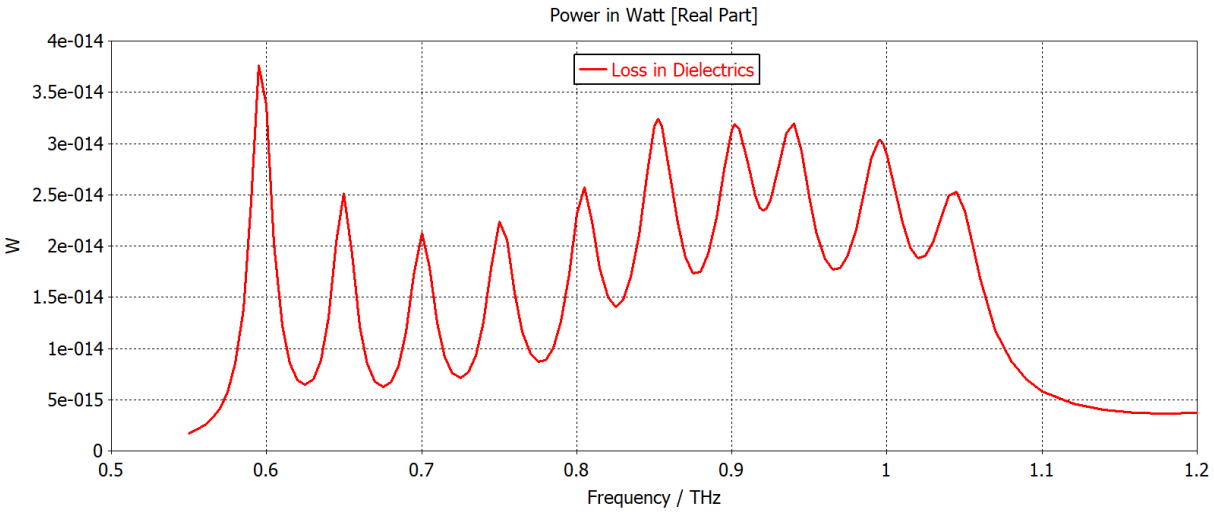

Fig. 3.4 - Dielectric losses, in watt, of the tag of Figs. 3.1 and 3.2 as a function of frequency.

In this image, the maximum power peaks indicate resonator resonances, and such a result can be proved when the structure of Fig. 3.1 is simulated on a specific platform to find resonant frequencies and coupled modes. To put it in another way, the resonators store the energy of the sent signal at the resonance locations. The concentration of fields between the resonator and the ground plane results in losses in the dielectric, so that the more intense the field, the greater the losses. The result can also be seen in a radar cross-section (RCS) plot.

Fig. 3.5 exhibits the electric field modulus at the frequency at which the first and largest resonator resonates, 0.6 THz.

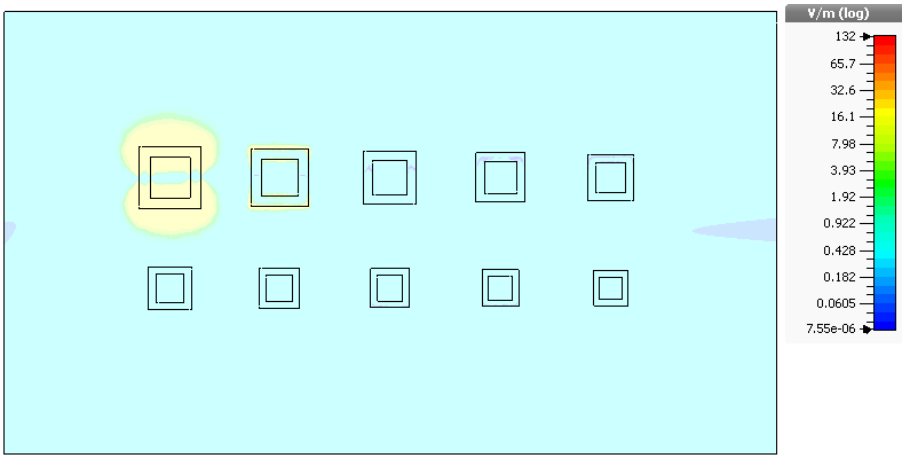

Fig. 3.5 - Electric field modulus at the frequency of 0.6 THz.

For a RFID system with a tag like that, the reading of the information contained in the tag would be based on the frequency domain. Briefly, the reader would send a broadband interrogation signal to the tag, and this signal would be reflected back to the reader so that the resonances were processed in the frequency domain.

As can be seen, there are results for a terahertz-band tag. However, as explained earlier in Section 2.1 of Chapter 2, such devices are difficult to construct mainly due to the thickness of the substrate, in addition to the scarce availability of measuring devices in the terahertz range.

3.3. Microwave Tag Modelings

In this section, the characteristics of the proposed system will be presented in a descriptive character, as well as numerical modelings throughout the development of the project. The models range from the simple spire to the ternary data encoding system.

3.3.1 Description of the Proposed System

Chipless RFID is a very attractive solution due to the non-existence of a data storage chip or battery, leading the final product to be cheap when considering the tagging of low cost objects such as banknotes and documents. In the literature, there are systems for identification of banknotes using chipless tags in which the whole transmission line, the receiving and transmitting antennas and all the resonators are embedded in the banknote; such a set is termed tag. In these systems, a reader sends a signal over a certain frequency range so that the tag receiving antenna transmits the received signal to the transmission line. This

signal is altered by the resonant pattern of the resonators and retransmitted through the tag transmission antenna to the reader. The reader then checks the received signal pattern and identifies the object code.

The proposed system operates differently, the transmission line and the resonators are placed only in the reader and not in each of the objects to be identified, so that these objects would only have metallic marks that would inhibit or weaken the resonance of a given resonator located in the reader. The system would work with the use of a reader composed of a transmission line and several lateral resonators, each resonator acting as a bit. The metal marks of identification would be embedded inside the banknotes or documents themselves, in an inner layer of the paper, since banknotes are manufactured in layers. Each banknote would have its specific printed metal pattern, which, when placed on the reader and properly aligned, would modify the reader's frequency response or, in other words, would nullify or weaken some resonances of some resonators in order to define its specific code.

Therefore, a larger number of resonators, in the case of this work, spiral resonators, can be positioned along a meandered transmission line, so that each spire can assume two or three states. The system can be binary with the two options being the presence or absence of resonance, but can also be ternary with the three options being presence, absence and presence of weak resonance or half resonance. For the latter case, a metallic shape must be drawn inside the banknote in order to keep the resonance at the same frequency while it is weakened. In the case of presence of resonance, there is no metal covering the resonator, that is, the resonator resonates freely without the metallic shield. In the case of the absence of resonance, the metallic mark completely covers the entire region corresponding to the resonator.

Throughout the description in the preceding paragraphs of the proposed system, the codes of each banknote or document would be defined by the banknote itself or by the document itself with metal marks printed on its inner layers. As an example, a system with N spires along the transmission line of the reader would result in a total of 2^N combinations of different codes using the binary system, that is, with presence or absence of resonances. When concerning the ternary system, a system with N spires would result in a total of 3^N combinations of different codes. The latter option allows the encoding of a larger amount of data, corresponding to a multiplicative factor of 1.5^N to be more specific.

Fig. 3.6 illustrates, in general terms, how the proposed system works. On the left, it is illustrated what would be the core component of the reader composed of a transmission line, together with the spiral resonators coupled to the line by gaps, numbered in ascending

order of resonant frequencies in the spectrum. Moreover, a paper sheet is placed over the microstrip line and resonators representing what would be the placement of a banknote or document. On the paper, the metal marks are positioned over the resonators in order to extinguish some resonances, as can be seen in the images on the right where the transmission curves of the structures are shown.

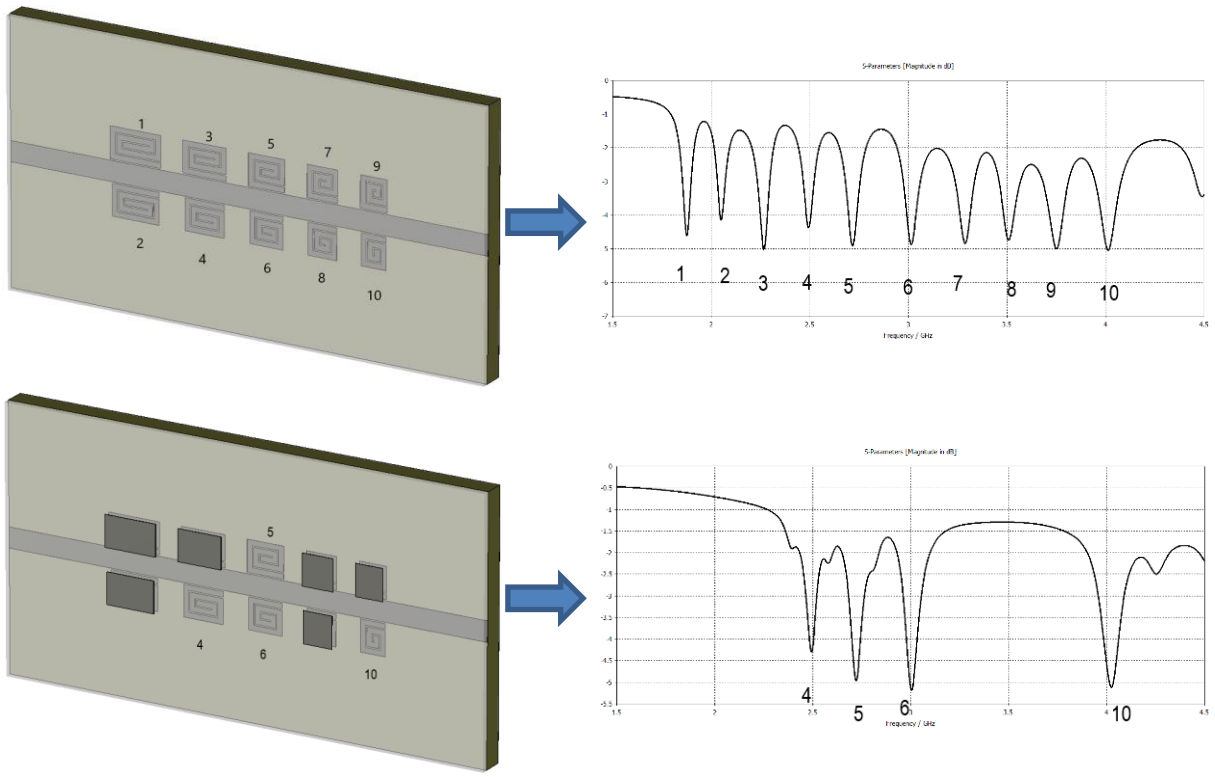

Fig. 3.6 - Illustration of the proposed system considering a binary system with ten spiral resonators. It is noted that the metal marks effectively suppress the resonances modifying the bit state.

Among the advantages of the system, the following stand out:

1) Low manufacturing cost. Since the system is designed for tagging of large number of objects, the total cost of the system is primarily dependent on the cost of the tag as presented in section 2.5 of Chapter 2. The tag cost, in this case, is for the printing of only small metal marks on the banknotes or documents.
2) Greater security. The metallic marks are printed on the internal layer of the banknote or document; in addition, there is the possibility of the use of transparent conductive inks, which makes counterfeiting even more difficult. For instance, in a bar code system, the bars would need to be visible and well established on the banknote surface, because the system uses visible light for identification. The exposed bars facilitates falsification. In a situation of falsification, the proposed system could identify, for example, the use of a different paper in the confection of the banknote by

the displacement of the resonances in the spectrum. Possible fake banknotes could also present misaligned metal marks so that the system could also identify by resonance pattern. Furthermore, software logical encryption can raise the security of the system.

3) Great potential for data encoding. In this regard, the proposed system allows increasing the possibility of resonance states of the resonators. For instance, the system could be endowed with three states in each resonator, being able to encode 3^N different codes, where N is the total number of resonators of the system.
4) Robustness. The metal mark completely suppresses the resonance along with its harmonics, unlike the system presented in [6], and cited in section 2.5 of Chapter 2, in which the arms of the spiral resonator are short-circuited and the resonance is shifted to a higher frequency. Another reason for robustness concerns the fact that the proposed system is not based on signal transmission through free space, since the code reading is carried out through a guided transmission line and there is no power loss in free space, also there is less random factors that could modify the spectrum. That way, the curves and resonances are more behaved compared to a system whose detection is made by distance. Furthermore, metal marks can be replaced with graphene marks because this material is stainless and relatively flexible, since banknotes and documents may be subject to mechanical stresses and humidity.

Graphene is an atomically thin, but stable, hexagonal carbon form that has attracted the attention of the scientific community since 2004. Along with its unique electronic properties, graphene has shown interesting optical, mechanical and thermal properties [20]. As the system proposed in this work is intended for use in banknotes and documents, adverse conditions such as mechanical stresses and moisture exposures have been taken into account. Hence, the use of graphene is adequate, because it is conductive, thin, low reactive, strong and somewhat flexible.

The next topics better clarify the development of the project in more detail with a step-by-step construction along with their respective charts and illustrations.

3.3.2 Software Modeling of the Spiral Resonator

To better clarify the system, a parametric study is carried out to verify the resonance sensitivity of the spiral resonator in relation to its main dimensional parameters. Fig. 3.7 shows a spiral-shaped resonator near to a microstrip line.

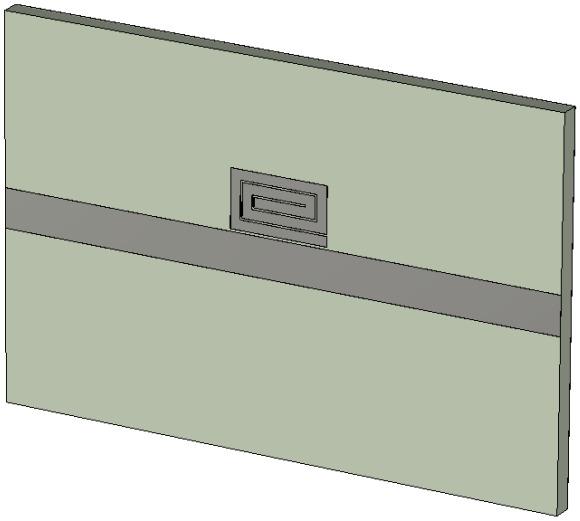

Fig. 3.7 - Spiral-shaped resonator near to microstrip line.

In the image, the line and the spire are on a FR-4 substrate whose electrical characteristics used in the simulations are dielectric constant $\varepsilon r = 4.3$ and loss tangent $\tan \delta = 25 \times 10^{-3}$. At first, for simulation purposes, the metal used was Perfect Electric Conductor (PEC). The boundaries of the structure were open, that is, there is the presence of perfectly matched layers (PML - Perfect Match Layer).

The spiral has physical parameters that allow the tuning of the resonance at a given frequency, as well as adjusting its width and depth to a certain resonance limit. However, it is known that the quality factor is limited by the inevitable losses in a real structure. Fig. 3.8 illustrates the variables of interest for adjusting the spiral resonance. They are the width of the spire arms *wr*, the horizontal length of the spire *1b*, the gap between the spire and the transmission line *gl* and the internal gap *gi* between the spire arms. The vertical length depends only on the internal gap, the width of the arms and the number of spire turns, which in the case of this work is kept fixed.

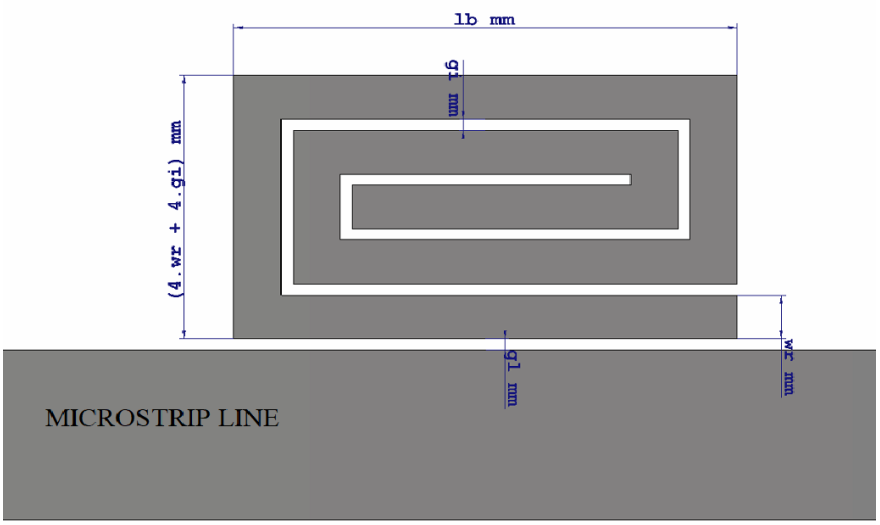

Fig. 3.8 - Variables of interest in adjusting the resonance of the spiral resonator.

The effects of the variations of these parameters will be presented below. Curves of the transmission parameter S21 of the resonator of Fig. 3.7 in dB will be presented as a function of frequency, which varies between 1.2 GHz and 2.4 GHz, in different situations of variation of dimensional parameters. Ports 1 and 2 are placed at the ends of the microstrip line. The quoted transmission parameter indicates a power ratio received at port 2 relative to the input power at port 1. In other words, at the spire resonance frequency, part of the power inserted into the transmission line is coupled into the spire and this fact can be observed in the transmission curve of the device.

First, it is showed the variation of *lb* and its effect on the resonance. In this case, the values of the other variables are maintained and are equal to: *gi* = 0.2 mm; *gl* = 0.2 mm and *wr* = 0.8 mm. Fig. 3.9 illustrates what happens. The frequency range varies from 1.2 GHz to 2.4 GHz and the attenuation range varies from 0 to -7 dB for better viewing.

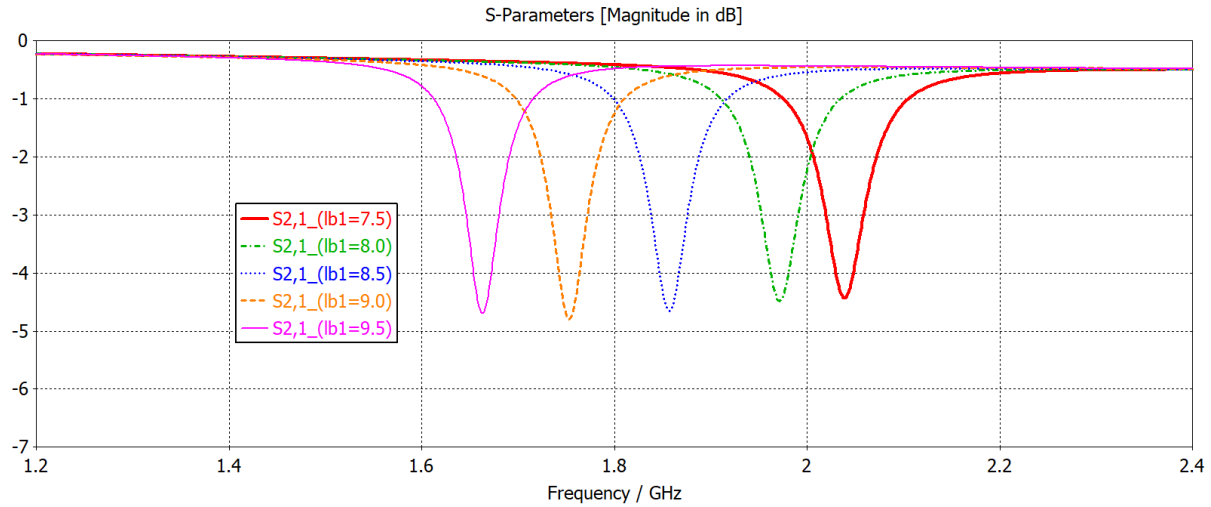

Fig. 3.9 - Parameter *lb* ranging from 7.5 mm to 9.5 mm with steps of 0.5 mm. Note the considerable displacement of the resonance in frequency.

As expected, the resonant frequency of the spiral resonator increases as its length is increased. The attenuation has practically no considerable change.

It will now be verified the effect of the variation of the width of the arms of the spiral resonator, corresponding to the variable *wr*. For this case, the values of the other variables are fixed: *gi* = 0.2 mm; *gl* = 0.2 mm and *lb* = 8.5 mm. Fig. 3.10 shows the results.

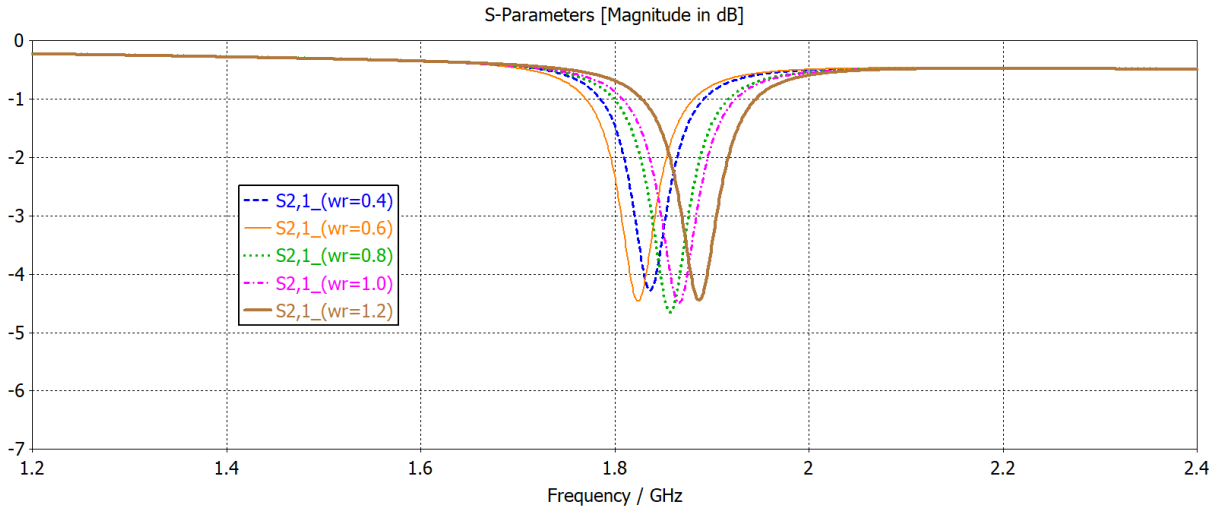

Fig. 3.10 - Parameter *wr* ranging from 0.4 mm to 1.2 mm with steps of 0.2 mm.

From the image, it can be seen that the width of the resonator arms has a small but notable influence at the resonance position compared to the horizontal length of the resonator. This behavior results, among other reasons, from the variation of the capacitance between the ground plane and the spire when varying *wr*. The attenuation is also little influenced,

however, the value of *wr* = 0.8 mm showed to be the best attenuation for the project follow-up.

The next parameter is the gap *gl* between the resonator and the transmission line. In this case, the values of the fixed variables are: *gi* = 0.2 mm; *wr* = 0.8 mm and *lb* = 8.5 mm. Fig. 3.11 presents the results.

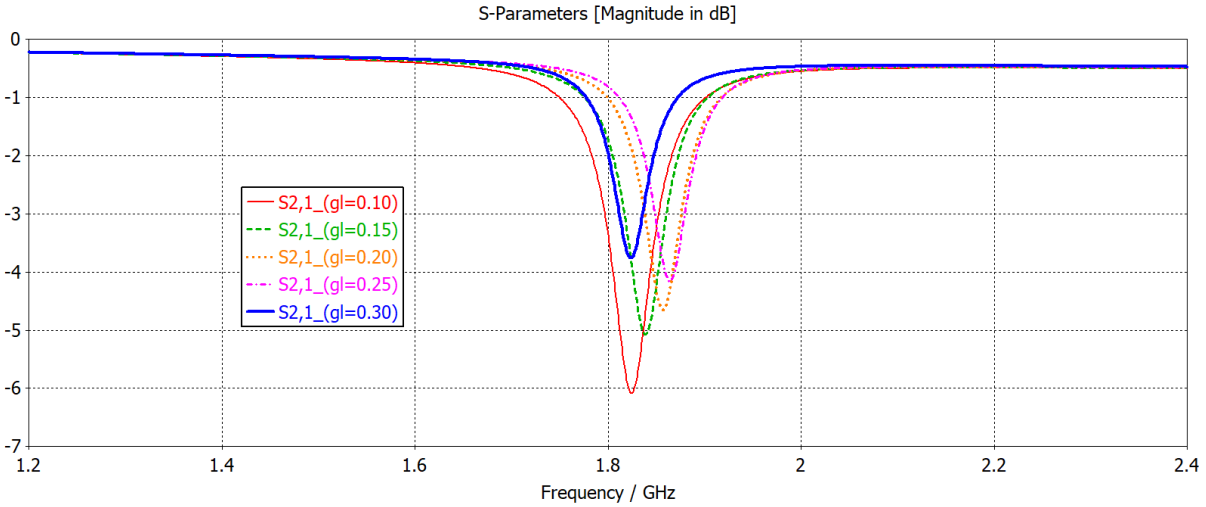

Fig. 3.11 - Parameter *gl* ranging from 0.10 mm to 0.30 mm with steps of 0.05 mm.

As can be noted, the displacement of the resonant frequency of the resonator relative to the distance between the microstrip line and the resonator is minimal. On the other hand, the attenuation of the resonance is greater when the resonator is closer to the line, as shown in Fig. 3.11, due to the greater coupling between the 50 Ω line and the spiral resonator.

The last analyzed parameter is the internal gap *gi* of the spiral resonator. In this situation, the values of the fixed variables are: *gl* = 0.2 mm; *wr* = 0.8 mm and *lb* = 8.5 mm. Fig. 3.12 exhibits the results of the variation of *gi*.

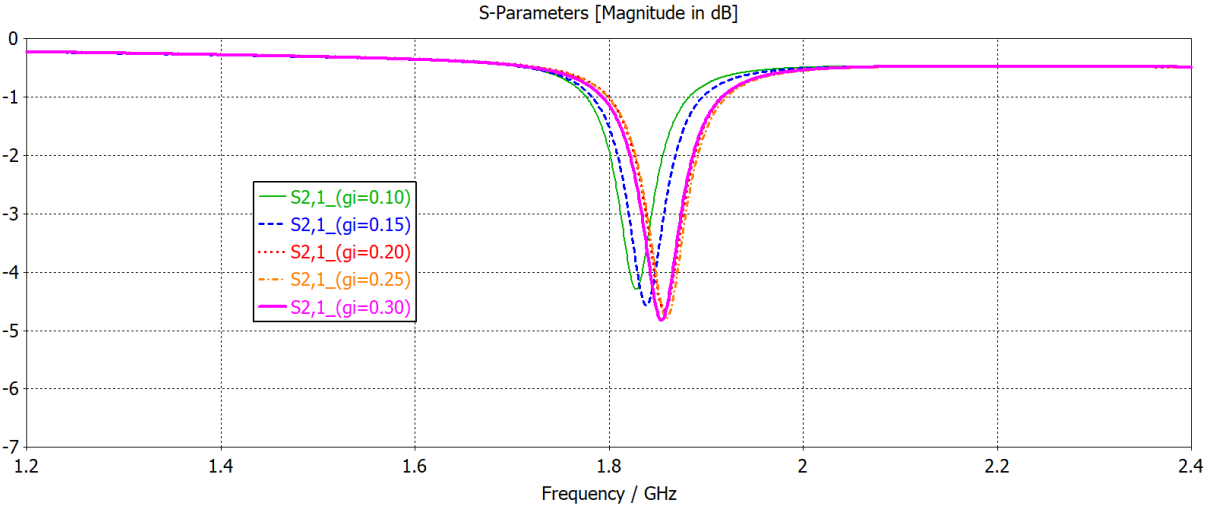

Fig. 3.12 - Parameter *gi* ranging from 0.10 mm to 0.30 mm with steps of 0.05 mm.

From this image, it is found that the resonance frequency is very little sensitive to the internal gap of the spiral resonator. However, it is slightly displaced due, among other factors, to the modification of the capacitance value between the spire arms, with the narrowing or enlargement of the gaps. Nevertheless, the attenuation receives an influence, although small, but remarkable, resulting from the variation of this parameter.

The parametric study has shown that the position of the resonant frequency depends strongly on the length of the spire *lb* and, to a lesser extent, on the width of the spire arms *wr*. The attenuation, on the other hand, depends essentially on the distance between the spire and the microstrip line *gl*, and to a lesser extent, depends on the widths of the internal gap *gi* and of the spire arms *wr*. In view of this, the values of the parameters defined for follow-up of the simulations and prototype construction are shown in Table I along with a summary of the effect of each parameter on the resonance.

Parameter	**Value (mm)**	**Resonance Displacement**	**Attenuation**
lb	8.0	Great effect	Very little effect
wr	0.8	Little effect	Little effect
gl	0.2	Very little effect	Great effect
gi	0.2	Very little effect	Little effect

Table I - Summary of the results of the parametric study of the spiral resonator.

An important observation is that the values of *gl* and *gi* were defined according to the available fabrication technique. The value of 0.2 mm is the minimum that can be obtained in the manufacturing conditions adopted in this work.

3.3.3 Software Modeling of the Proposed System

In this topic, a descriptive step-by-step will be demonstrated to better clarify the idea of the proposed system described in section 3.3.1. Considering the spiral resonator of Fig. 3.7 with the parameters defined in Table I, it is obtained that its resonance is situated at 1.97 GHz as seen in Fig. 3.13.

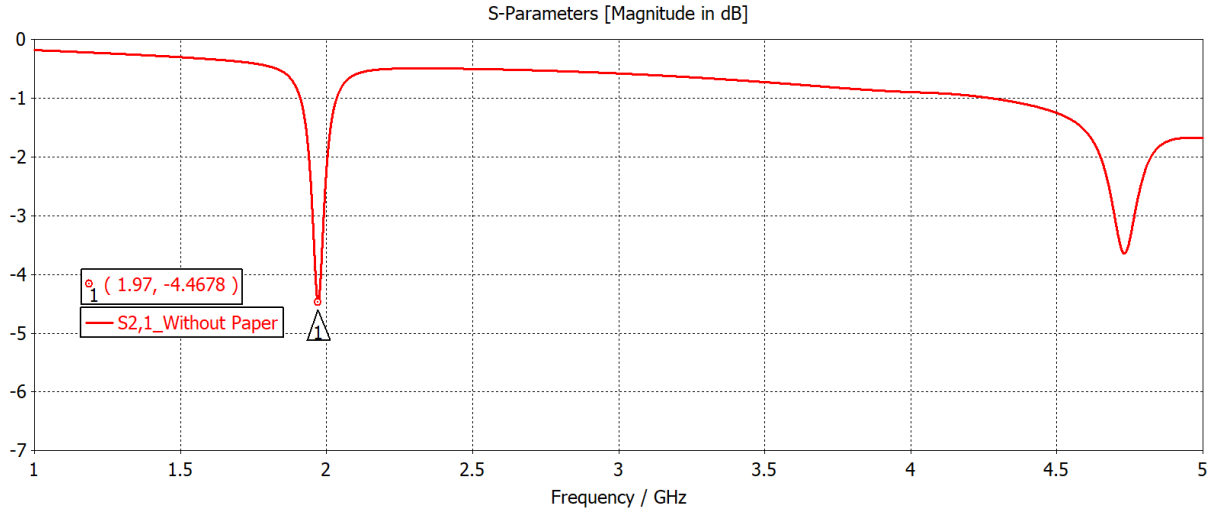

Fig. 3.13 - S21 transmission parameter of the structure of Fig. 3.7 with the parameter values of Table I.

Another resonance between 4.5 GHz and 5 GHz is also shown in Fig. 3.13. It represents the harmonic resonance of the main resonance. This resonance is undesirable since it limits the spectrum to a smaller amount of spires along the microstrip line.

Fig. 3.14 exposes a paper sheet over the structure. This situation is analogous to the positioning of a banknote or document on the spiral resonator and the transmission line.

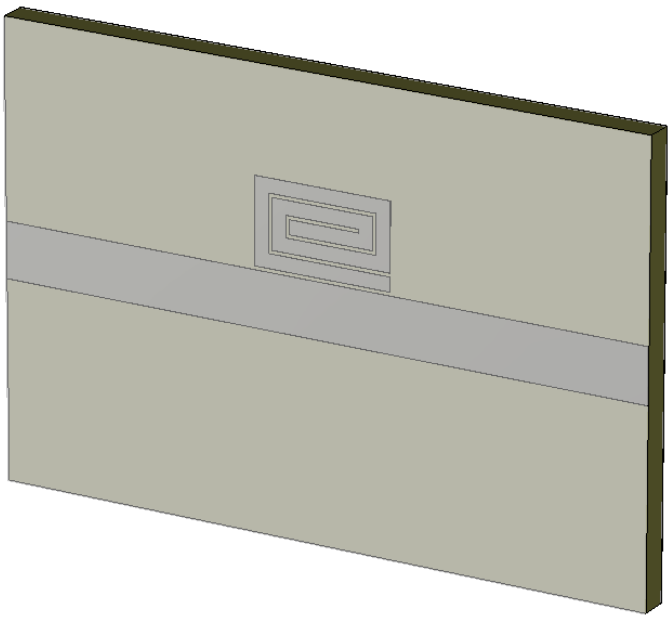

Fig. 3.14 - Structure with paper sheet covering line and spiral resonator (transparent white paper).

Fig. 3.15 reveals what happens to the S21 transmission parameter when occurs the placement of the paper sheet.

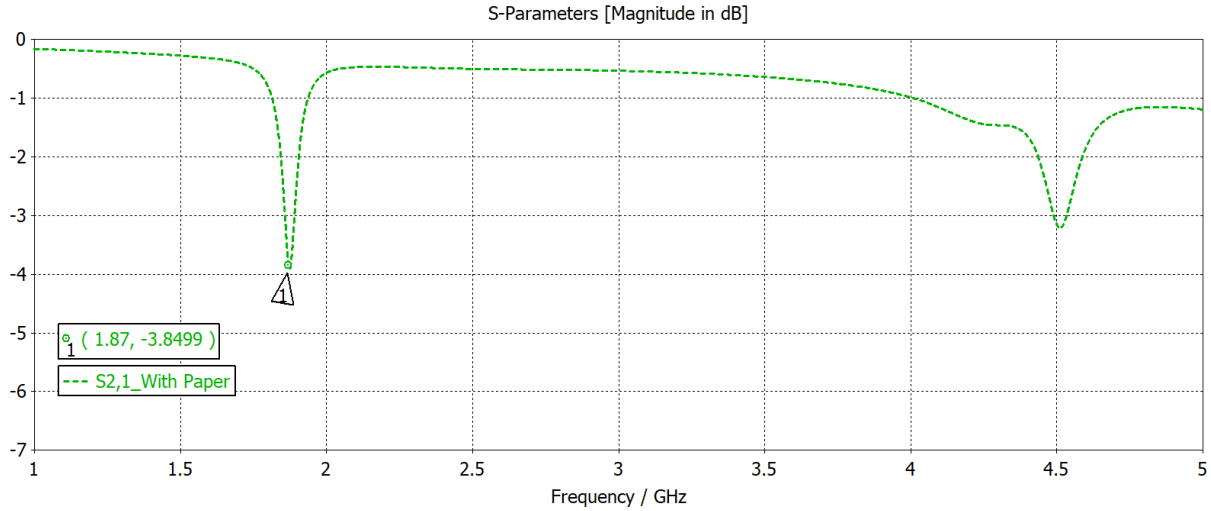

Fig. 3.15 - S21 of the structure of Fig. 3.14.

For better visualization, Fig. 3.16 shows the two curves in the same chart.

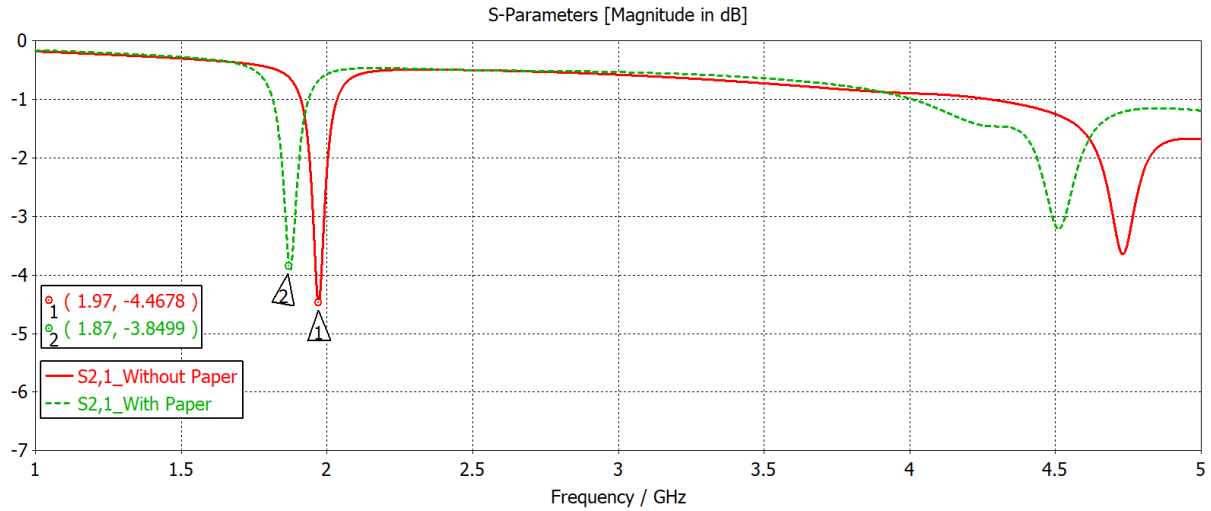

Fig. 3.16 - S21 of the spiral resonator with and without paper sheet.

From Fig. 3.16, it is noticed that the placement of the paper sheet displaces the resonance and reduces its depth by approximately 0.6 dB, that is, it reduces its quality factor. The displacement is due to the paper different dielectric constant in comparison to the substrate and the attenuation is due to its losses.

In the next image, it is observed the behavior of the electric and magnetic field lines of the spiral resonator with paper sheet at 1.87 GHz resonance frequency.

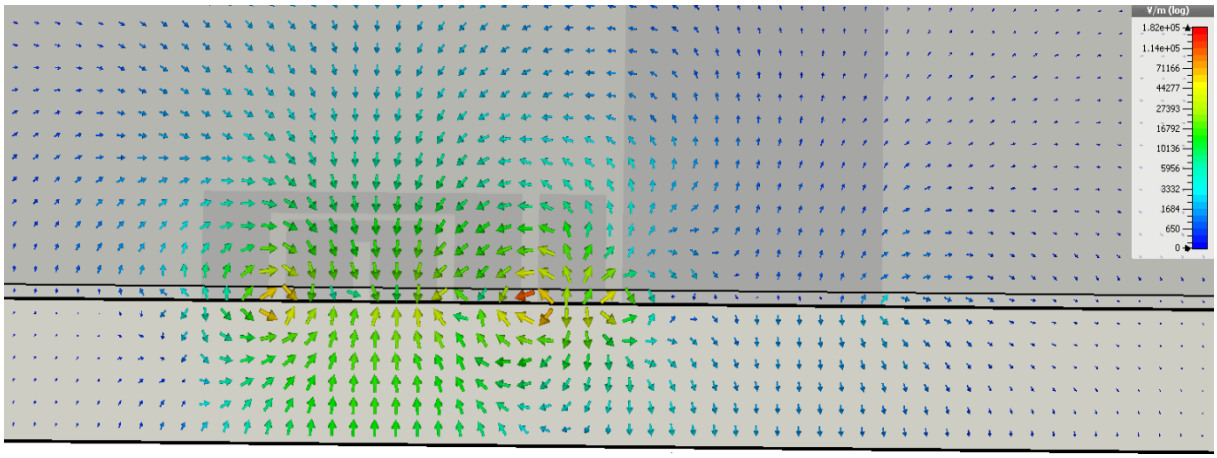

a)

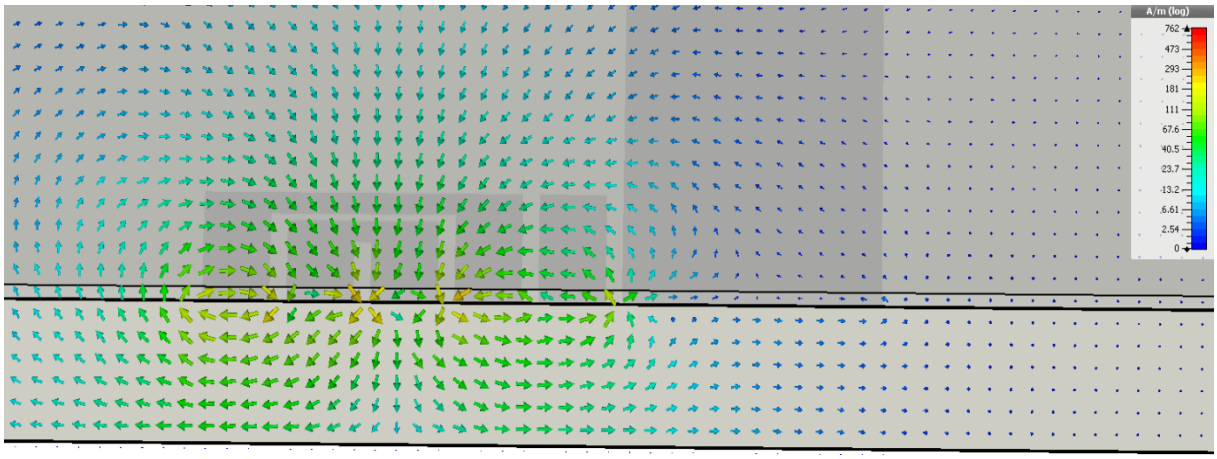

b)

Fig. 3.17 - Cross-section view of the behavior of the electric field a) and magnetic field b) lines at the resonance frequency of 1.87 GHz. Interfaces mark the substrate and paper.

From these images, it is noticed that there are enough field lines leaving the spire and crossing the paper. If these fields are prevented from freely flowing in this region, the resonance can be effectively attenuated.

In Fig. 3.18, the resonator is seen with a paper sheet and a metal plate positioned on the paper exactly over the position of the spiral resonator. It is important to note that the metal plate never touches the spiral resonator.

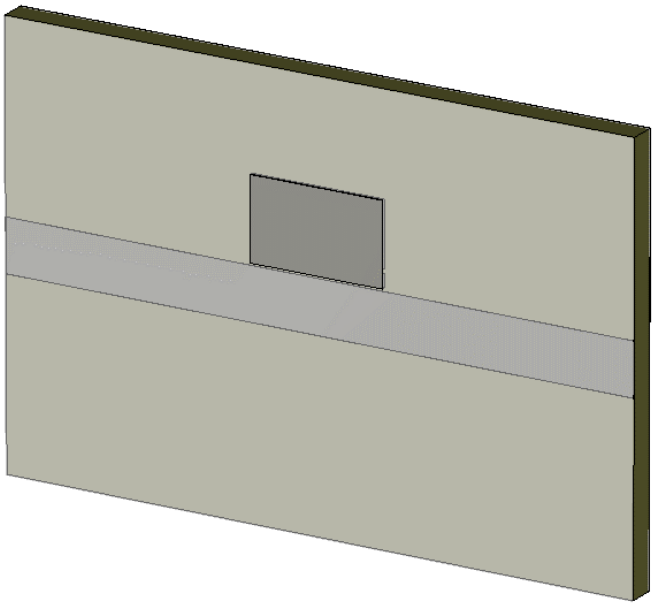

Fig. 3.18 - Set formed by the spiral resonator, paper sheet and metal plate on paper.

The arrangements of the electric and magnetic field lines, in this situation, are depicted by arrows in Fig. 3.19. The same scale of electric and magnetic fields is being used at the 1.87 GHz frequency, as in the previous case.

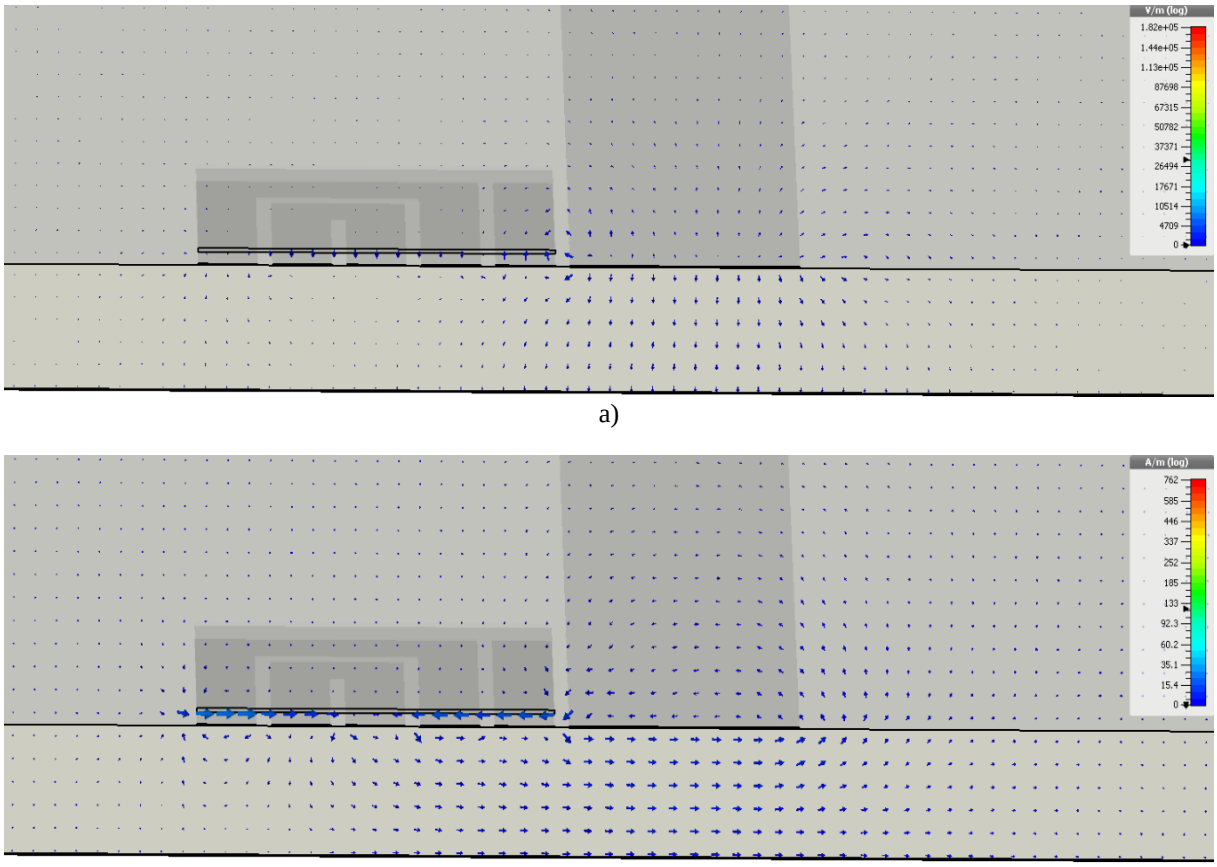

a)

b)

Fig. 3.19 - Cross-section view of the behavior of the electric field a) and magnetic field b) lines at the 1.87 GHz resonance frequency seen after placement of the metal plate over the paper. The interfaces mark the substrate, the paper sheet and the metal plate.

From Figs. 3.17 and 3.19 it is understood that the metal plate considerably weakens the electric and magnetic fields over the spire. This result can also be seen in the transmission curve of Fig. 3.20, where the three curves of the three described situations are plotted in the same graph. It can be seen that, in the case of paper and metal plate, there is a small resonance at approximately 2.33 GHz. This small resonance is not problematic in a system with multiple cascaded resonators, because its magnitude is practically negligible, as will be seen later. In addition, for the actual case, the metal plate would lie in an inner layer of the paper, which would further improve this result in terms of attenuation, because the plate would be located closer to the resonator.

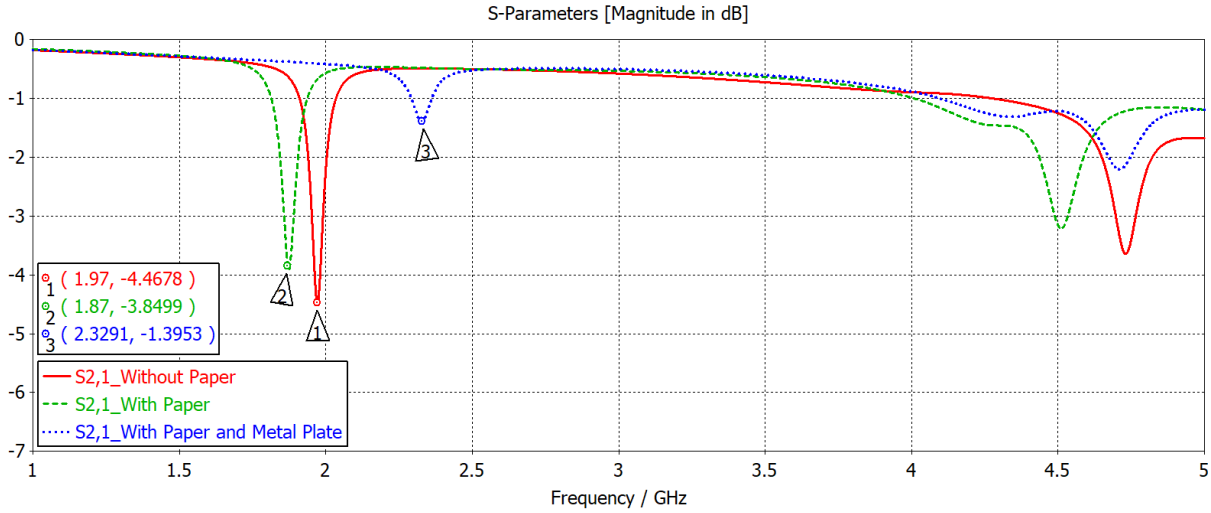

Fig. 3.20 - S21 curves illustrating the situations of the resonator without paper, with paper and with paper and metal plate.

The next results are a parametric study about the size of the metal plate on the paper. For example, tests were carried out with the plate covering not only the resonator, but also the extension of the corresponding microstrip line. For a better understanding, first consider Fig. 3.21, where the spiral resonator is displayed with the metal plate over it and the reference coordinate plane.

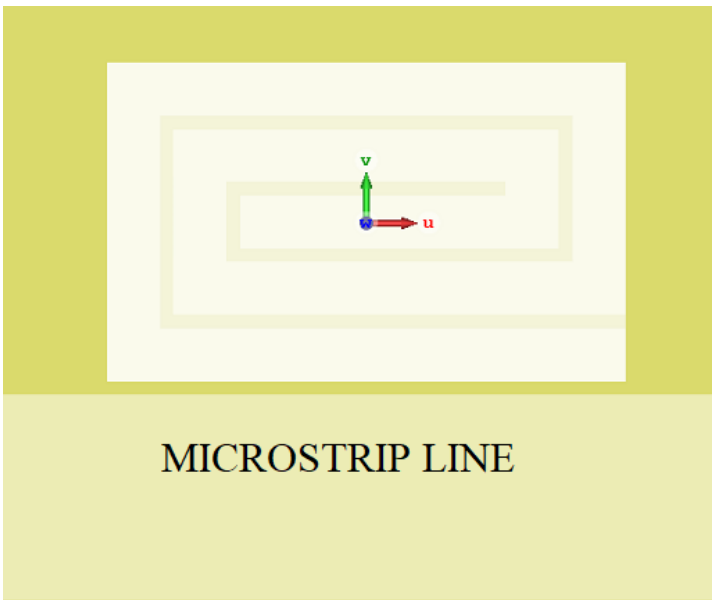

Fig. 3.21 - Spiral resonator with metallic plate on the paper along with the reference coordinate plane.

Consider that the circumstance given above, where the metal plate completely covers the extension of the spire without going beyond the edges is the condition given by the correspondence of the u, -u, v and -v directions, of the reference coordinate plane, to 0, 0, 0

and 0. This means that (u, -u, v, -v) = (0,0,0,0) and this is the reference condition. Thus, if the metal plate exceeds the edges of the spire, these values will be modified to the values in millimeters that has been exceeded. In order to better illustrate, the conditions given in Fig. 3.22 represent in (a): (u,-u,v,-v) = (1,1,1,1), i.e., there is an 1 mm spacing in the four directions of the reference plane beyond the edges of the spiral resonator. In b): (u, -u, v, -v) = [0,0,0 (*gl* + *wl*)], where there is metal plate spacing only in the –v direction, and this value is equal to the gap *gl* between the resonator and the microstrip line plus the width of the microstrip line *wl*.

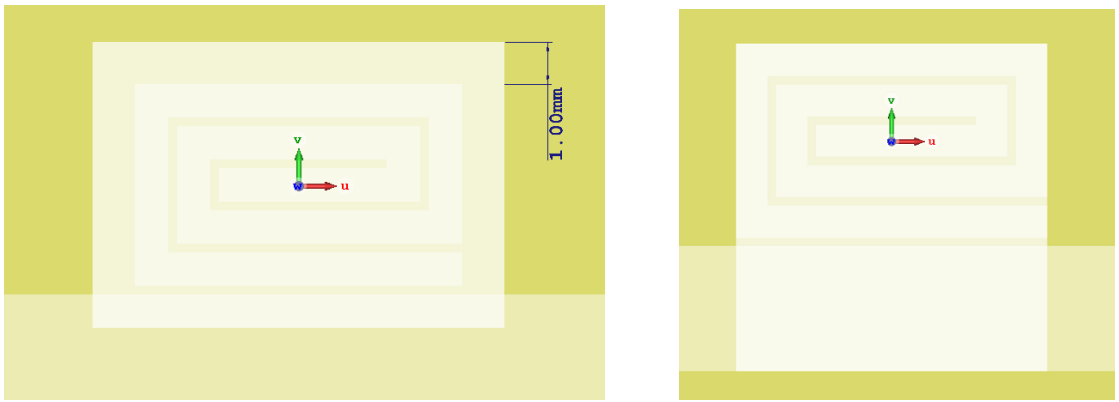

a) b)

Fig. 3.22 - Situation where the metal plate a) exceeds the limits of the spiral in the four edges by 1 mm and b) exceeds in (gl + wl) the limits of the spiral only in the -v direction.

In this context, some situations were simulated in order to find out which position and metal plate size would have the best performance along the spectrum. Fig. 3.23 illustrates the results in a spectrum ranging from 1.0 GHz to 5.0 GHz. There is an axis marker at the 1.87 GHz resonance frequency of the spire.

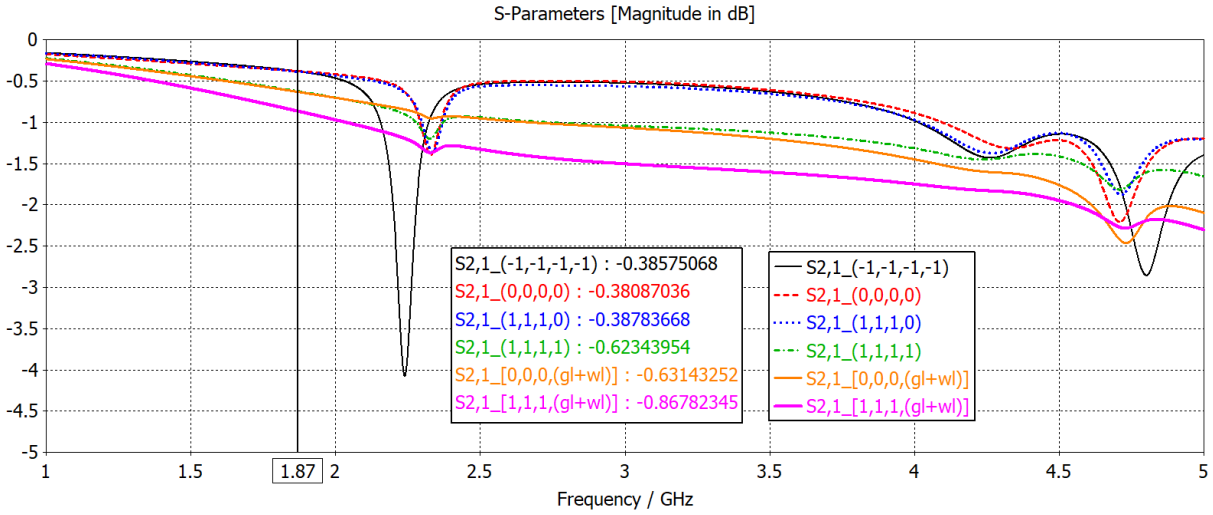

Fig. 3.23 - Transmission curves of six different situations of metal plate dimensioning on the paper.

Other configurations were tested but not placed in Fig. 3.23 to avoid problems in identifying the curves. Therefore, only the curves of greater interest are shown here. From Fig. 3.23, it can be observed that some curves differ more in higher frequencies. The curves (0,0,0,0) and (1,1,1,0) are very similar. The curves corresponding to [0,0,0,(*gl* + *w1*)] and [1,1,1,(*gl* + *wl*)] are characterized by a greater signal attenuation, since their metal plates are covering a considerable region of the microstrip line. Finally, the curve corresponding to (-1,-1,-1,-1) has a resonance of much greater magnitude resulting from the total non-covering of the spire by the metal plate. Given these results, it is reached that the best curve is that corresponding to (0,0,0,0), that is, when the plate completely covers the spire without going beyond the edges. Although it is similar to the curve (1,1,1,0), the curve (0,0,0,0) uses less metal, which would be advantageous in mass tagging.

The next steps are relative to the cascading of the spiral resonators along the microstrip line. First of all, it is necessary to analyze the behavior of two spirals in relation to the physical proximity and spectrum spacing. In [21], it is presented a study about the frequency guard bands of chipless RFID spiral resonators. Too close adjacent resonances in the spectrum could result in reading errors, but that is a question of future concern since the guard band of the resonance frequencies should be defined in accordance to the reading capability of the reader.

Fig. 3.24 presents a set with four spiral resonators, two on each side of the line, along with the variable *dist* representing the distance from one spire to another on one side of the line. The four resonators have the same dimensions except the horizontal length which, as analyzed in the previous section, is the parameter that most influences the position of the resonance in the transmission spectrum.

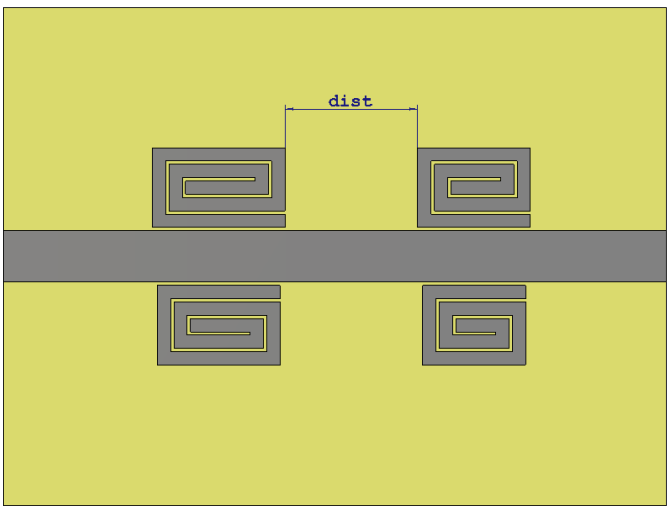

Fig. 3.24 - Two spires on each side along the microstrip line.

Fig. 3.25 shows the results of the transmission curves of the *dist* parameter sweep with values of 1.0 mm, 2.0 mm, 3.0 mm, 4.0 mm and 5.0 mm.

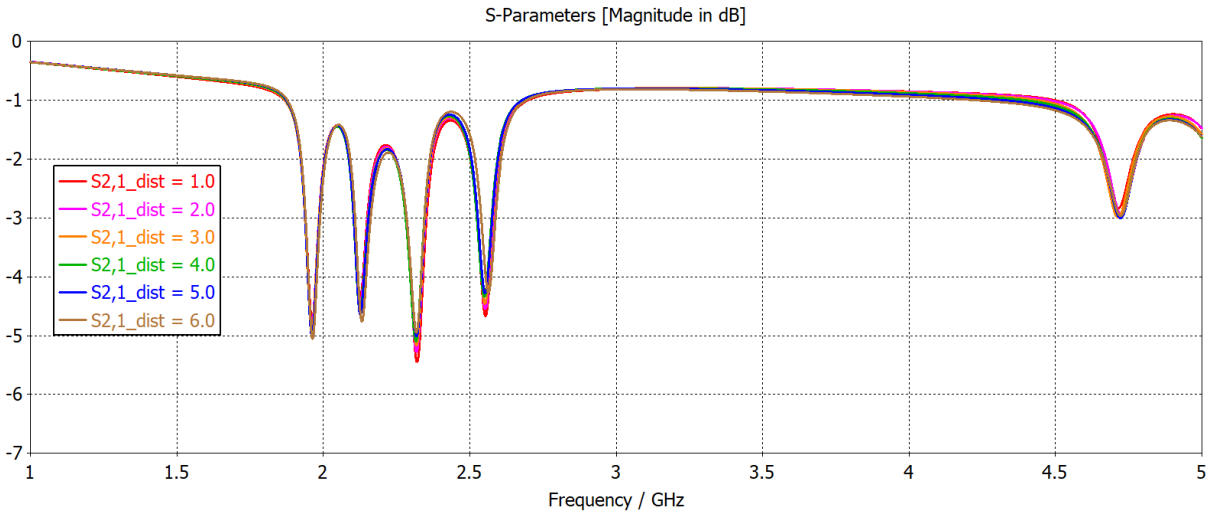

Fig. 3.25 - S21 curves of the structure of Fig. 3.24 as a function of the distance between the resonators.

As can be noted, there are no apparent changes in the transmission curves resulted from the variation in the distance between resonators. However, in order to avoid possible mutual couplings between the resonators and to facilitate the prototype handling at the time of placing the metal plates on the paper (copper tape), the distance of 3.5 mm was adopted for the project follow-up.

Following up the project, the next image features a model with ten spiral resonators. This is the final model for initial fabrication and measurement.

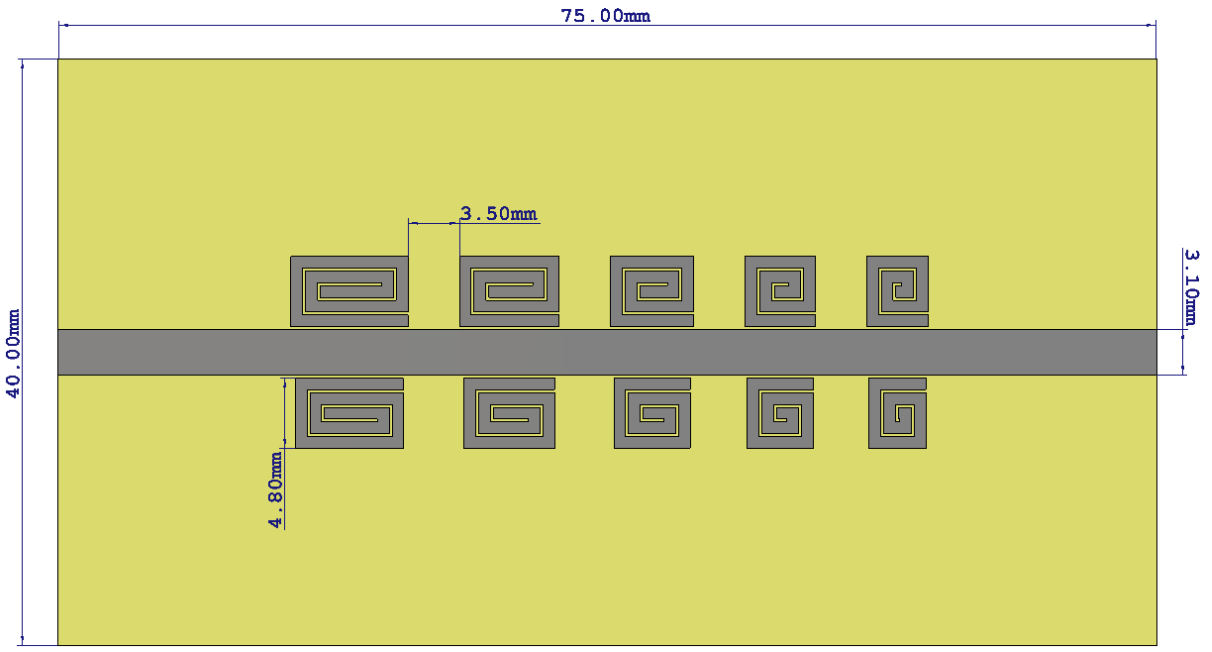

Fig. 3.26 - Device with ten spiral resonators along microstrip line in FR-4 substrate.

In Fig. 3.26, all spires have the same vertical dimension, with value of 4.80 mm, so that only the horizontal lengths are modified to reach the resonance shifts. The largest spire, the one located in the upper left, is the one with the lowest frequency resonance. The spire located just below the first represents the second tag resonance or the second bit, while the second spire of the top alongside the first spire represents the third bit, and so on. The smaller horizontal spire resonates at the highest frequency and represents the tenth bit of the tag. Table II presents the dimensions and resonance frequencies of the ten spiral resonators.

Spire	**Length (mm)**	**Width (mm)**	**Resonance Frequency (GHz)**
1ª	8.00	4.80	1.97
2ª	7.40	4.80	2.15
3ª	6.80	4.80	2.35
4ª	6.20	4.80	2.60
5ª	5.70	4.80	2.84
6ª	5.20	4.80	3.13
7ª	4.80	4.80	3.39
8ª	4.50	4.80	3.65
9ª	4.20	4.80	3.90
10ª	3.90	4.80	4.19

Tabela II - Dimensions and resonance frequencies of the ten spiral resonators.

From Table II, it can be seen that the ten resonators occupy a total band of just over 2.0 GHz. Fig. 3.27 shows the transmission curve of the ten spiral resonators without the placement of the paper sheet. It can be seen the ten resonances, and the beginning of its harmonics after 4.5 GHz.

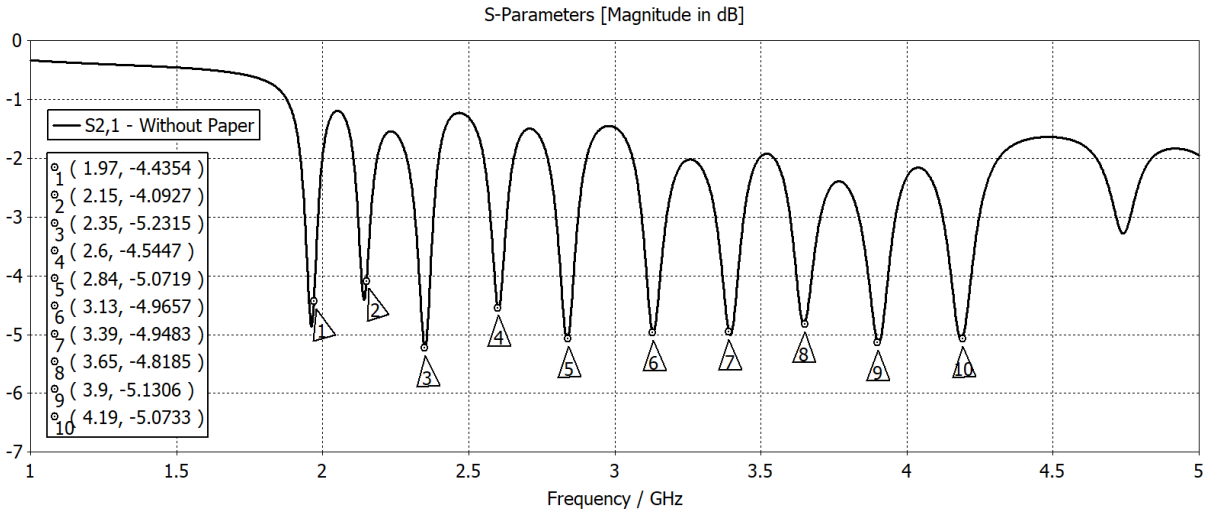

Fig. 3.27 - S21 curve of the structure of Fig. 3.26. Markers indicate the attenuation magnitude and the resonant frequency of each resonator.

The resonators were designed so that the resonances were well spaced in the spectrum. This caution was taken to avoid manufacturing problems, because the precision was not very fine. In this way, the spires were defined with lengths well spaced from each other, as can be seen in Table II.

In Fig. 3.28, the ten resonators are shown when a paper sheet is placed on them. Fig. 3.29 shows the two transmission curves to illustrate the effect of the paper placement, that is, paper adds losses to the resonances and shifts them in the spectrum to the left, as happened to the case of the individual resonator.

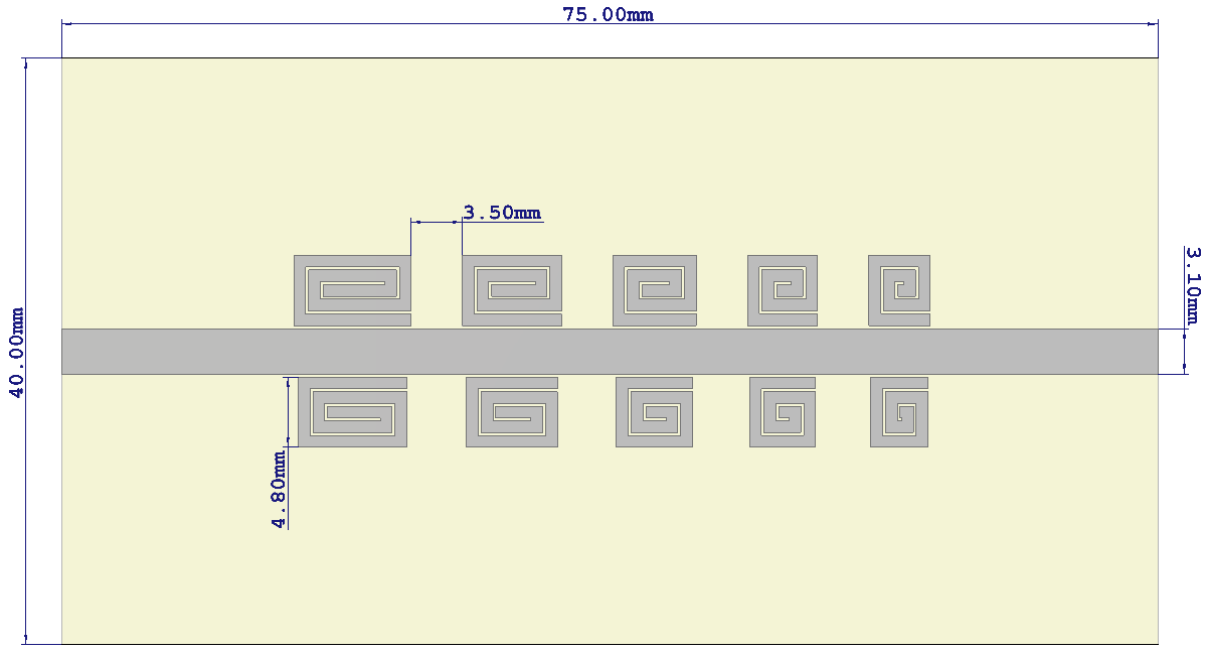

Fig. 3.28 - Device with ten resonators along a microstrip line on FR-4 substrate and with a paper sheet.

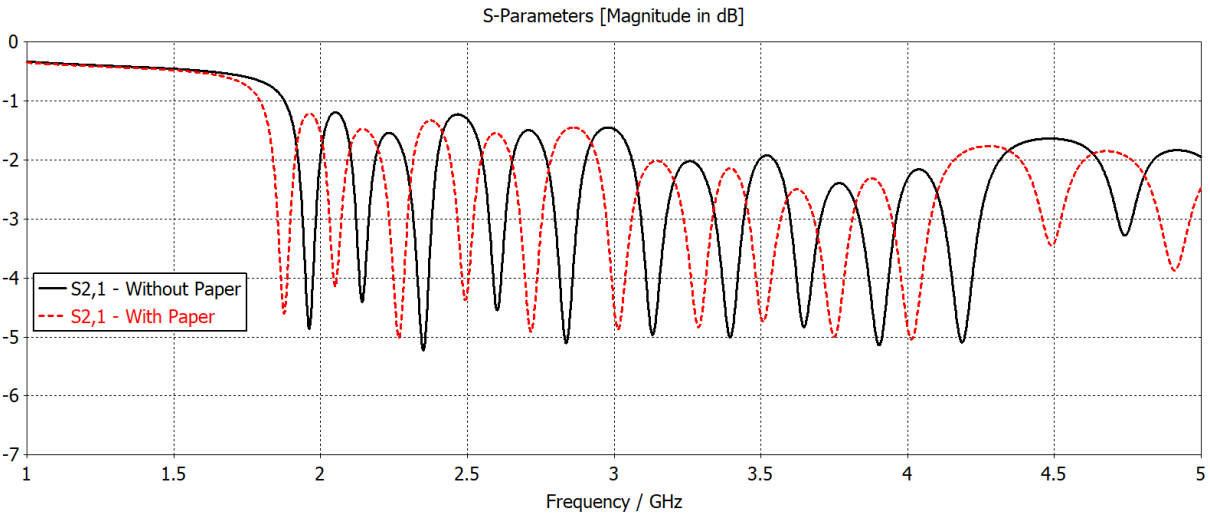

Fig. 3.29 - Transmission curves of the ten spiral resonators with and without paper sheet.

The next step is to define the binary codes for simulation. As shown, each spiral resonator has the potential to define two states, i.e., presence and absence of resonance. The presence of resonance is manifested when there is only the paper sheet over the resonator; the absence of resonance is achieved when the metal plate over the paper completely covers the region of the resonator. Hence, for the structure of Fig. 3.28, there are 2^{10} combinations of possible binary codes. These codes will be defined as follows: the bit state will be considered 0 when resonance is present, and the bit state will be considered 1 when there is no resonance.

The next image shows the condition in which all resonances are suppressed. Put into another way, metal plates were placed over all the resonators. This condition indicates

that all bits have value 1 resulting in the definition of the binary code given by (1111111111). In contrast, the structure shown in Fig. 3.28, where there is only the placement of the paper sheet on the resonators, corresponds to the binary code given by (0000000000), namely, there is the presence of all the resonances in the spectrum.

Fig. 3.30 reveals the spiral resonators with paper sheet and metal plates on all resonators. As described in the previous paragraph, such a structure represents the code (1111111111). Furthermore, the respective transmission curve plotted together with the reference curve, given by the code (0000000000), is also shown in Fig 3.30. It is observed that the small resonances resulting from the placement of the metal plates would not imply a reading error since their magnitudes are small. From 4.5 GHz on, it begins to appear the harmonic resonances.

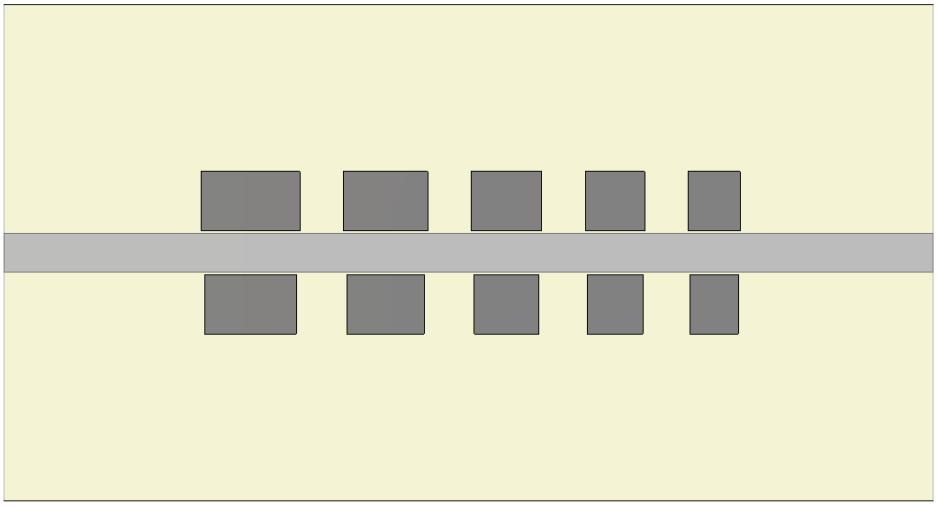

a)

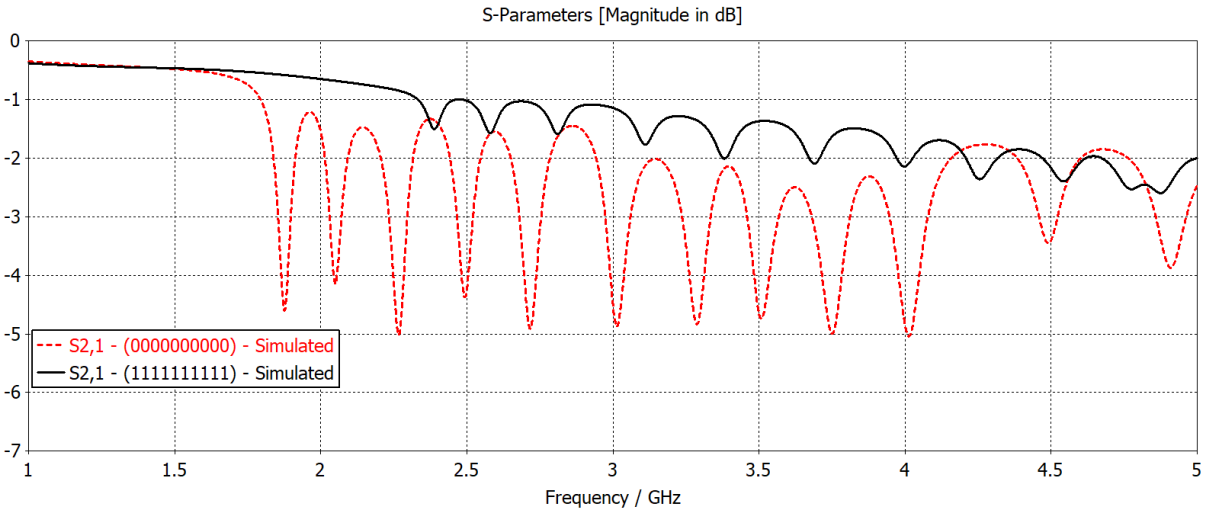

b)

Fig. 3.30 - a) Structure representative of the code (1111111111). b) Transmission curve representing code (1111111111) as well as reference curve which represents code (0000000000).

Fig. 3.31 shows the results referring to the code (0110101001). It is noticed here that the metal plates effectively suppress the resonances at their respective frequencies.

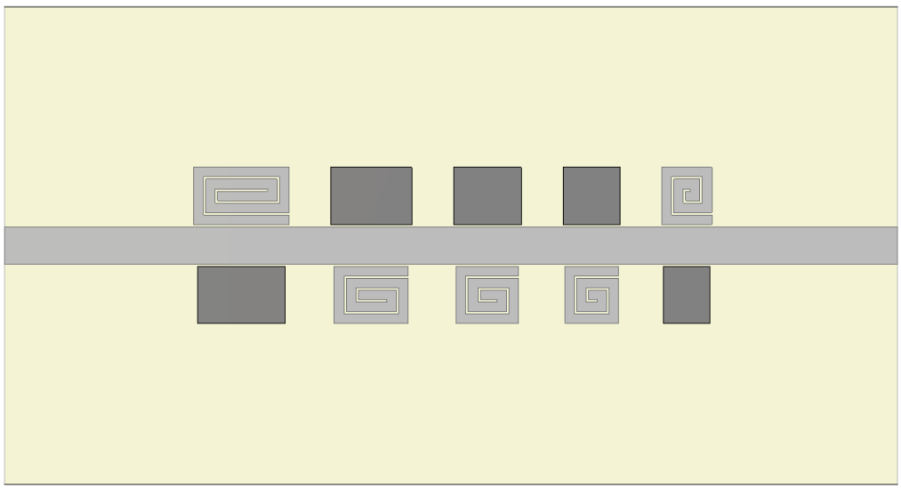

a)

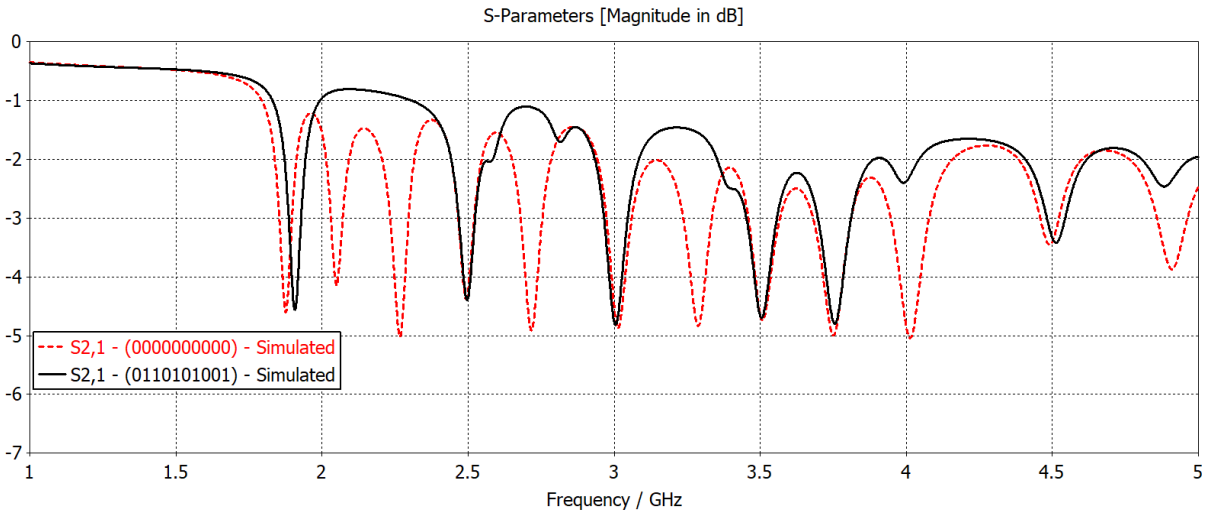

b)

Fig. 3.31 - a) Structure representative of the code (0110101001). b) Transmission curves representing the code along with its reference.

Fig. 3.32 presents the results referring to the code (1001010011).

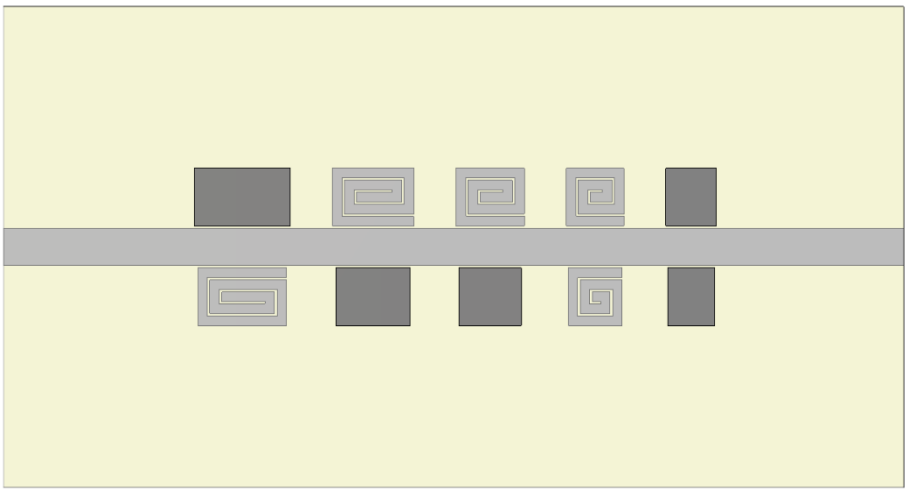

a)

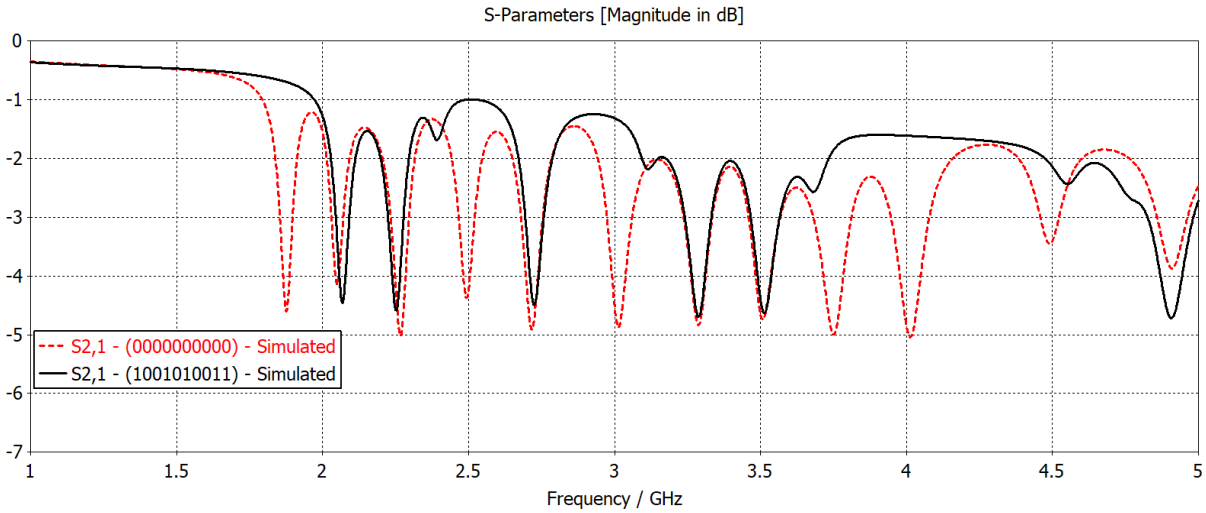

b)

Fig. 3.32 - a) Structure representative of the code (1001010011). b) Transmission curves representing the code along with its reference.

Fig. 3.33 brings the results referring to the code (1110001110).

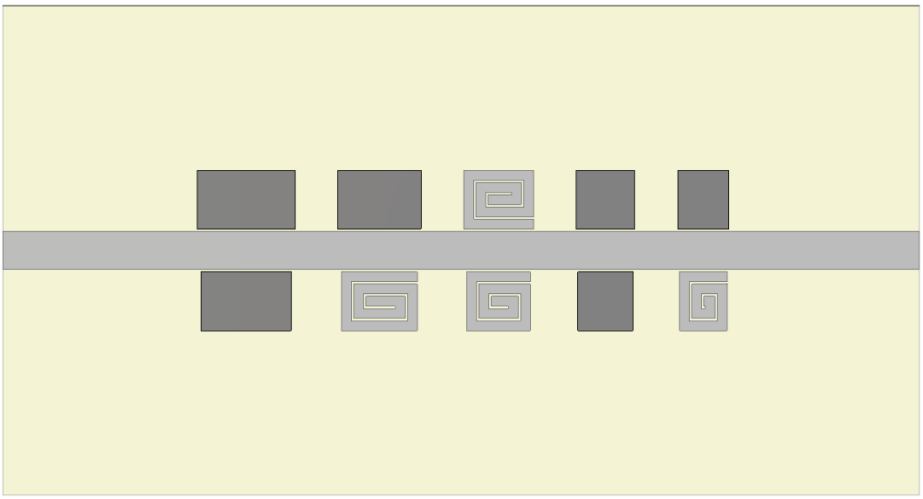

a)

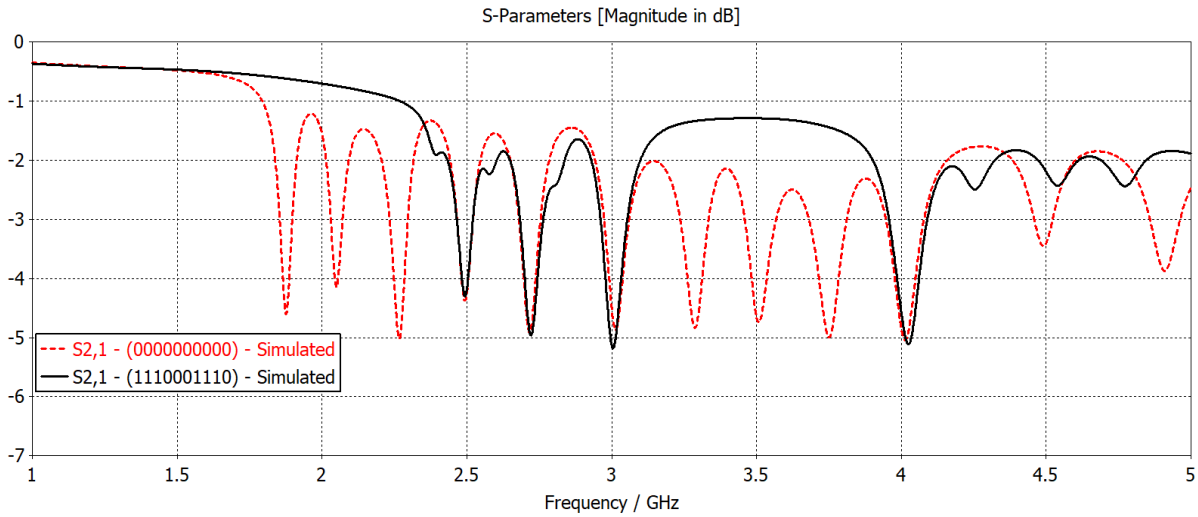

b)

Fig. 3.33 - a) Structure representative of the code (1110001110). b) Transmission curves representing the code along with its reference.

As could be seen from the presented results, the proposed system works. The metal plates satisfactorily eliminate the resonances at the designated locations and the resonators resonate freely in the absence of them.

3.3.4 Ternary System

As previously mentioned, the proposed system can also be ternary, that is, a spiral resonator may assume three states which are described as presence, absence, and presence of weak resonance or half resonance. For the latter state, the metal plate on the paper (or printed in its inner layer) must have a peculiar shape so that the new resonator, composed by the spire plus the metal plate, has a resonance frequency equal to the original spire resonance frequency and the attenuation in the transmission curve must be reduced.

In order for the above statement to be reached, care must be taken with the placement of the plate on the spiral resonator, since misplacement can significantly shift the position of the resonance and lead to undesirable reading errors. It is in this context that Fig. 3.34 again presents the spiral resonator to begin the analysis of the ternary system. The substrate used is the same as that described in section 3.3.2.

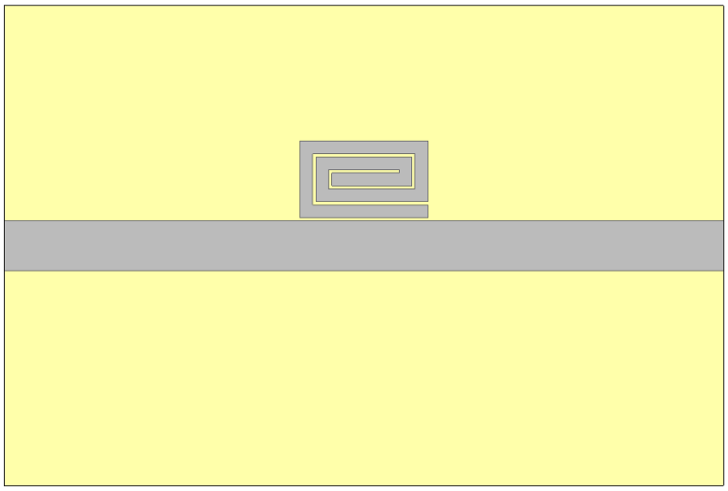

Fig. 3.34 - Spiral-shaped resonator near to microstrip line.

Fig. 3.35 exhibits the transmission curve of this spiral resonator, where it can be seen the resonance at 1.87 GHz, this is the full resonance state of the resonator. It is necessary to define a metallic pattern on the resonator so that the resonance is weakened while it is maintained at the same frequency.

Therefore, it has been found that placing a metal plate on the central region of the resonator over the paper, so as to take a fraction of its area as can be seen in Fig. 3.36, shifts the resonance frequency to the right. It is seen in Fig. 3.37 the displacement of the position of the resonance resulting from the placement of this metal plate. The curves are the transmission parameters of the resonator without metal plate and the resonator with this central plate.

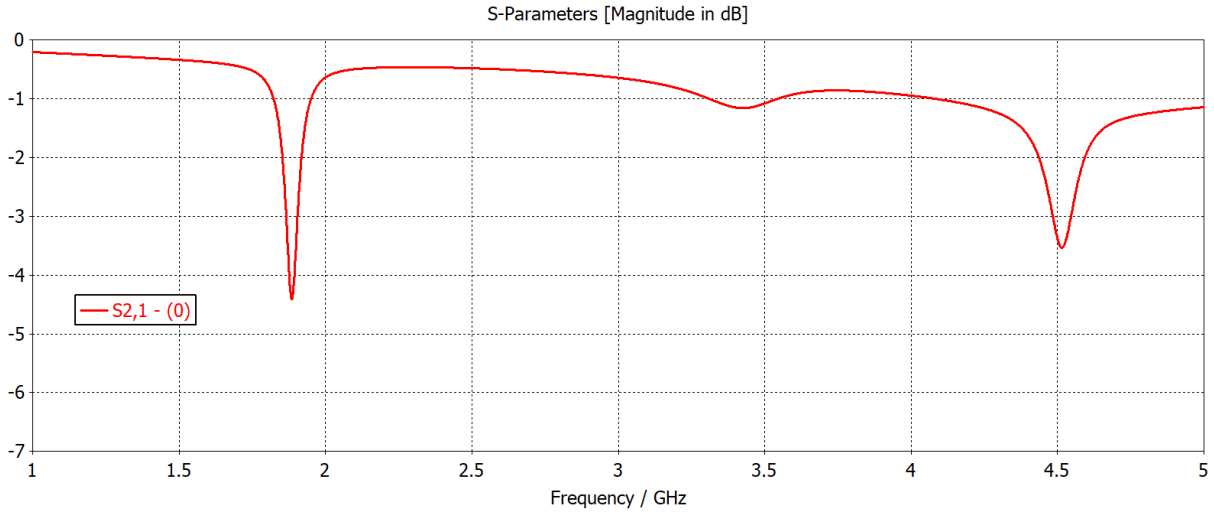

Fig. 3.35 - Transmission parameter (S21) of the structure of Fig. 3.34.

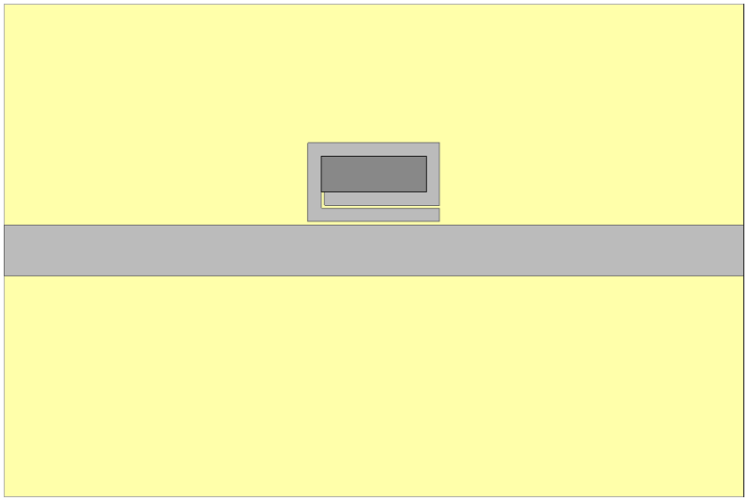

Fig. 3.36 - Central metal plate on paper covering fraction of the resonator area.

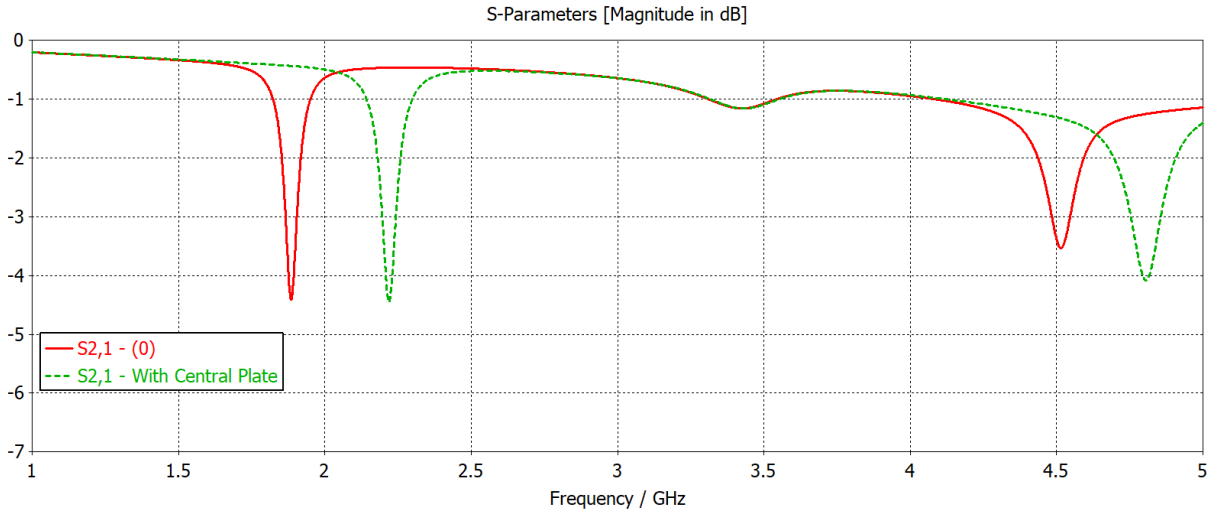

Fig. 3.37 - S21 parameters of the spiral resonator with and without the metal plate shown in Fig. 3.36.

On the other hand, placing plates on paper in a position covering the lateral edges of the spiral resonator, as shown in Fig. 3.38, shifts the original position of the resonance to the left. Fig. 3.39 reveals the displacement of the resonance position to the left on the transmission curve.

In view of this, the two plate placement possibilities shown can be combined so that the resonance remains at the same frequency at the same time as it is weakened, since much of the area of the spiral resonator on the paper will be covered. In Fig. 3.40 the resonator is presented as the combination of the central plate together with the lateral plates on the paper. This plate is referred to as half-resonance plate. Fig. 3.41 shows the effect of the placement of this peculiar metal plate on the transmission curves of the structure.

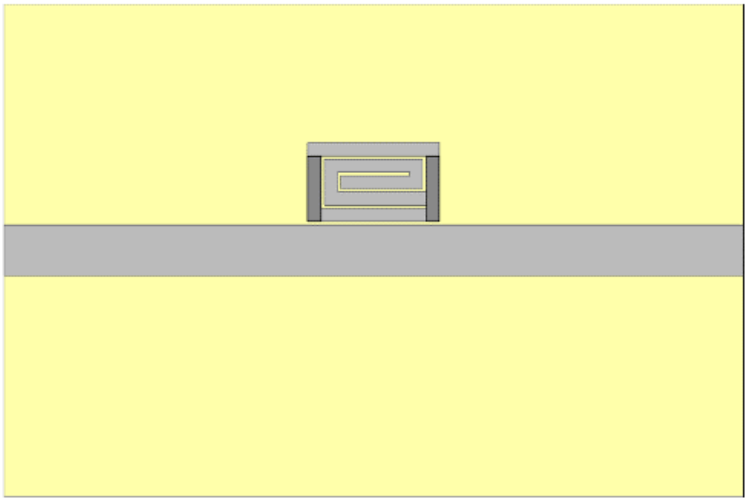

Fig. 3.38 - Lateral metal plates on paper.

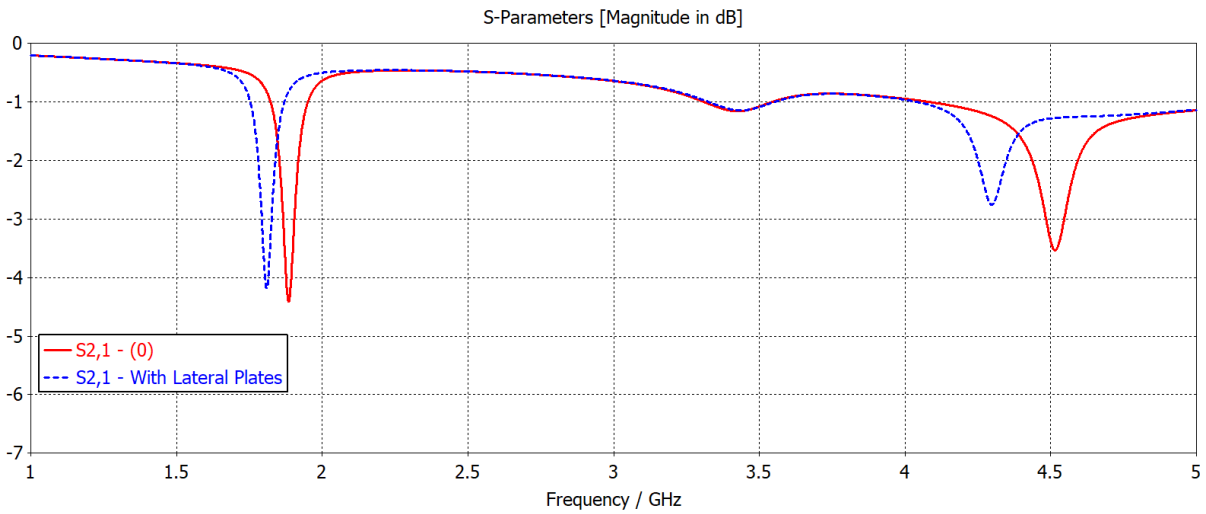

Fig. 3.39 - S21 parameters of the spiral resonator with and without lateral plates.

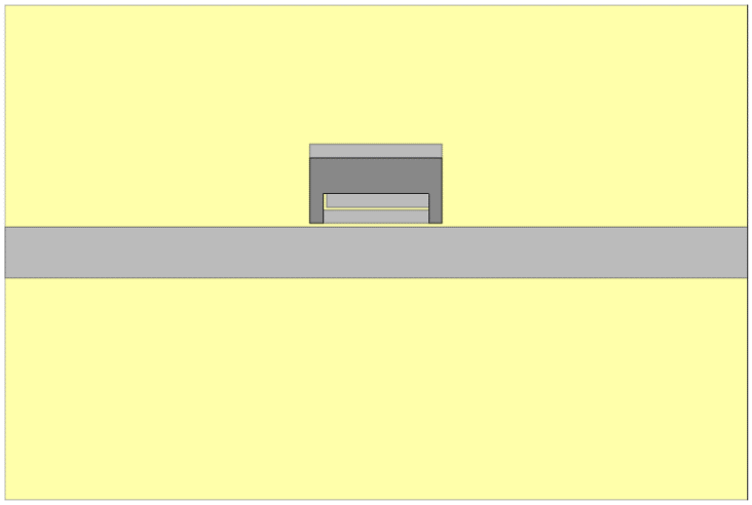

Fig. 3.40 - Spiral resonator with half-resonance plate on paper.

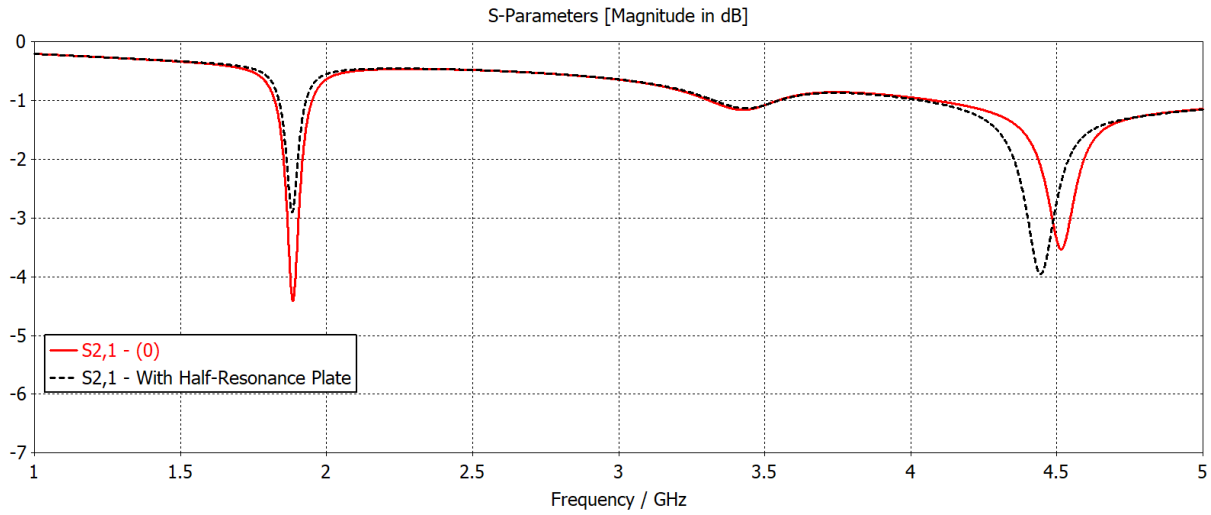

Fig. 3.41 - S21 parameters of the spiral resonator with and without the half-resonance plate.

It is noted in this image that the combination of the central plate and the lateral plates of Fig. 3.40 maintains the resonance at the expected frequency and attenuates it to form a new state or the third resonance state of the spiral resonator, as quoted earlier.

Nevertheless, the position of this resonance in the spectrum was very sensitive to the small variations in the positions of the half-resonance plate. In a practical system, the guard band of each spiral resonator would be increased in order to avoid reading errors by virtue of these possible displacements of the resonances caused by small misalignments of the banknote or document. In other words, the implementation of the ternary system increases the amount of coded data of the system, but slightly increases the frequency bands used by the resonators to avoid reading problems due to half-resonance displacements. This fact does not compromise its superiority in relation to the binary system.

Chapter 4

Measurement Results and Comparisons

This chapter presents the measurement results of the system. Two sets of measurements were performed. The first one was used to identify the precise values of the electrical characteristics of the available substrate. In the second, extra measurements were taken along with measurements using graphene buckypaper which is a flexible, low-cost and paper-like material made out of several stacked graphene flakes. The measurement results of this chapter will always be compared to the results obtained from the electromagnetic simulations.

4.1. First Set of Measurements

For the first measurements, a FR-4 substrate with dielectric constant εr = 4.3 and loss tangent = 25 x 10^{-3} was considered in the simulations, as these are the most common values for FR-4. The frequency band of the resonators was 1.80 to 4.10 GHz. However, the results of this section reveal that the electrical parameter values used in the simulations differ from those of the available physical FR-4 substrate.

The board was made by a milling machine whose minimum drill bit available at the time of manufacture was 0.2 mm. That is the reason why the gaps of the resonators are 0.2 mm. Fig. 4.1 shows a photo of the built board.

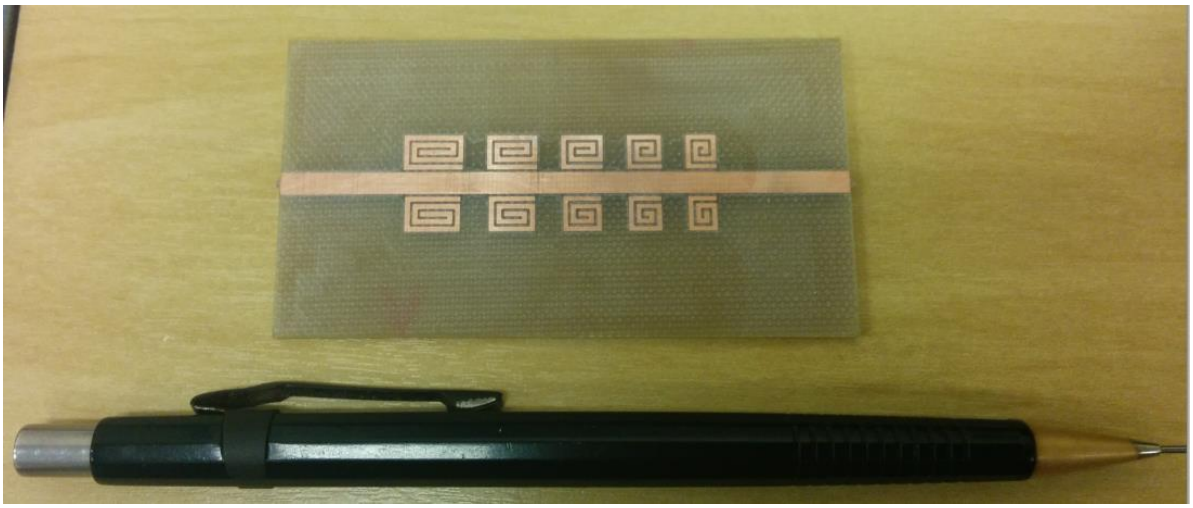

Fig. 4.1 - First board built with resonators and line.

Fig. 4.2 exhibits how the masks were made, that is, the paper on which the copper tape was glued. The paper masks represent what would be the banknotes or documents with their respective codes embedded, in other words, represent the tags. The exact length and width measurements of both resonator and plate were drawn on paper. The figure also shows the board with 50 Ω connectors welded at the ends and one of the masks, that representing the code (1111111111), positioned and fixed thereon.

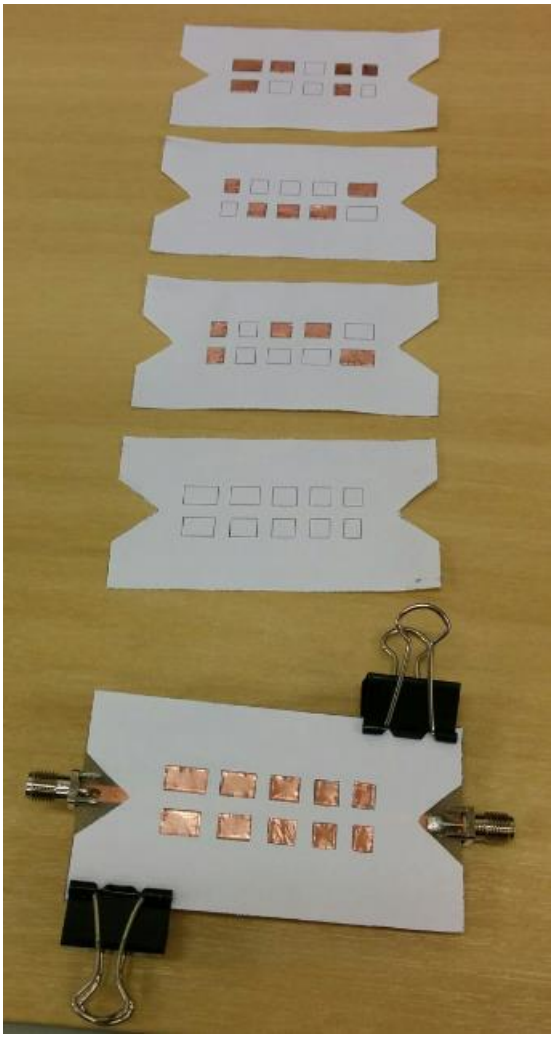

Fig. 4.2 - Photo of paper masks and the board with the attached (1111111111) tag.

Measurements were performed using a network analyzer in the 1.0 to 6.0 GHz frequency range. The measurement configuration is shown in the following figure, where the board is connected directly to the network analyzer port in one of its ends. A 50 Ω cable connects the other end to the second port of the network analyzer. Everything was properly calibrated. Tags were affixed to the board with binder clips and paper clips.

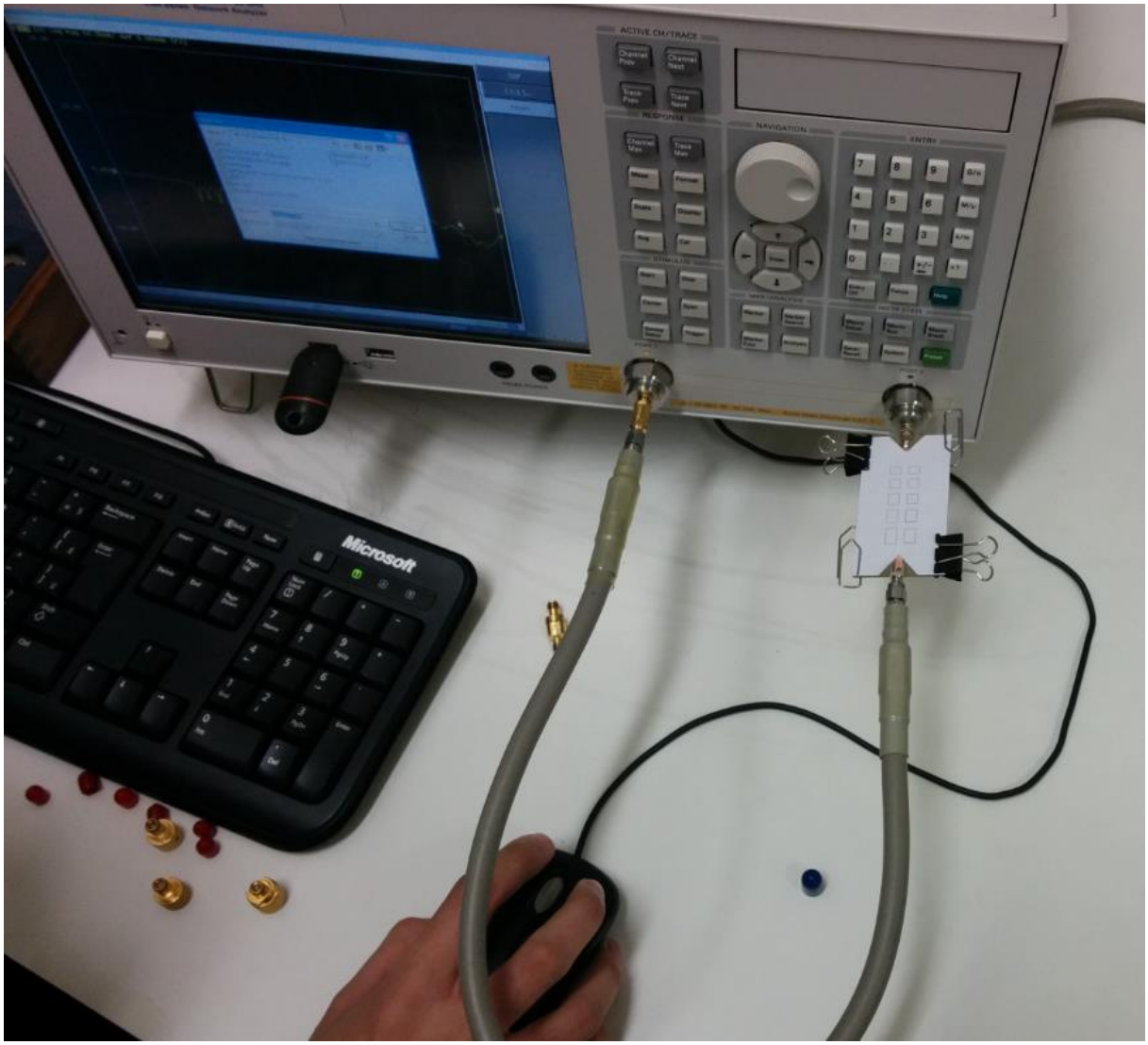

Fig. 4.3 - Measurement bench.

The next figures present the results of the measurements together with the results of the simulations. Fig. 4.4 presents code (0000000000) both simulated (solid curve) and measured (dashed curve). This situation represents the case where the paper sheet is placed on the resonators without any copper tape.

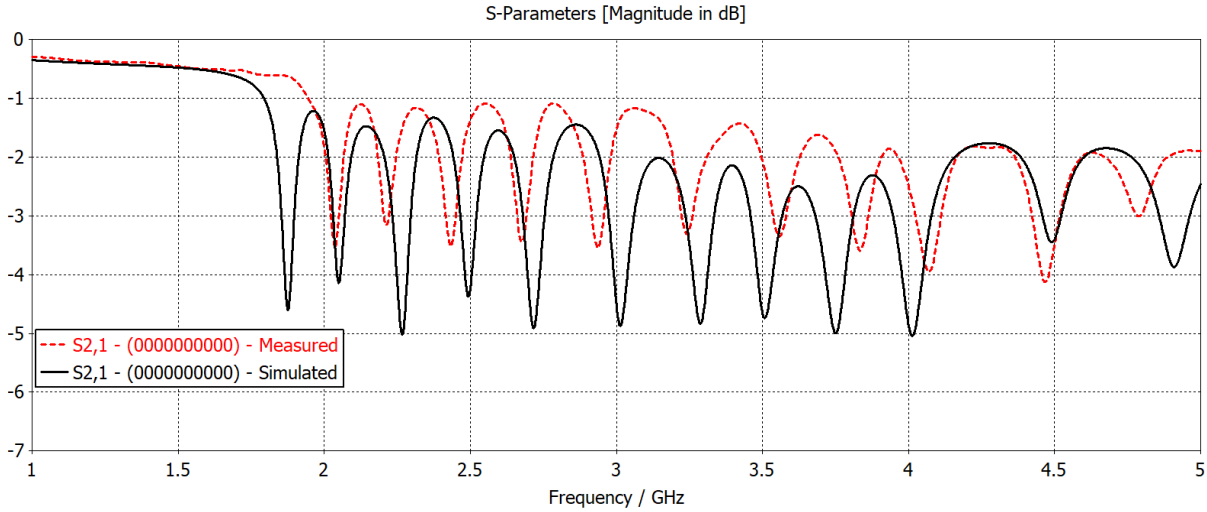

Fig. 4.4 - Measured and simulated transmission curves representing code (0000000000).

Fig. 4.5 displays the curves for the code (1111111111), situation in which all resonators have copper tape on the paper.

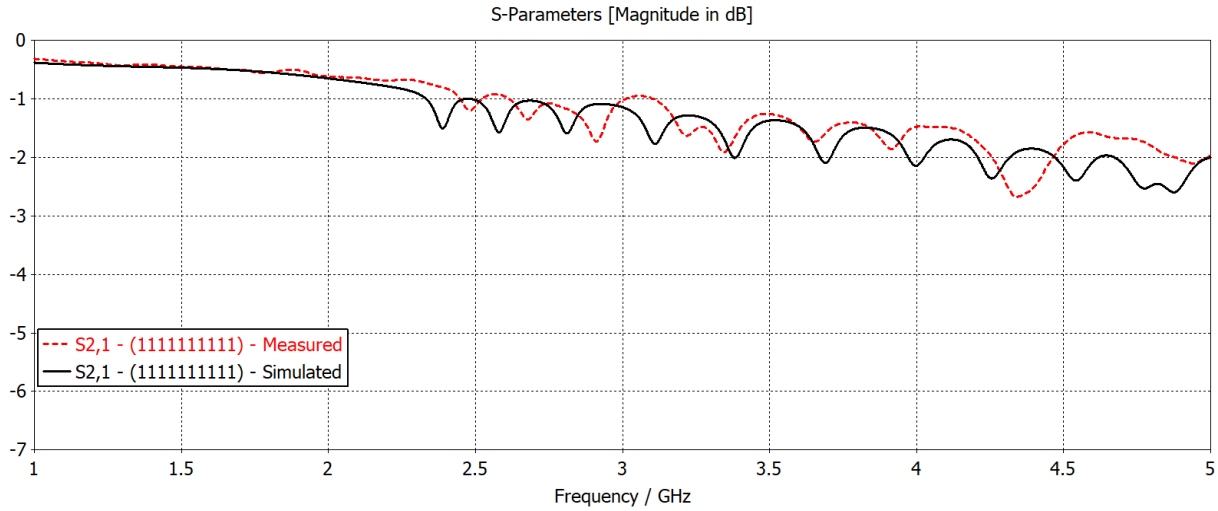

Fig. 4.5 - Measured and simulated transmission curves representing code (1111111111).

Fig. 4.6 presents the curves for the code (0110101001).

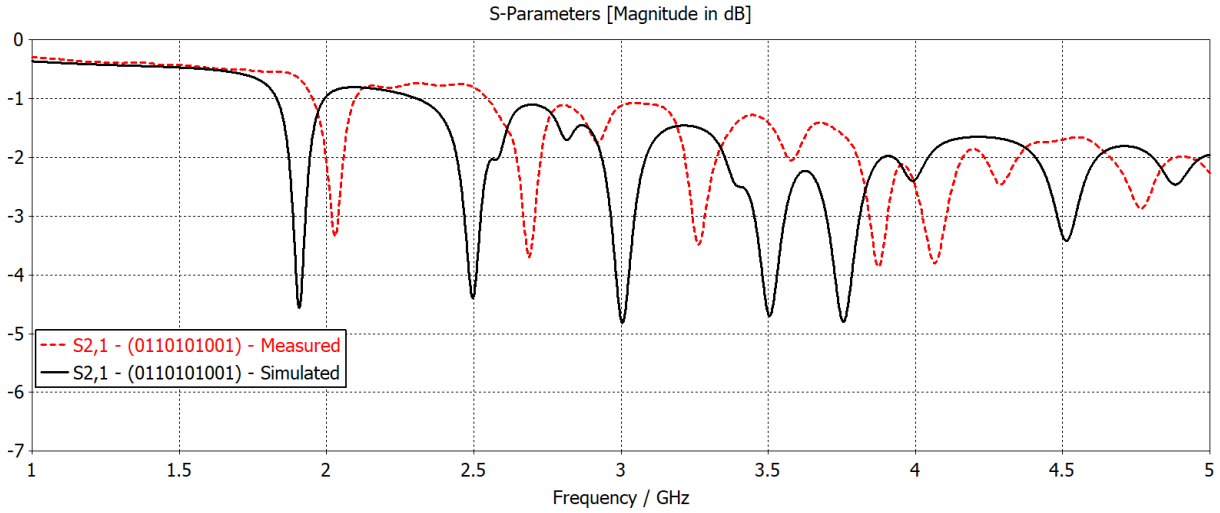

Fig. 4.6 - Measured and simulated transmission curves representing code (0110101001).

It is seen in Fig 4.7 curves for the code (1001010011).

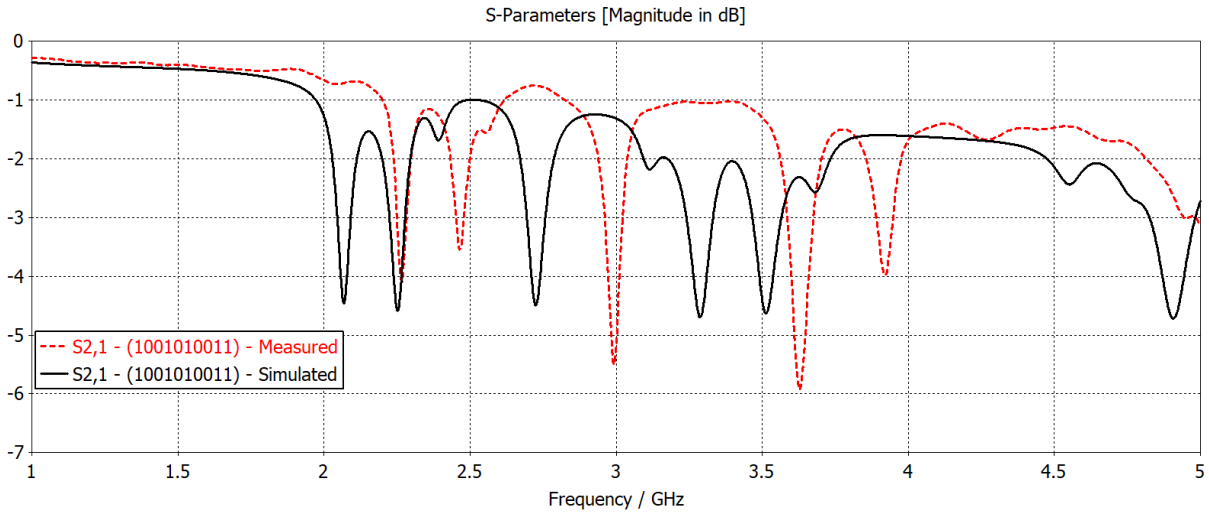

Fig. 4.7 - Measured and simulated transmission curves representing code (1001010011).

Fig. 4.8 brings the last set of curves representing code (1110001110).

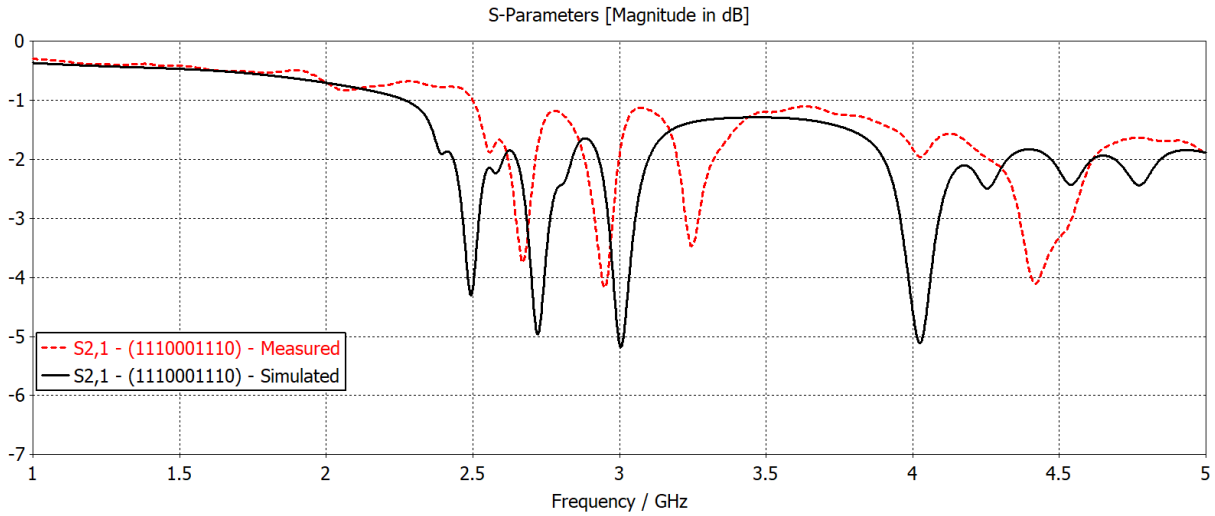

Fig. 4.8 - Measured and simulated transmission curves representing code (1110001110).

From the images, it can be observed that all the measured curves are shifted to the right by approximately 200 MHz. Also, the measured curves suggest that there are less losses in the system in relation to the simulations. This frequency shift arose as a result of the different values of the electric characteristics of the substrate compared to the values used in the simulations. Another reason was the difference in thickness of the substrate that after measured with a digital caliper had a value of 1.32 mm, which is lower than 1.60 mm used in the simulations. Moreover, the minimum available drill bit of 0.2 mm was not suitable for radiofrequency measurements; the minimum available and adequate drill bit was 0.4 mm. To complete, the simulations did not consider the effect of the connectors nor the metal losses (copper).

Therefore, an improved model has been developed in software taking into account all the involved losses, connectors and the exact dimensions of the structure. The model is shown in Fig. 4.9.

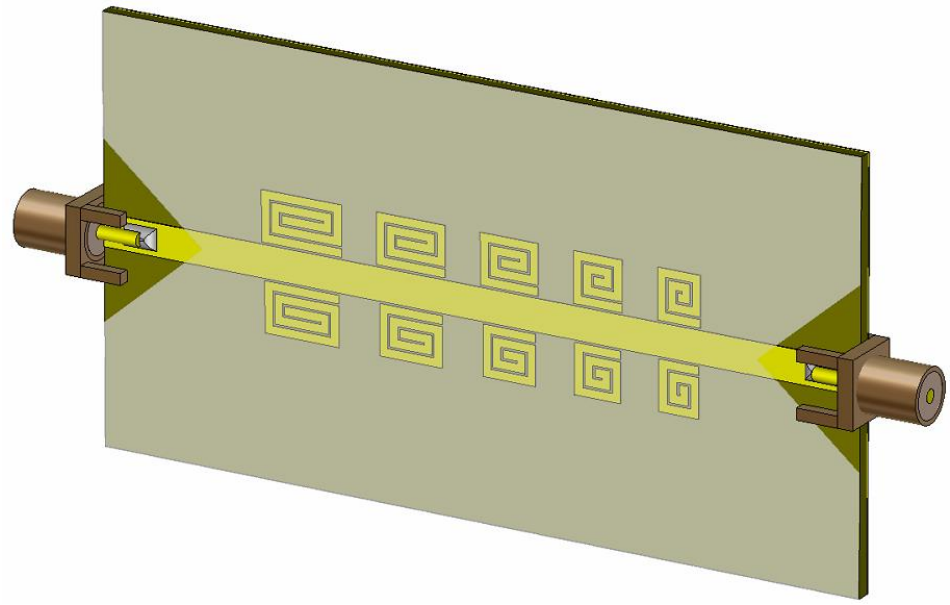

Fig. 4.9 - Improved model for simulations.

Hence, using the model of Fig. 4.9 and adjusting the simulated curves with the measured curves, the values of εr = 3.67 and loss tangent tan δ = 12.7 x 10^{-3} were found for the substrate. These values are lower than those used in simulations. For the paper sheet, the values of εr = 1.4 and loss tangent tan δ = 40 x 10^{-3} were found from the measured and simulated curves with and without paper sheet.

Figs. 4.10 to 4.14 show how the curves were better adjusted with these new values.

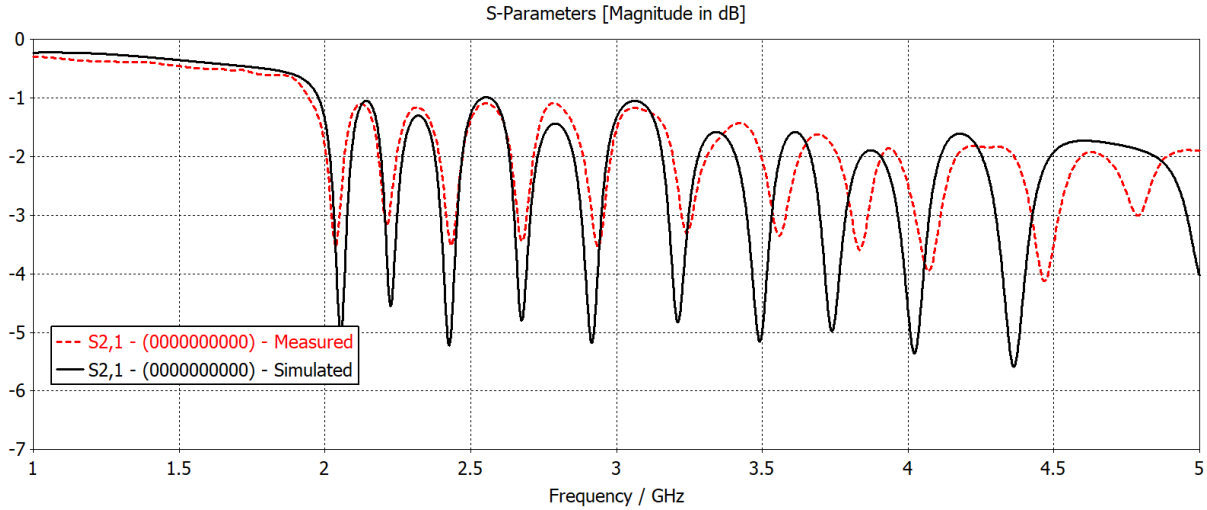

Fig. 4.10 - Measured and simulated transmission curves with adjusted electrical characteristics of the substrate and paper sheet, representing code (0000000000).

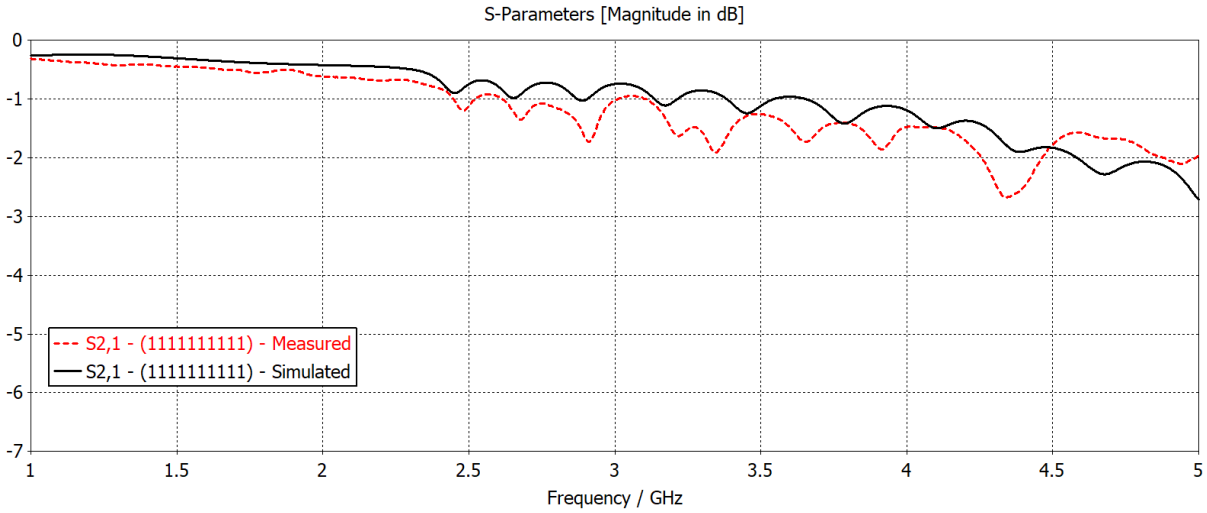

Fig. 4.11 - Measured and simulated transmission curves with adjusted electrical characteristics of the substrate and paper sheet, representing code (1111111111).

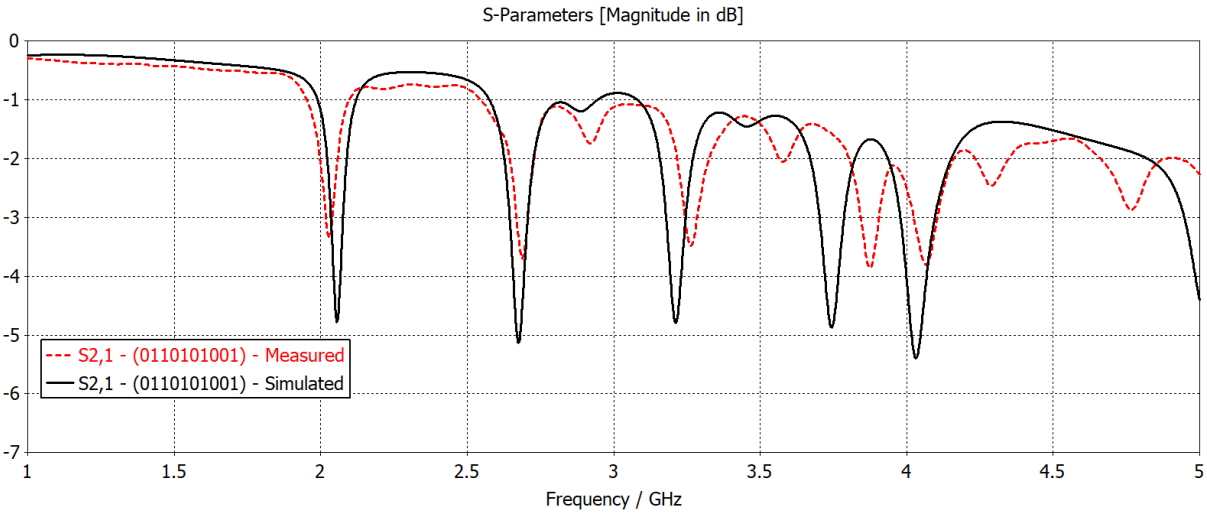

Fig. 4.12 - Measured and simulated transmission curves with adjusted electrical characteristics of the substrate and paper sheet, representing code (0110101001).

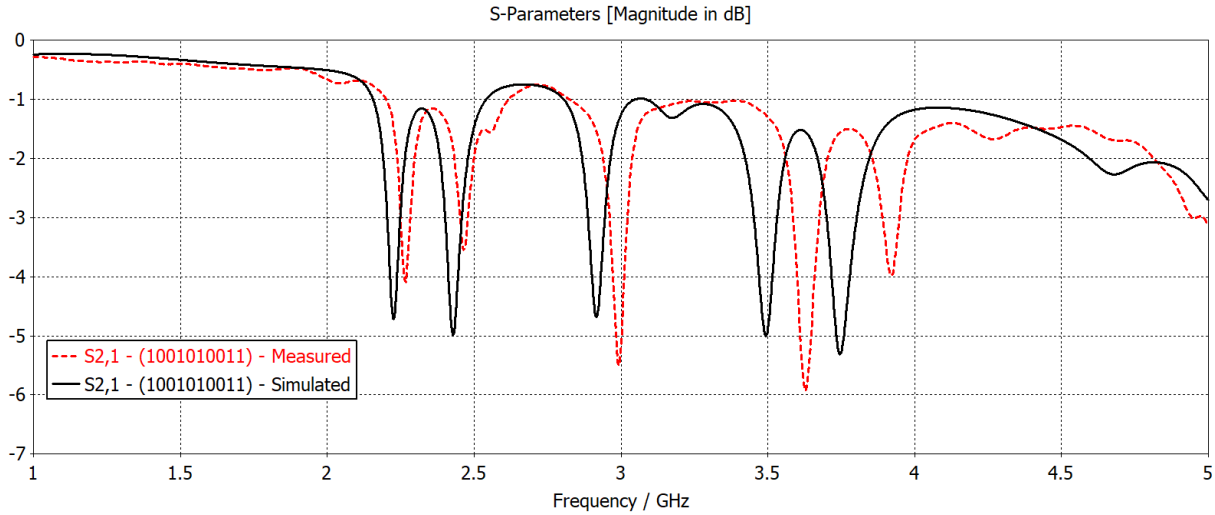

Fig. 4.13 - Measured and simulated transmission curves with adjusted electrical characteristics of the substrate and paper sheet, representing code (1001010011).

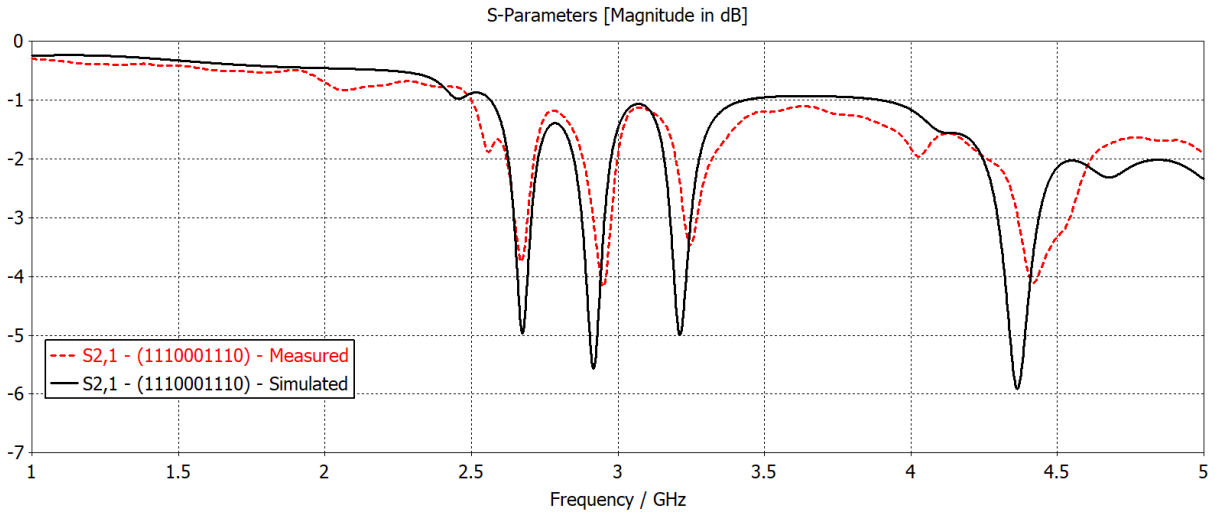

Fig. 4.14 - Measured and simulated transmission curves with adjusted electrical characteristics of the substrate and paper sheet, representing code (1110001110).

4.2 Second Set of Measurements

In the second set of measurements, it was taken into account that the electrical characteristics of the materials are those found in the previous section, namely, εr = 3.67 and tan δ = 12.7 x 10-3 for the substrate, and εr = 1.4 and tan δ = 40 x 10-3 for the paper sheet. That way, a new model was developed with these adjustments, new resonator dimensions; new microstrip line width and new resonator band of 1.80 to 3.60 GHz. Fig. 4.15 shows the new board with seven tags.

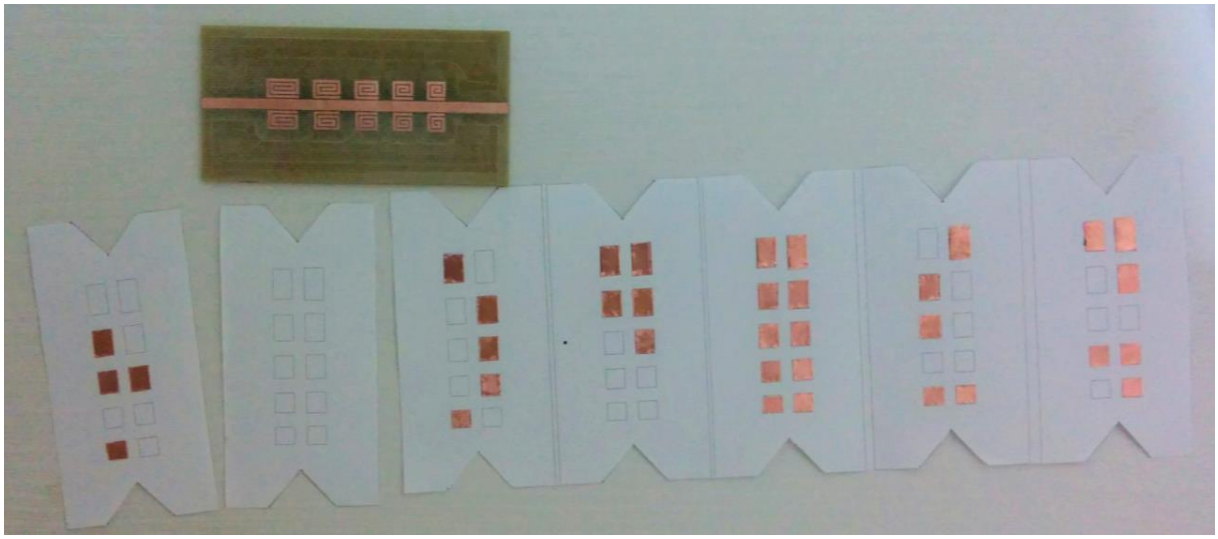

Fig. 4.15 - Second manufactured prototype next to the tags used.

Nevertheless, from the measurement results, it was noted that the dielectric constant of the substrate was not εr = 3.67, and a new readjustment of curves indicated that the value was εr = 4.20. Moreover, the height of the substrate again differed slightly from the simulated thickness, being 1.49 mm while the simulated thickness was 1.32 mm. The other variables remained the same. This was one of the difficulties of this project, the substrates used are made available by the faculty and do not have well defined electrical characteristics, that is, they vary from lot to lot.

Since the numerical model was designed with a dielectric constant different from its actual value, the results shown below are not the best possible because there is a small mismatch between the microstrip line and the 50 Ω transmission line. The calculation of the microstrip line impedance, according to section 2.2 of Chapter 2, with the characteristics of the physical model being: substrate thickness of 1.49 mm, εr = 4.20 and line width of 2.75 mm, reaches the impedance value of 52.4 Ω. This little mismatch is not a big deal.

Figs. 4.16 to 4.22 show the results for the seven binary codes inherent to the seven tags of Fig. 4.15.

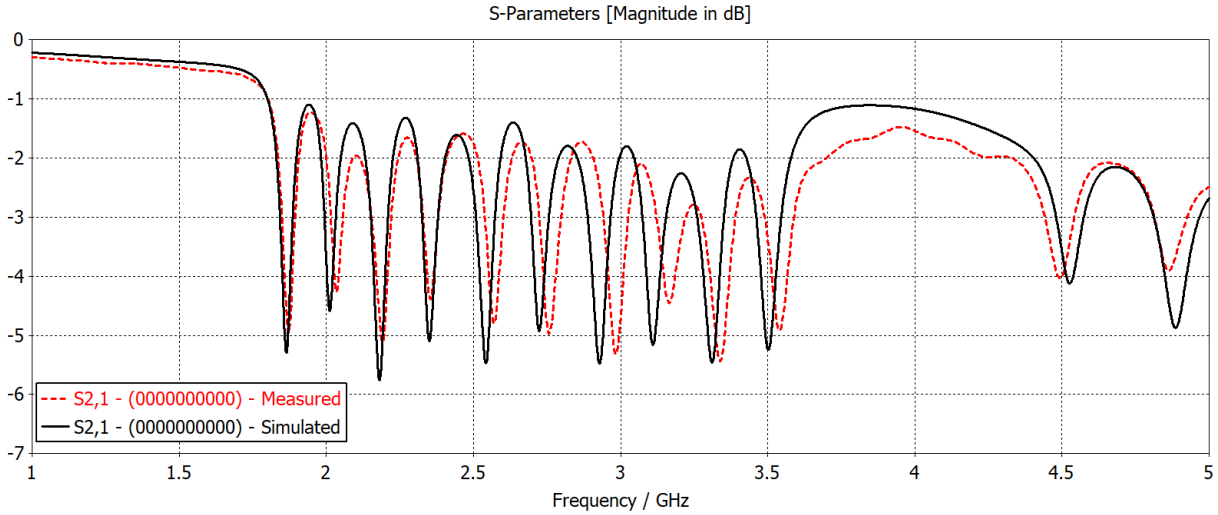

Fig. 4.16 - Measured and simulated transmission curves of the second set of measurements and simulations representing code (0000000000).

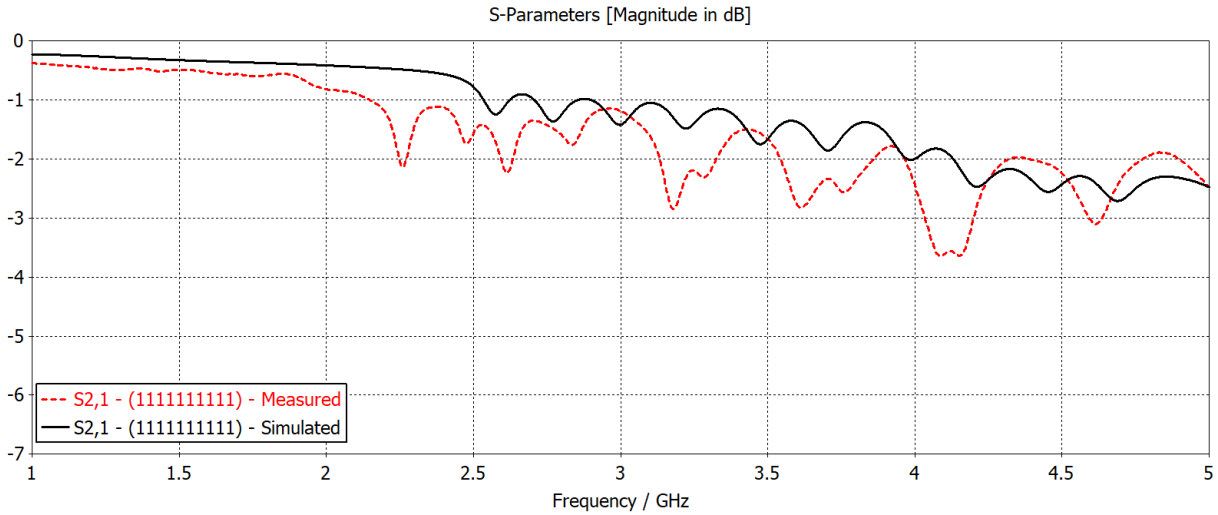

Fig. 4.17 - Measured and simulated transmission curves of the second set of measurements and simulations representing code (1111111111).

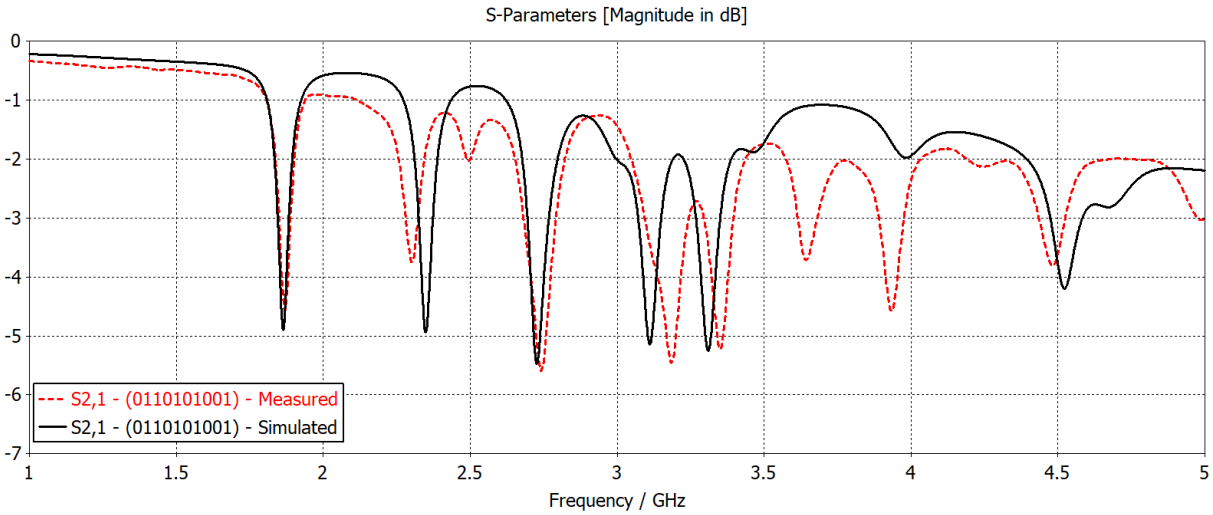

Fig. 4.18 - Measured and simulated transmission curves of the second set of measurements and simulations representing code (0110101001).

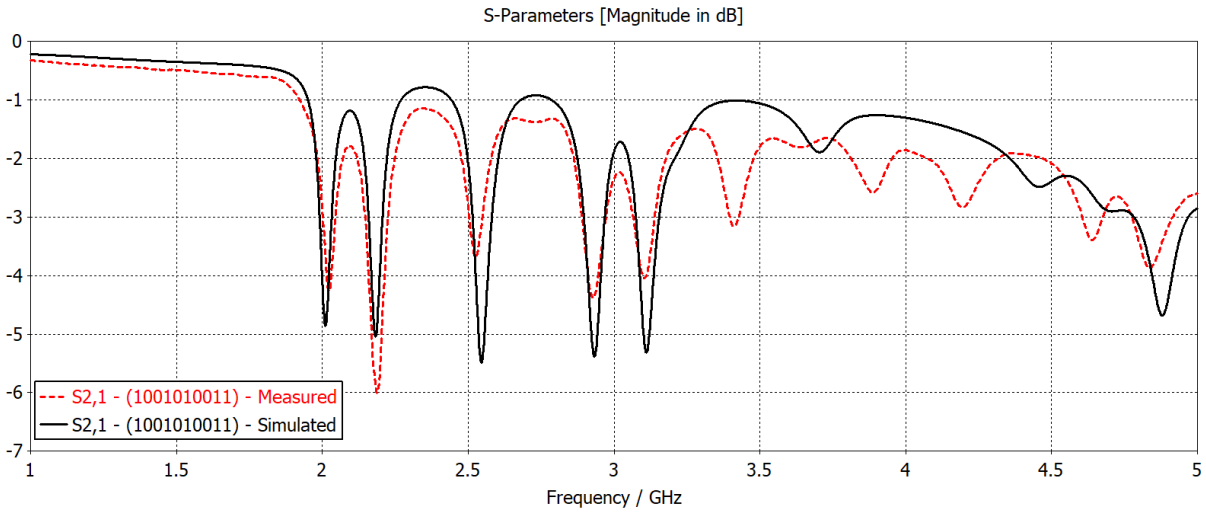

Fig. 4.19 - Measured and simulated transmission curves of the second set of measurements and simulations representing code (1001010011).

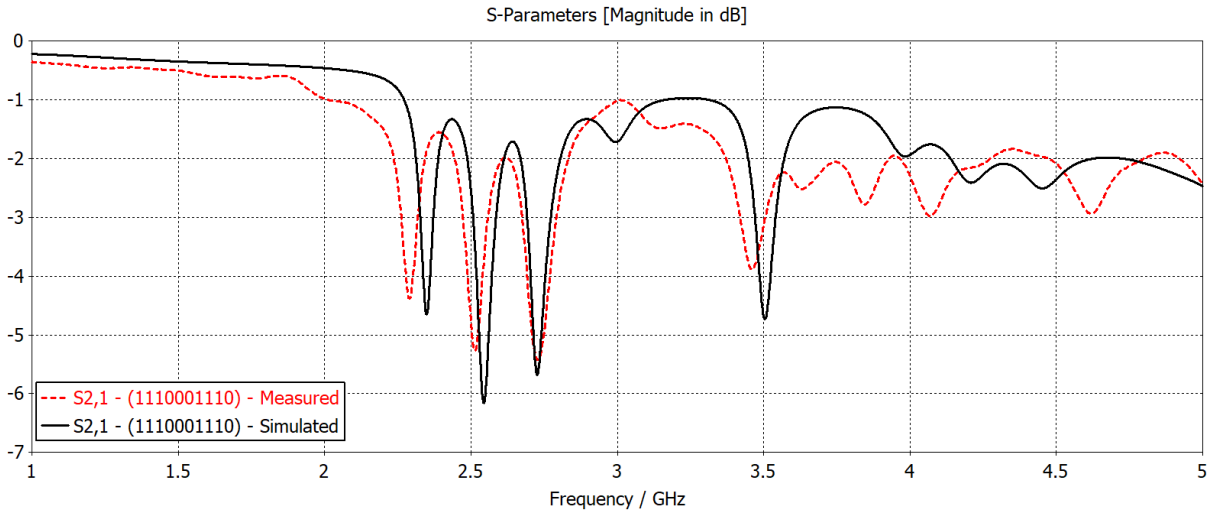

Fig. 4.20 - Measured and simulated transmission curves of the second set of measurements and simulations representing code (1110001110).

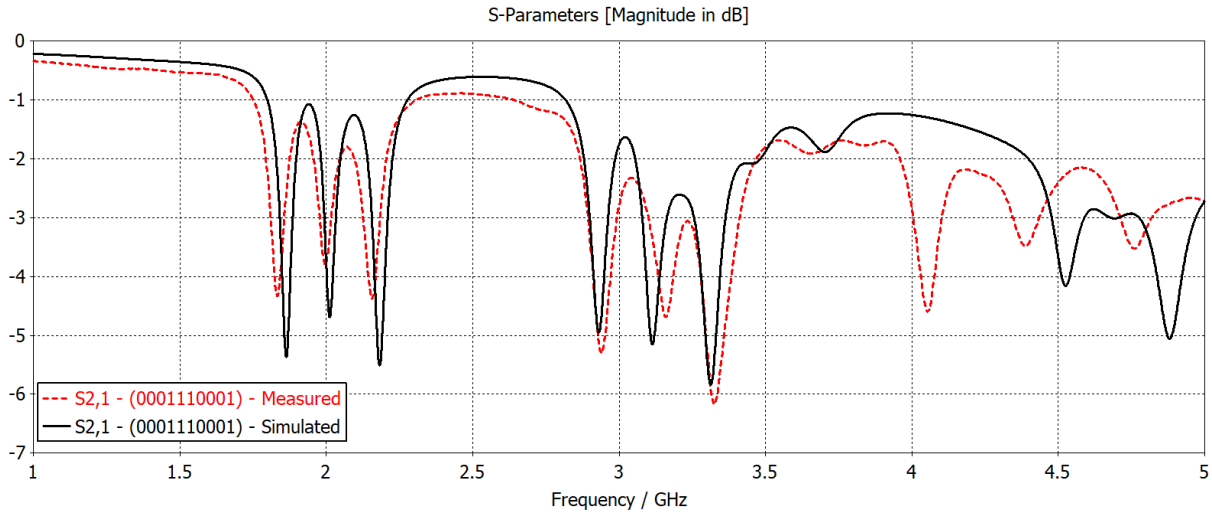

Fig. 4.21 - Measured and simulated transmission curves of the second set of measurements and simulations representing code (0001110001).

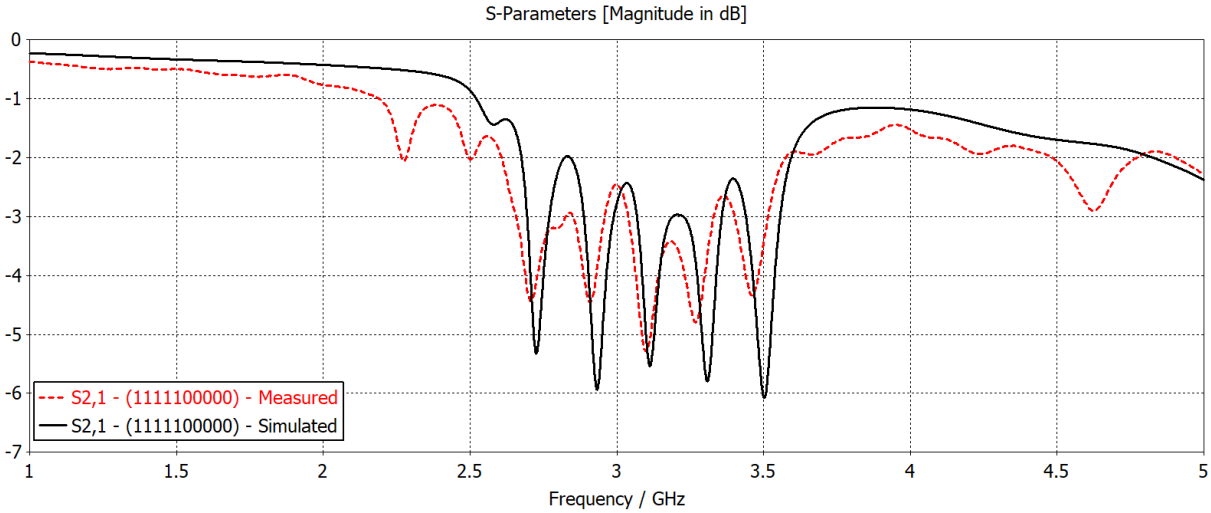

Fig. 4.22 - Measured and simulated transmission curves of the second set of measurements and simulations representing code (1111100000).

In addition to the mentioned mismatch, in Figs. 4.18 and 4.19, it can be noticed that some resonances have not been properly suppressed. This result is due to the manufacture inaccuracies of the tags, since the copper tape bonding and the tag alignment over the board were not as perfect as in the simulations. Another error factor of the measurements in relation to the simulations is the presence of air gaps between the tags and the board. These gaps could be canceled out in a system using stripline or even microstrip by submitting the banknote or document to pressure.

4.2.1 Complementary Measurements: Graphene Buckypaper and Tests with Banknotes.

In this subsection, graphene results and tests of the system using banknotes will be presented. Graphene buckypaper was manufactured within the CCS Nano (Center for Semiconductor Components and Nanotechnologies) of the State University of Campinas. The manufacturing process and some of the characteristics of the material are detailed in [22]. Fig. 4.23 shows a photo of the tags with graphene buckypaper, approximately 1 mm thick, fixed in the proper positions representing the codes (1111111001) and (1110001110).

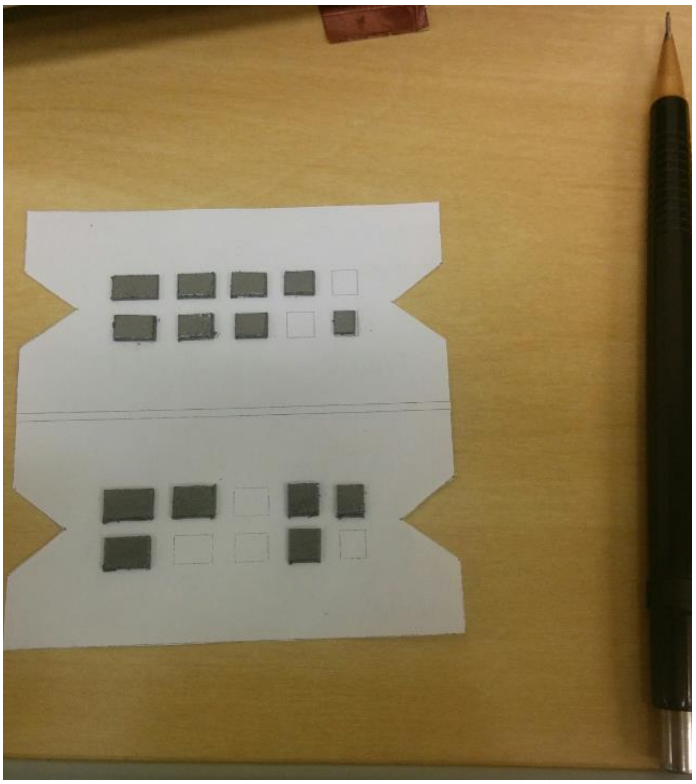

Fig. 4.23 - Two graphene buckypaper tags, the codes are: (1111111001) and (1110001110).

Figs. 4.24 and 4.25 present the measurement results of these two tags and prove that the system is also functional with graphene buckypaper. Besides, it is noted that the curves are smoother than the copper tape ones due to the absence of low magnitude resonances through the spectrum, perhaps due to the absorptive characteristic of the graphite. This is an attractive solution because of the advantages of graphene already previously presented.

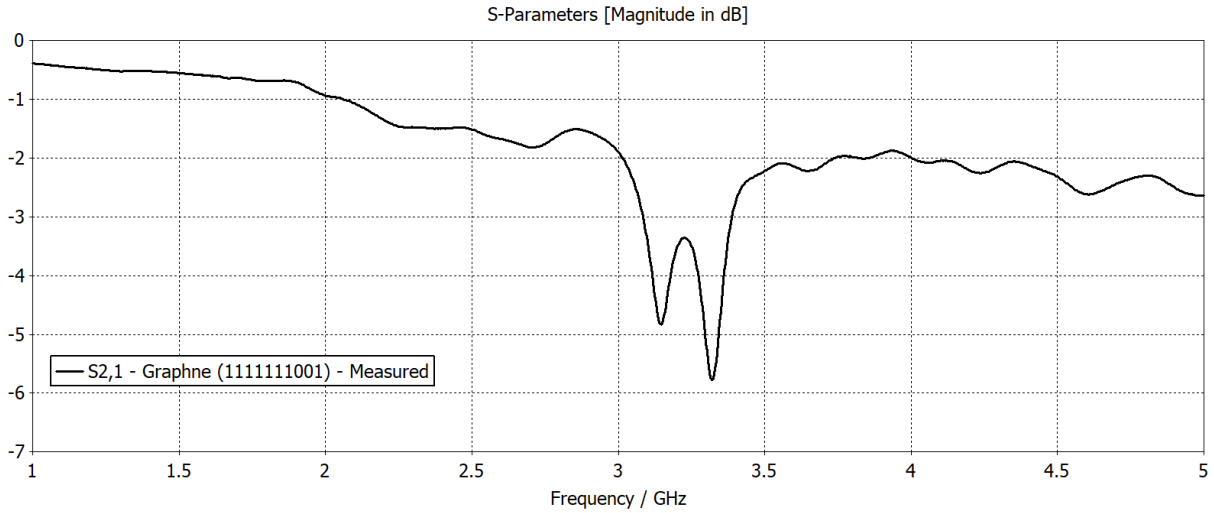

Fig. 4.24 - Measured transmission curve with graphene buckypaper representing code (1111111001).

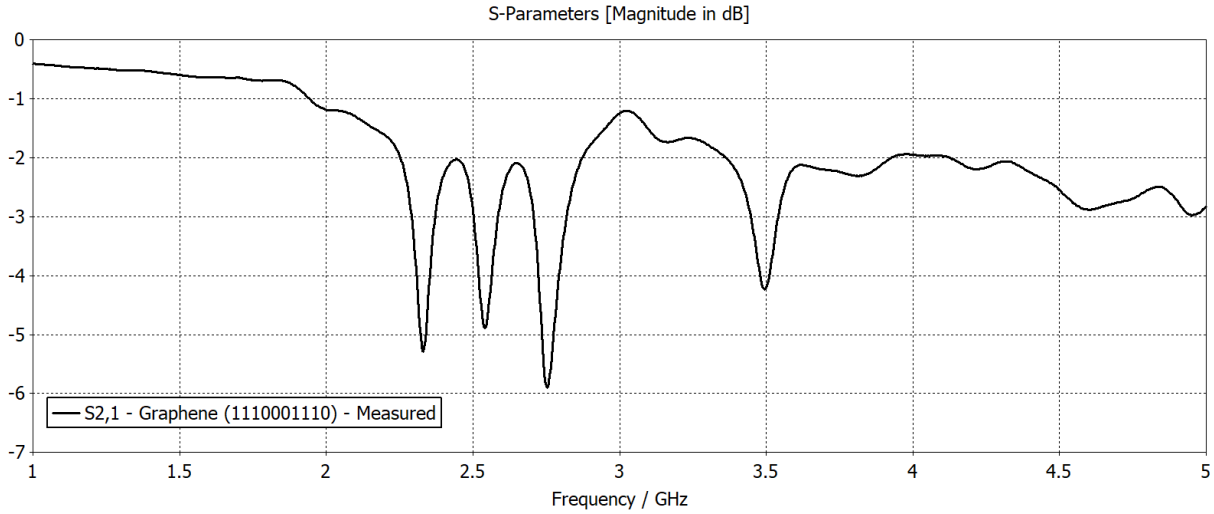

Fig. 4.25 - Measured transmission curve with graphene buckypaper representing code (1110001110).

Now, the next results are about banknotes over the board.

Figs. 4.26 to 4.29 present the measured curves of the system for the following four situations of banknotes on the resonators: new and dry banknote; old banknote; new and little wet and new and wet banknotes. These measurement situations have the objective of testing the effect of certain adverse conditions to which banknotes or documents can be submitted, such as humidity and aging, in order to verify and prove the system viability. The transmission curves of these situations are placed along with the transmission curve of the board without banknote placement.

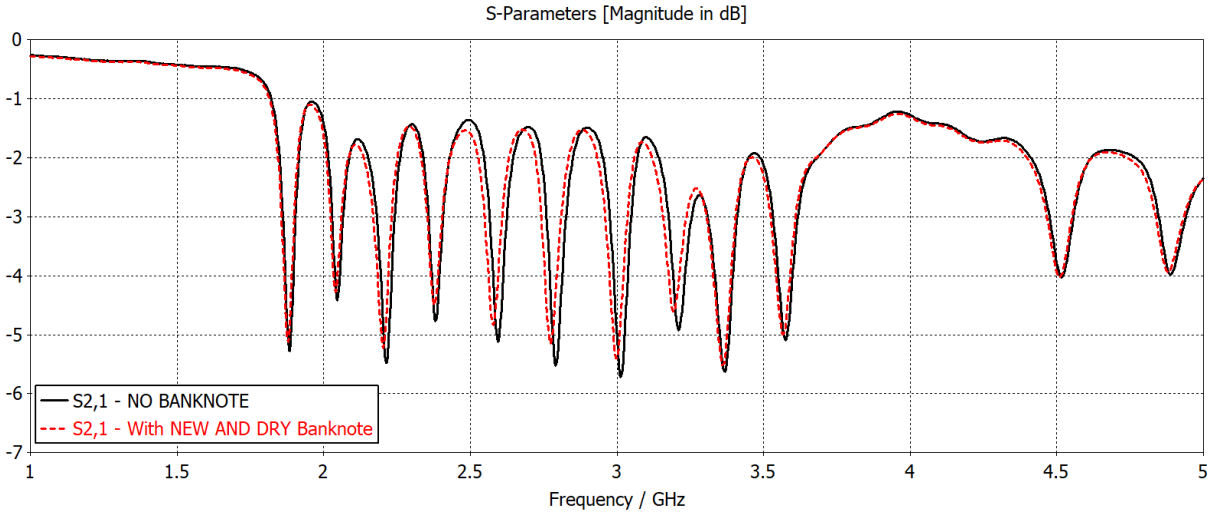

Fig. 4.26 - Measured transmission curves: board with new and dry banknote x board without banknote.

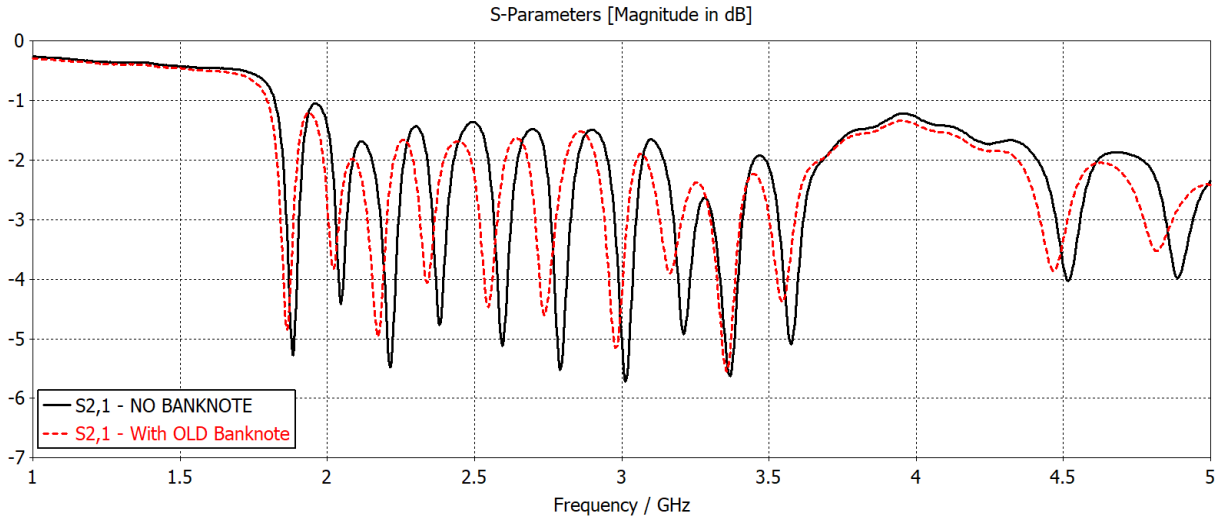

Fig. 4.27 - Measured transmission curves: board with old banknote x board without banknote.

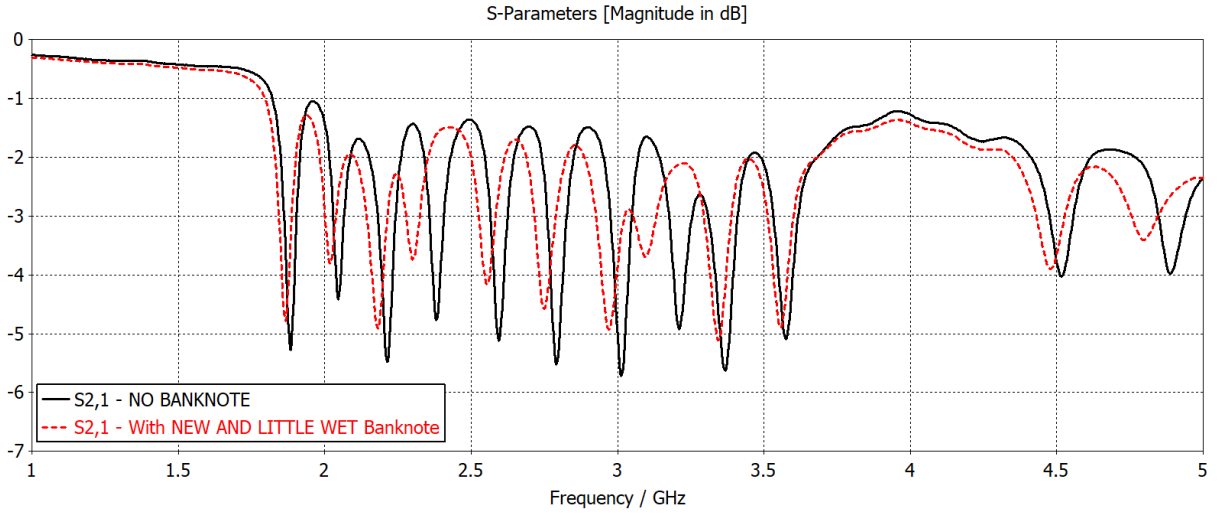

Fig. 4.28 - Measured transmission curves: board with new and little wet banknote x board without banknote.

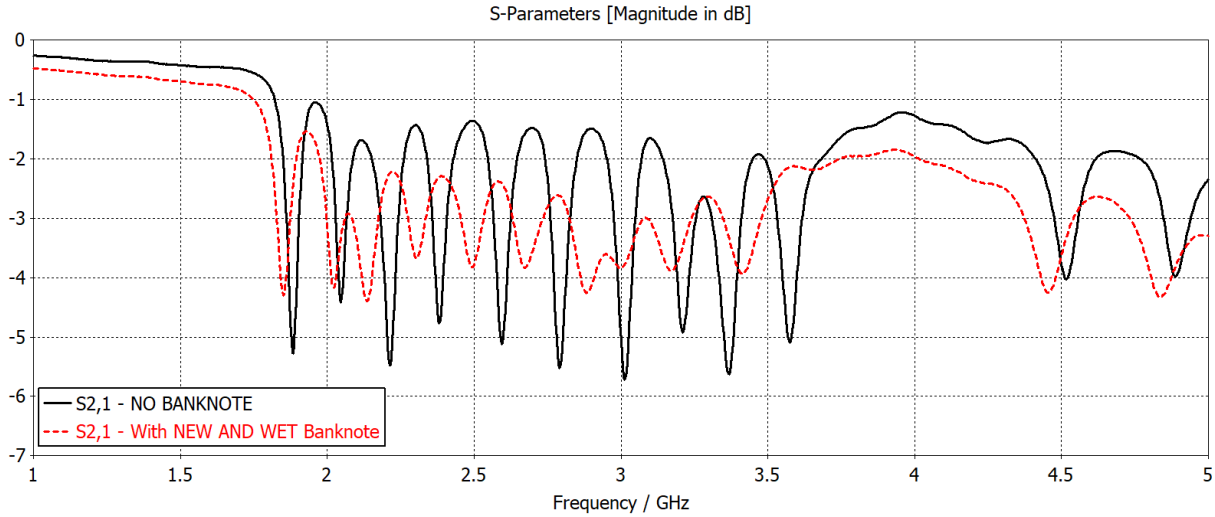

Fig. 4.29 - Measured transmission curves: board with new and wet banknote x board without banknote.

The results show that a new and dry banknote practically does not displace the transmission curve and has very little attenuation, indicating that a banknote like that has a dielectric constant close to 1.0 and low losses. In the case of the old banknote, this adds a greater displacement in the curves in relation to the new one and causes more losses; these results mean that the old banknote has greater dielectric constant and loss tangent resulting from the impregnation of dust particles and moisture. The little wet and wet banknotes shift and attenuate the curves more significantly, as a result of the electromagnetic wave absorption by the water and the modification of the dielectric constant of the banknote.

Therefore, it is realized that a wet or even little wet banknote might result in reading errors in the system due to the resonance attenuation caused by the water. However, for the implementation of such a system, a much better substrate would be used than FR-4 such as Arlon 25N whose dielectric constant is 3.38 and loss tangent is 25 x 10^{-4}, that is, a loss factor about five times lower than that of FR-4. The problem of resonance attenuation resulting from moisture or aging of the banknotes or documents can thus be reduced by using a substrate with smaller losses where the resonances would be deeper and detached in the spectrum. The issue of the resonance displacement can be bypassed with the increase of the allocated frequency from each resonator.

Chapter 5

Conclusions and Future Works

The project development presented throughout this text brings a practical and cost-effective solution to a long-standing problem, with its historical examples, that could threaten a country's economy: the problem of banknote and document counterfeiting.

The developed system can work on both the microstrip and stripline technologies, each with its specific advantages and disadvantages. The resonators with the microstrip line or stripline constitute the reader core. The resonator used was the one with a spiral shape because it is compact and simple, but the possibility of using other types of resonators is not ruled out, as long as the resonances can be extinguished by means of a metallic pattern printed in the banknotes or documents.

The chipless radiofrequency identification technology was the technological basis of this project, through which it is possible for data to be encoded in a large number of objects by reducing the total cost of the identification system and making it comparable to the cost of a barcode system, however, with much more security. The proposed developed system reduces the tag manufacturing activity to the impression of a simple metallic pattern without the need of a transmission line, resonators and/or receiving and transmitting antennas as in [6]. That is because the transmission line and the resonators are located in the reader and there are no antennas because the reading is achieved through the contact of the banknote with the reader. In a system where it is necessary the tagging of a very large amount of objects, it is indispensable that the tags be cheap so that the system is plausible and advantageous.

The numerical analysis performed throughout this work demonstrated the viability of the proposed developed system, from the simple spiral resonator with variations and adjustments of its physical parameters to the demonstration of the possibility of greater data encoding. Moreover, the proposed system has several advantages such as low cost of tag manufacturing, very convenient in an identification system with numerous objects. Also, the metallic pattern can be printed inside the banknotes or documents. Besides, there is the possibility of greater data encoding, using the idea of the ternary system. Lastly, the system has great robustness.

The S parameter measurements in laboratory validated the results obtained in the simulations, despite the encountered difficulties with the electrical parameters of the substrates. The first set of measurements served to better estimate these parameters and to prepare the ground for a second set of measurements. The second set allowed better results and complementary measurements such as those in which graphene buckypaper was used in the production of the tags and the tests with the utilization of banknotes in different situations.

For future works, the following activities are considered of importance: the development of the system reader with its RF and digital modules; the modeling and construction of the resonators in a substrate of better quality, as Arlon 25N or Taconic TLX; the development of a model with more resonators for greater data encoding; and size reduction by increasing the frequency, so that the tag takes up a not too large area of the banknote or document.

References

[1] 9 fatos sobre Isaac Newton que surpreenderão você. Available on: https://seuhistory.com/noticias/9-fatos-sobre-isaac-newton-que-surpreenderao-voce. Accessed on: Jun. 22, 2017.

[2] M. Singh, Review: “Isaac the torturer”. Available on: https://www.newscientist.com/article/mg15621055-800-review-isaac-the-torturer/. Accessed on: Jun. 22, 2017.

[3] Dinheiro sim: durável, seguro, secreto. Como são feitas as notas brasileiras. Available on: http://super.abril.com.br/comportamento/dinheiro-sim-duravel-seguro-secreto-como-sao-feitas-as-notas-brasileiras/. Accessed on: Jun. 22, 2017.

[4] S. Preradovic; N. C. Karmakar, “Multiresonator-Based Chipless RFID, Barcode of the Future”. Springer, 2012.

[5] N. C. Karmakar; M. Zomorrodi; C. Divarathne, “Advanced Chipless RFID: MIMO-Based Imaging at 60 GHz – ML Detection”. John Wiley & Sons, Inc. 2016.

[6] S. Preradovic, I. Balbin, N. C. Karmakar and G. F. Swiegers, "Multiresonator-Based Chipless RFID System for Low-Cost Item Tracking," in *IEEE Transactions on Microwave Theory and Techniques*, vol. 57, no. 5, pp. 1411-1419, May 2009. doi: 10.1109/TMTT.2009.2017323

[7] X. –C. Zhang; J. Xu, “Introduction to THz Wave Photonics”, USA: Springer, 2010.

[8] K. Aydin; I. Bulu; K. Guven; M. Kafesaki; C. M. Soukoulis; E. Ozbay, “Investigation of magnetic resonances for different split-ring resonator parameters and designs”. New Journal of Physics 7, p. 10, August 2005.

[9] “High Speed PCB Layout Techniques”. Available on: http://www.ti.com/lit/ml/slyp173/slyp173.pdf.

[10] A. C. Balanis, “Advanced Engineering Electromagnetics”, 2012, Chapter 8, pp. 455-466.

[11] D. M. Pozar, “Microwave Engineering”, Fourth Edition, John Wiley & Sons, Inc.

[12] S. Tedjini, N. Karmakar, E. Perret, A. Vena, R. Koswatta and R. E-Azim, "Hold the Chips: Chipless Technology, an Alternative Technique for RFID," in *IEEE Microwave Magazine*, vol. 14, no. 5, pp. 56-65, July-Aug. 2013. doi: 10.1109/MMM.2013.2259393

[13] RFSAW Inc. “The global SAW tag – a new technical approach to RFID”,

2004. Available on: http://www.rfsaw.com/Pages/TechnicalPublications.aspx. Accessed on: Jun. 26, 2017.

[14] C. S. Hartmann, "A global SAW ID tag with large data capacity," *2002 IEEE Ultrasonics Symposium, 2002. Proceedings.*, 2002, pp. 65-69 vol.1. doi: 10.1109/ULTSYM.2002.1193354

[15] Y. F. Weng, S. W. Cheung, T. I. Yuk and L. Liu, "Design of Chipless UWB RFID System Using A CPW Multi-Resonator," in *IEEE Antennas and Propagation Magazine*, vol. 55, no.1, pp. 13-31, Feb. 2013. doi: 10.1109/MAP.2013.6474480

[16] CST – Computer Simulation Technology. Available on: https://www.cst.com/.

[17] R. H. Giles, “Characterization of Material Properties at Terahertz Frequencies”. Submillimeter Technology Laboratory, University of Massachusetts, Lowell.

[18] “Terahertz Materials”. Available on: http://www.tydexoptics.com/en/products/thz_optics/thz_materials/. Accessed on: May 16, 2017.

[19] Z. Y. Pan, P. Zhang, Z. C. Chen, G. Vienne and M. H. Hong, "Hybrid SRRs Design and Fabrication for Broadband Terahertz Metamaterials," in *IEEE Photonics Journal*, vol. 4, no. 5, pp. 1267-1272, Oct.2012. doi: 10.1109/JPHOT.2012.2207711

[20] J. S. Moon and D. K. Gaskill, "Graphene: Its Fundamentals to Future Applications," in *IEEE Transactions on Microwave Theory and Techniques*, vol. 59, no. 10, pp. 2702-2708, Oct. 2011. doi: 10.1109/TMTT.2011.2164617

[21] G. T. Santos-Souza, A. A. d. C. Alves, L. L. Bravo-Roger and H. E. Hernandez-Figueroa, "Numerical determination of frequency guard band resonances for Chipless RFID Tags," *2014 IEEE Brasil RFID*, Sao Paulo, 2014, pp. 10-12. doi: 10.1109/BrasilRFID.2014.7128952

[22] J. P. Pantoja; R. Savu; M. A. Canesqui; S. A. Moshkalev e H. E. Hernandez-Figueroa, "Performance Comparison of Metallic and Graphene Buckypaper Microstrip Transmission Lines," IMOC – International Microwave and Optoelectronics Conference, Águas de Lindoia, Brasil, 2017.